KINETIC EFFECTS ON GLOBAL ALFVÉN WAVES

by

Riccardo Betti

Laurea: Universitá di Roma "La Sapienza"
1987

Submitted to the Department of
Nuclear Engineering in Partial Fulfillment of
the Requirements for the Degree of

DOCTOR OF PHILOSOPHY IN NUCLEAR ENGINEERING

at the

Massachusetts Institute of Technology

February 1992

Signature of the Author .....
Department of Nuclear Engineering
October 2, 1991

Certified by .....
Prof. Bruno Coppi
Thesis Supervisor

Certified by .....
Prof. Jeffrey P. Freidberg
Thesis Co-Supervisor

Accepted by.....
Prof. Allan Henry
Charmain, Committee for Graduate Students

KINETIC EFFECTS ON GLOBAL ALFVÉN WAVES

by

RICCARDO BETTI

Submitted to the Department of Nuclear Engineering
on October 2, 1991 in partial fulfillment of the
requirements for the degree of Doctor of Philosophy in
Nuclear Engineering

ABSTRACT

A theoretical investigation is carried out on the effects of the kinetic particle response on global type shear-Alfvén waves in tokamaks. Two kinds of wave-particle interactions have been identified: (1) resonant interaction between energetic circulating particles and high frequency Alfvén waves ($\omega \simeq \omega_A$), (2) nonresonant interaction between trapped particles and low frequency modes ($\omega = \omega_{*i}$).

Among the high frequency global type shear-Alfvén modes we focus on gap modes which are discrete modes whose real frequency lies in gaps of the Alfvén continuum induced by geometrical effects. In particular it is discovered the existence of a new gap mode, the Ellipticity Induced Alfvén Eigenmode (EAE) which is induced by the ellipticity of the plasma cross section that couples the m and $m+2$ poloidal harmonics. This mode is of the same general class as the Toroidicity Induced Alfvén Eigenmode (TAE). In configurations with finite ellipticity, the EAE $(n; m, m+2)$ has a global structure centered about the $q = (m+1)/n$ surface. The region of "localization" is of order $\kappa - 1$ which is often much larger than ϵ. Thus, the EAE may be more "global" than the TAE in such configurations.

In the presence of an energetic ion species any Alfvén wave can be destabilized via transit resonance with circulating particles. A sufficient stability criterion is derived for energetic particle-Alfvén mode. The criterion is valid for arbitrary aspect ratio, arbitrary β, noncircular, axisymmetric tori. The plasma is modeled by a magnetohydrodynamic (MHD) core plus a fully kinetic Vlasov species of hot particles. Electron and bulk ion kinetic effects are neglected. In spite of the complexity associated with the analysis of the Vlasov species, a simple but exact stability boundary is derived. The criterion is very fluid-like in nature, suggesting that accurate evaluation in realistic geometries can be accomplished with only minor modifications to any one of the existing MHD stability codes.

In order to include the stabilizing effects of the electron and ion Landau damping a more general treatment using a newly derived drift kinetic description of each species is carried out. The analysis has been restricted on Alfvén gap modes. Three modes have been identified: the Toroidicity, Ellipticity and Triangularity induced Alfvén Eigenmodes (TAE,EAE and NAE). It is found that electron Landau damping in highly elongated plasmas has a strong stabilizing influence on the $n = 1, m = 1$ EAE, while the ion Landau damping stabilizes the $n = 1, m = 1$ TAE in high density regimes. Furthermore, the NAE turns out to be stable for all currently proposed ignition experiments. The stability analysis of a typical burning plasma device (BPX) shows that $n > 1$ gap modes pose a serious threat to the achievement of ignition conditions.

Low frequency modes ($\omega \simeq \omega_{*i}$) have also been investigated using the new drift kinetic model. Focusing on the internal kink mode, the main kinetic contribution arises from trapped particles (both ions and electrons) which precess in the toroidal direction with angular velocity $\omega_{Dh}(\epsilon, \Lambda)$ where ϵ and Λ are the particle energy and pitch angle. It is found that the trapped bulk ions can destabilize the high frequency branch ($\omega \simeq \omega_{*i}$) of the internal kink. The instability is driven by the trapped bulk ions and requires a somewhat large value of ω_{*i}/ω_{Dh}. The numerical solution of the dispersion relation shows that a sharp threshold in β_p exists for the instability to grow and that stabilizing effects come from the trapped electron response. Although a more detailed analysis is needed, these preliminary studies indicates that the trapped electrons are not able to bring the mode to a complete stabilization.

Thesis Supervisor: Dr. B. Coppi

Title: Professor of Physics

Thesis Co-Supervisor: Dr. J.P. Freidberg

Title: Professor of Nuclear Engineering

ACKNOWLEDGEMENTS

The journey of about four years now comes to a close. Looking back I realize that MIT is a great place to be. Throughout the journey I have found individuals who have supported me, who have guided me, and who have accompanied me.

I am very grateful to my two advisors, Prof. B. Coppi and Prof. J.P. Freidberg. I really believe I could not have made a better choice. If combined together Jeff and Bruno give rise to the "absolutely perfect advisor".

I would like to thank Dr. S. Migliuolo and Dr. J.U. Brackbill for their friendship and collaboration. I am also very grateful to Prof. D.J. Sigmar for his wise advice (scientific and otherwise) and for pointing out the importance of energetic particle-Alfvén modes to future large tokamaks. Special thanks to Dr. C.T. Hsu for many useful discussions on gap modes.

I owe a special gratitude to my parents Renato and Anna Maria and to my brother Raimondo for their endless support and to all my friends that have been close to me during the struggle. I do believe that during the past four years at MIT I have met the most valuable and interesting people. I am sure they will be friends for life.

Very special thanks to Marco and Giulia, Yvette and Simone, Sergio and Stefano. Given the limited number of pages available I cannot express in these acknowledgements all my gratitude to the six of them. Nevertheless I would like to spend few words on one of them who had the misfortune to share the office with me for the last three years. I am conviced I'll be very sorry to have met Marco Nassi. From now on I will have to compare myself with him and suffer eternal frustration. My only hope is that my expertise in dealing with ideal models in physics (such as Ideal MHD) will help me to deal with ideal models in life (such as Marco).

I am extremely grateful to my girlfriend Suzanne who has tolerated my crazy mood while typing this thesis.

Special thanks to my favorite room-mate Ana L., to my office-mate Paolo , to Catherine L. and Ana K. for their assistance and to my colleagues at the PFC and RLE: Bob, James, Darin and Luigi. I would also like to thank Mi for the delicious food she provided for me during the last phase of this thesis.

TABLE OF CONTENTS

CHAPTER 1.

Introduction

1.1 Kinetic effects on MHD modes

The study of kinetic effects on the stability of magnetohydrodynamic modes has received considerable attention in the last decade.

Due to the present efforts put forth to design an ignition experiment, in which the plasma heating provided by the charged fusion reaction products can compensate for all forms of energy loss, it has become necessary to investigate how plasma instabilities can deteriorate alpha particle confinement. In particular, if one refers to a deuterium-tritium plasma mixture, relevant questions concern whether or not the 3.5 Mev alpha particles produced by the DT reactions can be confined within the plasma column for the duration of their slowing down; and if confined, whether or not they will affect the plasma stability and energy transport. The classical aspects of the energetic particle confinement, namely "prompt" losses caused by intersection of their orbits with the wall of the vessel, as well as classical diffusion across the magnetic field, "ripple losses," etc., have been extensively investigated[1,2].

From the experimental side there has been convincing evidence that kinetic effects, due to a high-energy particle population, can affect the stability of global modes. In high power, nearly perpendicular neutral beam injection experiments[3], bursts of large amplitude poloidal magnetic field fluctuations with frequency in the range of the ion diamagnetic frequency were correlated to reductions of neutron

emissivity that corresponds to significant losses of energetic beam ions. The observed mode reveals a dominant $m = n = 1$ structure (m is the poloidal mode number and n is the toroidal mode number)

Since the magnetic field fluctuations associated with this instability showed a characteristic skeletal signature on the soft X-ray imaging system, the name of "fishbone oscillations" was suggested. A reduction of the mode rotational frequency was also observed in combination with the particle bursts, showing a dependence of the mode frequency on the energetic particle density. These bursts are usually superimposed on the sawtooth oscillations; however, in a few cases they have also been observed during sawtooth-free periods. Soft X-ray tomographic analyses of the fishbone bursts shows the presence of a magnetic island about the $q = 1$ surface. This can be considered as an indication that the fishbone mode is an $m = n = 1$ resistive internal kink. Significant amounts of beam power have been lost during fishbone activity in PDX and Doublet III, while only minor losses have been observed in JET. Theoretical investigations of fishbone oscillations[5,6], suggest that an $n = 1$, $m = 1$ internal kink with a frequency of oscillation ω , approximately equal to the ion diamagnetic frequency ω_{*i} , is destabilized by resonant interaction with trapped hot particles precessing at their magnetic drift frequency. In an alternative interpretation[4], the limit $\omega_{*i}/\omega_{Dh} = 0$ was considered and a mode with $\omega = \omega_{Dh}$ was proposed as a relevant candidate.

High-frequency activity has also been observed in conjunction with fishbone oscillations. In PBX, modes with poloidal mode numbers larger than one and with frequencies in the range 140-220 kHz, have been detected[7]. During these high frequency bursts, the neutron emission dropped only two percent indicating beam losses much smaller than the one reported during the low frequency activity (20 percent).

Very recently, MHD activity, with frequency in the range of the Alfvén frequency, has been observed in the TFTR[8] and DIII-D[9] when quasi-tangential neutral beams were injected with velocities close to the Alfvén speed. The unstable mode

had toroidal wave number $n > 1$ in both experiments. In TFTR, the mode excited at 82kHz was identifed as having toroidal wavenumber $n = 2$. The measured frequency coincides with one of a $n = 2$, $m = 2$ TAE mode. A fundamental problem in the TFTR experiment is that poloidal wavelengths were measured, corresponding to poloidal mode number of $m = 6$ and $m = 8$ respectively. An $n = 2$, $m = 6$ TAE mode would resonate at the $q = 13/4 > 3$ surface that is close to the plasma edge. Since poloidal wavelength measurements are performed on the outer region of the plasma column, it is likely that a wide variety of $n = 2$ TAE modes were excited, but only the ones localized at the plasma edge were detected. Decrease in neutron emission during bursts indicates that a significant amount of energetic particles are ejected from the plasma core.

MHD activity in the frequency range $\omega \sim \omega_A$ was later observed in DIII-D. Several modes with frequency between 50-200kHz were associated with high frequency bursts. These modes had a toroidal mode number of $n > 2$, and a large variety of poloidal harmonics were detected. A more detailed analysis of the DIII-D experimental results will be given in Chapter 6. A review of the theory of toroidicity-induced Alfvén eigenmodes will be presented in the next section.

The most threatening aspect of MHD mode excitation via energetic particle resonance is the hot particle losses during bursts. A realistic evaluation in an ignition experiment scenario has been proposed by Sigmar et al[10]. Provided that the fluctuation level of toroidicity-induced Alfvén modes is $\tilde{B}_r/B > 10^{-4}$, Sigmar et al. showed that the α particle loss rate can reach the value of $\nu_{loss} \sim 100s^{-1}$, overwhelming the α production rate of $\nu_{prod} \sim 60s^{-1}$. The TAEs mainly resonate with high energy alphas and only stop when $\beta_\alpha < \beta_{\alpha crit}$ is reached. Also, the dependence of the loss rate on initial α energy shows a decrease with decreasing α energy. Thus, the TAE seems to remove very efficiently only high energy alphas, leaving the Helium ash almost undisturbed.

Besides the resonant interaction destabilization of MHD modes, energetic particles may have beneficial effects on macroscopic plasma stability. During ICRF

heating and perpendicular neutral beam injection, sawtooth-free operation has been possible[11]. In both cases, a large population of trapped hot ions has been created. The proposed mechanism of the observed stabilization has been clearly presented by F. Porcelli[12]. The hot, trapped particles precess very rapidly in the toroidal direction generating a net current $J_{prec.}$. The flux enclosed by the correspondent current ring is a constant of the trapped particle motion provided $\omega << \omega_{Dh}$ (the magnetic drift frequency of the hot particles). A magnetic perturbation, such as an $n = m = 1$ kink mode that leads to an increase in the magnetic flux enclosed by the torus, causes the contraction of the current rings and consequent positive work is done against the fast particle pressure. The theory of sawtooth suppression was first presented by Coppi et al.[13] in the case of anisotropic energetic particle population. In this case, the sign of ω_{Dh} is constant and the effect of the energetic particles is always stabilizing. When isotropic alpha particles are considered, ω_{Dh} no longer has a unique sign and the overall effect can be destabilizing. An accurate numerical analysis in a finite β , finite aspect ratio configuration shows a stability threshold for the $m = 1$, $n = 1$ internal kink, lower than ideal MHD[16].

Stabilization of high-n ballooning modes by energetic particles was also proposed by Rosenbluth et al.[14] (1983). The stabilizing effect is similar to the one proposed for the $m = n = 1$ internal kink. Later, D. Spong et al.[15] showed that the high-frequency branch of the kinetic ballooning modes at $\omega \sim \omega_{Dh\alpha}$ can be destabilized by resonant interaction. From those results, it is clear that in a plasma, with an energetic ion component, two kinds of effects can be identified: 1) Destabilization of MHD modes via resonant interaction, and 2) Enhanced "rigidity" to $\tilde{\mathbf{E}} \times \mathbf{B}$ displacement when a significant fraction of fast particles is trapped.

2.1 Outline of the thesis

The linear theory of kinetically modified magnetohydrodynamics will be discussed in the course of this thesis. Great effort has been devoted to develop a general theory of low-n kinetic-MHD modes in tokamak plasmas. We shall be concerned with the excitation of global modes, i.e. modes whose structure is dominated by the Fourier components with low poloidal and toroidal wavenumbers (m, n).

In Chapter 2, we focus on real frequency Alfvén waves, which are modes with frequency in the range of the Alfvén frequency and that are stable in the frame of ideal MHD theory. In particular we study the effects of the noncircularity of the plasma column on the ideal Alfvén modes and we show that the ellipticity of the flux surfaces leads to frequency gaps in the Alfvén continuum spectrum. Within these gaps we discover the existence of discrete modes (Ellipticity Induced Alfvén Eigenmodes, EAE) having macroscopic structure and many common features with toroidally induced Alfvén eigenmodes (TAE). In particular both can be driven unstable by a small population of high energy particles. Since the ellipticity is larger than toroidicity in many tokamaks, the EAE is typically a more "global" mode than the TAE. The EAE results from the poloidal coupling induced by the ellipticity of the plasma cross section, and its eigenfuction is centered about the $q = (m + 1)/n$ surface, with m being the lowest poloidal harmonic.

In Chapter 3 a stability criterion is derived for energetic particle Alfvén modes. The criterion is valid for arbitrary aspect ratio, arbitrary β, noncircular, axisymmetric tori. The plasma is modeled by a magnetohydrodynamic core plus a fully kinetic Vlasov species of hot particles. The stabilizing bulk electron and ion kinetic effects are neglected. In spite of the complexity associated with the analysis of the Vlasov species, a simple but exact stability boundary is derived. The criterion is very fluidlike in nature, suggesting that accurate evaluation in realistic geometries can be accomplished with perhaps only minor modifications to any one of the existing ideal MHD stability codes.

In Chapter 4 the stability analysis is carried out for energetic particle-Alfvén gap modes in the small gyroradius approximation. The growth rate for the EAE and TAE is derived including the stabilizing effects of the ion and electron Landau damping. A general solution of the perturbed Vlasov equation valid for low-(m, n) numbers is also proposed. It is found that the electron Landau damping in highly elongated plasmas has a strong stabilizing influence on the $n = 1$ EAE, while the ion Landau damping on the sideband resonance stabilizes the $n = 1$ TAE in the high density regimes.

In Chapter 5 the effects of the kinetic response of trapped particles on the internal kink modes is examined. It is found that the main contribution arises from trapped particles (both ions and electrons) which precess in the toroidal direction with angular velocity $\omega_D(\varepsilon, \Lambda)$ where ε and Λ are the particle energy and pitch angle. For sufficiently high β_p, the high frequency branch of the internal kink ($\omega \simeq \omega_{*i}$) can be destabilized by the nonresonant trapped bulk ion response. The trapped electrons are found to have a stabilizing effect, but it is usually insufficient to stabilize the mode.

In Chapter 6 we analyze the experimental data on high frequency MHD activity during tangential neutral beam injection that are avalaible in the literature and we compare it with the theoretical predictions derived in this thesis. We find that in the DIII-D experiment there may be some evidence of the existence of the Ellipticity Induced Alfvén Eigenmodes.

CHAPTER 2:

Alfvén waves in Tokamaks

2.1 Introduction

In this chapter we investigate the properties of shear Alfvén waves in a tokamak plasma. These oscillations are polarized so that the perturbed magnetic field $\tilde{\mathbf{B}}$ and velocity $\tilde{v}$ are mainly perpendicular to the equilibrium field $\mathbf{B}_0$ and the wavevector $\mathbf{k}$; the wave is purely transverse causing the magnetic field lines to bend. The shear Alfvén wave describes a basic oscillation between plasma kinetic energy and magnetic field line tension. The plasma dynamics is almost perpendicular and produces no density fluctuations (incompressible motion). The spectral properties of shear Alfvén modes in toroidal plasma are quite distinctive and have been investigated by several authors[1,2]. Our analysis is carried out within the framework of the ideal MHD theory and is focused on modes with a nonvanishing real frequency. It is well known that such modes are always stable in ideal MHD. However, kinetic effects such as resonant interactions with energetic particles, can drive these modes unstable[3]. Normally resonant effects are so small that they can be treated perturbatively, implying that the lowest order eigenfunction is still the one given by the ideal MHD equations. A detailed analysis of shear Alfvén waves in an ideal tokamak plasma is therefore necessary.

2.2 Model

The basic equation describing Alfvén waves in a noncircular tokamak is derived from the standard MHD Lagrangian $\mathcal{L} \equiv \delta W - \omega^2 K$. In order to carry out the analysis, we introduce the ohmic tokamak aspect ratio expansion which assumes (1) the plasma minor radius a is small compared to the major radius R_0, i.e. $\epsilon = a/R_0 << 1$, (2) the plasma pressure is small compared to the magnetic field pressure $\beta = 2\mu_0 P/B^2 \sim \epsilon^2$ and (3) the poloidal magnetic field component is small compared to the toroidal component $B_\theta/B_\phi \sim \epsilon$. Furthermore, we assume that the current distribution is such that the safety factor $q(r) \simeq rB_\phi/RB_\theta$ is of order unity for $r < a$. In particular, for a low-β plasma in which $B_\phi \simeq$ constant over the plasma column, the variation of $q(r)$ is mainly related to the axial component of the current density $J_\parallel$,

$$J_\parallel \simeq J_0 \frac{1 - s/2}{q(r)/q_0}$$

where $q_0 = q(0)$, $s = rdlnq/dr$ and $J_0 = J_\parallel(0)$.

The derivation requires that $\mathcal{L}$ be calculated to third order in ϵ: $\mathcal{L} = \epsilon^2 \mathcal{L}_2 + \epsilon^3 \mathcal{L}_3 + \ldots$

The analysis begins with the following forms for the potential and kinetic energies,

$$\delta W = \frac{1}{2} \int d\mathbf{r} \Big[|\mathbf{Q}_\perp|^2 + B^2 \, |\nabla \cdot \boldsymbol{\xi}_\perp + 2 \, \boldsymbol{\xi}_\perp \cdot \boldsymbol{\kappa}|^2 + \gamma p \, |\nabla \cdot \boldsymbol{\xi}|^2$$

$$-2(\boldsymbol{\xi}_\perp \cdot \nabla p)(\boldsymbol{\kappa} \cdot \boldsymbol{\xi}_\perp^*) - \frac{J_\parallel}{B}(\boldsymbol{\xi}_\perp^* \times \mathbf{B}) \cdot \mathbf{Q}_\perp \Big] \tag{1}$$

$$K = \frac{1}{2} \int d\mathbf{r} \, \rho \, |\boldsymbol{\xi}|^2. \tag{2}$$

The modes of interest are low n number shear Alfvén waves characterized by $\omega^2 \sim k_\parallel^2 v_a^2$. Since $k_\parallel a \sim \epsilon$, we are required to order $\nabla \cdot \boldsymbol{\xi}_\perp \sim \epsilon \, \boldsymbol{\xi}_\perp / a$, or else the magnetic compression term would dominate the behavior. This implies that $\xi_\parallel \sim \epsilon^2 \xi_\perp$ from which it then follows that the plasma compressibility $\gamma p |\nabla \cdot \boldsymbol{\xi}|^2$, and the parallel

kinetic energy $\rho|\xi_{||}|^2$ both give rise to contributions in $\mathcal{L}$ of order ϵ^4. Thus, both terms can be neglected.

The first step in the derivation is to minimize the magnetic compressibility term order by order. The value of $\nabla \cdot \boldsymbol{\xi}_\perp$ correct to the required accuracy is found by noting that the curvature $\boldsymbol{\kappa} = -\mathbf{e}_R/R + O(\epsilon^2)/a$. This yields

$$\nabla \cdot \boldsymbol{\xi}_\perp \approx \frac{2\xi_R}{R}. \tag{3}$$

Equation (3) can be solved by introducing a stream function as follows

$$\boldsymbol{\xi}_p = R\nabla_p X \times \mathbf{e}_\phi \tag{4}$$

where $\boldsymbol{\xi}_p = (\xi_R, 0, \xi_Z)$ is the poloidal component of $\boldsymbol{\xi}_\perp$ and ∇_p is the poloidal gradient. The toroidal component ξ_ϕ is of order $\xi_\phi \sim \epsilon\xi_p$ and never enters the calculation, even when evaluating $\mathcal{L}$ to order ϵ^3. The entire analysis is now expressed in terms of the single scalar unknown $X = X(R,Z)\exp(-i\omega t - in\phi)$.

The remaining terms in δW and K can be evaluated in a straightforward manner. For the kinetic energy we obtain

$$\rho|\boldsymbol{\xi}_\perp|^2 = \rho R^2|\nabla_p X|^2. \tag{5}$$

The evaluation of δW requires the quantity $\mathbf{Q}_\perp$, which after a short calculation can be written as

$$\mathbf{Q}_\perp \equiv (\nabla \times \boldsymbol{\xi}_\perp \times \mathbf{B})_\perp = \frac{1}{F_0}\nabla[R^2\mathbf{B}\cdot\nabla X] \times \mathbf{B} \tag{6}$$

where $F(\psi) \equiv RB_\phi = F_0[1 + O(\epsilon^2)]$; that is $F_0 = R_0B_0 = \text{const}$. The quantity $J_{||}$ appearing in the kink term reduces to $J_{||} = J_\phi[1 + O(\epsilon^2)]$ in the aspect ratio expansion. Similarly $\boldsymbol{\kappa} \approx -\mathbf{e}_R/R$ is only needed to leading order in the curvature term.

Upon combining these results we obtain the following form of $\mathcal{L}$ correct up to and including terms of order ϵ^3

$$\mathcal{L} = \int d\mathbf{r}\Big[\frac{|\nabla_p V|^2}{R^2} - J_\phi \nabla_p V \cdot \nabla_p X^* \times \mathbf{e}_\phi + 2R^2 p'(\mathbf{B}_p \cdot \nabla_p X)\frac{\partial X^*}{\partial Z} - \omega^2\rho R^2|\nabla_p X|^2\Big]. \tag{7}$$

Here, $V = R^2\mathbf{B}\cdot\nabla X$, $p' = dp(\psi)/d\psi$, $\mathbf{B}_p = (\nabla\psi\times\mathbf{e}_\phi)/R$, and ψ is the equilibrium flux function satisfying the Grad-Shafranov equation. From Eq. (7) it is straightforward to calculate the variation of $\mathcal{L}$ with respect to X. Setting $\delta\mathcal{L} = 0$ leads to an Euler-Lagrange equation that can be expressed as

$$\mathbf{B}\cdot\nabla\left[\Delta^*(R^2\mathbf{B}\cdot\nabla X)\right] + \frac{1}{R}\nabla_p(RJ_\phi)\times\mathbf{e}_\phi\cdot\nabla_p(R^2\mathbf{B}\cdot\nabla X) \\ - 2R^2\frac{\partial}{\partial Z}(p'\mathbf{B}_p\cdot\nabla_p X) + \omega^2\nabla_p\cdot(\rho R^2\nabla_p X) = 0 \tag{8}$$

where $\Delta^* V \equiv R^2\nabla\cdot(\nabla V/R^2)$. Equation (8) is the desired form of the basic stability equation for Alfvén waves in a general noncircular geometry, consistent with the ohmic tokamak aspect ratio expansion.

2.3 The straight circular Tokamak

In order to simulate an axisymmetric toroidal equilibrium having a relatively large aspect ratio with minor radius a and major radius R_0, we take the length of the cylinder to be $2\pi R_0$ and an equilibrium magnetic field of the form

$$\mathbf{B} = B_\theta(r)\mathbf{e}_\theta + B_z(r)\mathbf{e}_z. \tag{9}$$

The equilibrium of such a system is given by the basic radial pressure balance relation

$$\frac{d}{dz}(p + \frac{{B_\theta}^2 + {B_z}^2}{2\mu_0}) + \frac{{B_\theta}^2}{\mu_0 r} = 0 \tag{10}$$

where p is the plasma pressure. In terms of the original Lagrangian formulation $\mathcal{L} = \epsilon^2\mathcal{L}_2 + \epsilon^3\mathcal{L}_3$, we neglect $\mathcal{L}_3$ and the effect of toroidicity. The Euler-Lagrange equation in the limit of a low-β straight tokamak reduces to

$$\mathbf{B}\cdot\nabla[\nabla_p^2(\mathbf{B}\cdot\nabla X)] + \mu_0\nabla_p J_\phi\times e_\phi\cdot\nabla_p(\mathbf{B}\cdot\nabla X) + \omega^2\nabla_p\cdot(\rho\nabla_p X) = 0. \tag{12}$$

We consider perturbations about the equilibrium of the form

$$X(r,t) = X(r)\exp[i(-k_z z + m\theta - \omega t)] \tag{13}$$

where m is the poloidal wavenumber and $k_z = n/R_0$ is the longitudinal component of the wavevector. In the cylindrical geometry each poloidal harmonic is decoupled. It is then straightforward to show that

$$\mathbf{B} \cdot \nabla = -iB_0 k_{||}$$

$$\nabla_p^2 = \nabla^2 \tag{13}$$

where $k_{||}$ is the component of the wavevector parallel to the equilibrium magnetic field

$$k_{||} = \frac{1}{R_0}(n - \frac{m}{q(r)})$$

and ∇^2 is the cylindrical operator

$$\nabla^2 = \frac{1}{r}\frac{\partial}{\partial r} r \frac{\partial}{\partial r} + \frac{1}{r^2}\frac{\partial^2}{\partial \theta^2}.$$

All the toroidal corrections of order ϵ have been neglected. From the equilibrium relations, it is easy to derive the following expression for the toroidal current

$$\mu_0 J_\phi = \frac{1}{r}\frac{d}{dr} r B_\theta. \tag{14}$$

Substituting in Eq. (12) yields the following equation for the mth harmonic

$$\frac{1}{r}\frac{d}{dr} r(\omega^2 \rho - k_{||m}^2 B_0^2)\frac{dX_m}{dr} - \frac{1}{r^2}\left[m^2(\omega^2\rho - k_{||m}^2 B_0^2) - r B_0^2 \frac{dk_{||m}^2}{dr}\right] X_m = 0 \tag{15}$$

A simplified version of this equation is obtained by introducing the new variable $\xi_m = X_m/r$. Eq. (15) then reduces to the well-known Alfvén wave equation in cylindrical geometry (assuming for simplicity that $\rho = const.$)

$$\frac{1}{r}\frac{d}{dr} r^3(\rho\omega^2 - k_{||}^2 B_0^2)\frac{d\xi_m}{dr} = g(r)\xi_m \tag{16}$$

where

$$g(r) \simeq (m^2 - 1)[\rho\omega^2 - k_{||}^2 B_0^2]. \tag{17}$$

A more detailed minimization of the MHD Lagrangian up to order ϵ^4 can be easily carried out in the cylindrical limit, leading to a more complete form[4] of g

$$g = (m^2 - 1)[\rho\omega^2 - k_{||}^2 B_0^2] + \rho k_z^2 B_\theta^2 [\frac{2\mu_0 r p'}{B_\theta^2} + (3q + 1)(q - 1)] \tag{18}$$

where the second term on the RHS of Eq. (18) is of order ϵ^4. In Sec. (2.5) we show how the terms of order ϵ^4 are important in the theory of global type shear Alfvén waves. We start analyzing the lowest order solution, and therefore keep only terms of order ϵ^2. Focusing on Eq. (16), we note that for an arbitrary eigenvalue ω, such that $\omega_{Amin}^2 < \omega^2 < \omega_{Amax}^2$, one can find a corresponding eigenfuction ξ_m which has a logarithmic singularity at the point r_0 where $k_{||}^2(r_0)v_A^2(r_0) = \omega^2$. Such modes define the Alfvén continuum spectrum. The frequency spectrum is simply given by

$$\omega^2 = (n - \frac{m}{q(r)})^2 (\frac{v_A}{R_0})^2 \tag{19}$$

and it is plotted in Fig.1 for $n = 1$ and different poloidal mode numbers m. It is important to note that in cylindrical geometry two modes with different m's (m' and m) and equal n can be singular at the same location r_0 where $k_{||m}(r_0) = -k_{||m'}(r_0)$. When coupling between different poloidal harmonics is introduced, this degeneracy is removed and frequency gaps are generated.

2.4 The eigenfunction and the damping rate of the continuum spectrum

The solution of the eigenmode equation for shear Alfvén waves in the continuum demonstrates very interesting properties in the neighborhood of the magnetic surface where the local Alfvén frequency ω_A equals the wave frequency ω. A clear treatment of the eigenvalue problem can be found in Ref.[5] and Ref.[15] where the propagation of Alfvén waves in the heliosphere has been investigated. However, the reader should be aware that the results presented here do not agree with those derived in Ref.[5]. The discrepancy is resolved shortly.

Let us focus on Alfvén waves in cylindrical geometry. The eigenvalue equation, derived in the previous section Eq. (16), is repeated here for convenience.

$$\frac{1}{r}\frac{d}{dr}r^3(\rho\omega^2 - k_\parallel^2 B_0^2)\frac{d\xi}{dr} = (m^2-1)[\rho\omega^2 - k_\parallel^2 B_0^2]\xi. \tag{20}$$

The solution must satisfy appropriate boundary conditions such as $\xi(0) = \xi(a) = 0$ for $m > 1$ and $\xi(r \simeq 0) = \xi_0[1 + const.r^2]$, $\xi(a) = 0$ for $m = 1$. Multiplying both sides of Eq. (20) by ξ^* and integrating over the plasma volume, it is easily shown that $\omega_{Amin}^2 < \omega^2 < \omega_{Amax}^2$. Therefore, a point r_0 has to exist where $\omega^2 = \omega_A^2(r_0)$ has to exist within the plasma column. At that point Eq. (20) becomes singular and the ideal MHD model breaks down. As pointed out in Ref.[5], in the neighborhood of r_0, the dissipative processes become important. The properties of the Alfvén singularity are similar to those of shock waves where the jump of physical quantities is independent of the magnitude of the viscous dissipation in the limit of small viscosity. It is shown later that the damping rate of Alfvén waves is independent of the dissipation. A different conclusion holds for the case of an energy source located in the singular layer. In this case, the growth rate is proportional to the instability driving mechanism. The solution of Eq.(20) in the neighborhood of the singular point is, therefore, of crucial importance. Before proceeding to the solution of the eigenvalue problem, we invoke the validity of the causality condition and consider modes that vanish for $t \to -\infty$, i.e. $\omega_i > 0$. This is also the requirement for the integrability of the Laplace transform.

For $r \to r_0$ Eq. (20) can be written in the following form

$$\frac{d}{d\hat{x}}(i\hat{x} + \hat{\gamma})\frac{d\xi}{d\hat{x}} = 0 \tag{21}$$

where

$$\hat{\gamma} = 2\omega_i/|\omega_r| \tag{22}$$

and

$$\hat{x} = sgn(\omega_r \frac{d\ln\omega_A^2}{dr})\left|\frac{d\ln\omega_A^2}{dr}\right|_{r=r_0}(r - r_0). \tag{23}$$

It is important to choose the appropriate normalized variables. In fact we note that the choice of normalized variables has to lead to a solution which satisfies the causality condition $\omega_i > 0$. In order to clarify this point, we integrate Eq. (21), and obtain

$$\xi = A + B\ln(i\hat{x} + \hat{\gamma}) = \tag{24}$$

$$A + B[\ln(\hat{x}^2 + \hat{\gamma}^2)^{1/2} + i\arctan(\frac{\hat{x}}{\hat{\gamma}}) + i\pi sgn(\hat{x})\Theta(-\hat{\gamma})]$$

where Θ is the step function and the standard definition of the logarithm of a complex quantity with the branch cut along the $\hat{\gamma} < 0$ axis has been used. Notice that this solution is identical to the one obtained in Ref.[5], except for the definition of the normalized variables. The solution given in Eq. (24), which is valid in the limit of $\hat{x} \to 0$, is defined in the whole $(\hat{x}, \hat{\gamma})$ plane except the $(\hat{x} = 0, \hat{\gamma} < 0)$ semiaxis, which is in agreement with the causality condition that requires ω_i to be positive. We conclude that $\hat{\gamma}$ must be chosen with the condition that ω_i and $\hat{\gamma}$ have the same sign. Any other choice leads to a stable and non-physical unstable root depending on the sign of $\hat{\gamma}/\omega_i$. The solution given in Eq. (24) is a continuous function for growing modes and presents a discountinuity at $x = 0$ for $\hat{\gamma} < 0$. We first focus our attention on growing modes; and starting from Eq(20), we construct a quadratic form by multipying Eq. (20) by ξ^* and integrating over the plasma volume. Since the eigenfunction is continuous, we integrate by parts and obtain the following relation

$$\int dr\rho[\omega^2 - \omega_A^2(r)]r\{|\frac{d\xi}{dr}|^2 r^2 + (m^2 - 1)|\xi|^2\} = 0 \tag{25}$$

The imaginary part of Eq. (25) leads to $\omega_i = 0$. We conclude that growing solutions are not allowed for shear Alfvén waves in the framework of ideal MHD.

A different picture emerges in the case of damped modes. A discrepancy arises when $\hat{\gamma} < 0$, because negative values of ω_i violate the causality condition. Note first that taking the limit $\hat{\gamma} \to 0_+^-$ in Eq. (24) leads to the same solution

$$\xi(\gamma \to 0_+^-) = A + B\ln|\hat{x}| + i\frac{\pi}{2}Bsgn(\hat{x}). \tag{26}$$

The conclusion is that ξ is continuous for $\hat{\gamma} = 0$, and we can thus "continue" the singular solution to values of $\hat{\gamma} < 0$. This procedure is equivalent to the analytic continuation in the domain $\hat{\gamma} < 0$ of the Landau integral. In the present case, the eigenfunction is discontinuous in $\hat{x}$ and the integration by parts used in the derivation of the quadratic form Eq. (25), must be performed separately in the regions $0 < r < r_0^-$ and $r_0^+ < r < a$. The quadratic form for $\hat{\gamma} < 0$ can then be written as

$$P\int_0^a \rho(\omega^2 - \omega_A^2(r))r\left[\left|\frac{d\xi}{dr}\right|^2 r^2 + (m^2-1)|\xi|^2\right]dr = \rho r_0^3(\omega^2 - \omega_A^2(r))\xi^* \frac{d\xi}{dr}\Big|_{r_0^-}^{r_0^+} \quad (27)$$

where $P\int_0^a = \int_0^{r_0^-} + \int_{r_0^+}^a$ is the principal value of the integral. Eq. (27) reproduces the result of Ref.[5] in the case of slab geometry. Observe that the function $(\omega^2 - \omega_A^2(r))d\xi/dr$ is continuous across the singular point r_0 and, therefore, the jump in the RHS of Eq. (27) is due only to the term ξ^*. By considering the imaginary part of Eq. (27), we obtain

$$\omega_i P\int_0^a \rho r\left[\left|\frac{d\xi}{dr}\right|^2 r^2 + (m^2-1)|\xi|\right]dr = -2\pi\rho_0|B|^2 r_0^3\left|\frac{d\omega_A}{dr}\right|_{r_0} \quad (28)$$

This result was also obtained in Ref[5]. However according to our analysis another step is necessary to find ω_i since the ratio of A to B is unknown. We decompose the eigenfunction in a singular part (ξ_s) given by the logarithmic term in Eq. (24) and a regular part

$$\xi_r = \xi - \xi_s. \quad (29)$$

ξ_r has no singularity in the domain $0 < r < a$. We then assume that the amplitude of the singular solution is small compared to the regular part. Following the definition of ξ_s given in Eq. (24), and assuming $\log(-\hat{\gamma}) \sim 1$, we order $|\xi_s/\xi_r| \sim \hat{\gamma}^{1/2} << 1$. To justify this ordering, we recall that the energy dissipated in the singular layer depends on the magnitude of the electric field. Furthermore, the assumption of small damping requires the dissipation to be small. Since the poloidal electric field in the layer is proportional to $d\xi_s/dr$, with $a(\partial/\partial r) >> 1$, a small dissipation requires $|\xi_s|/|\xi_r| << 1$.

Next , we substitute Eq. (29) into Eq. (28) and use the definition of ξ_s to show that the LHS of Eq. (28) evaluated in the region about $r \simeq r_0$ yields an important contribution independent of ω_i

$$\omega_i P \int_0^a \rho r \left[\left| \frac{d\xi}{dr} \right|^2 r^2 + (m^2 - 1)|\xi|^2 \right] dr = \tag{30}$$

$$\omega_i \int_0^a \rho r \left[\left| \frac{d\xi_r}{dr} \right|^2 r^2 + (m^2 - 1)|\xi_r|^2 \right] dr - \pi r_0^3 \rho_0 |B|^2 \left| \frac{d\omega_A}{dr} \right|_{r_0}$$

The damping rate of the mode easily follows

$$\omega_i = -\pi \frac{\rho_0 r_0^3 |B|^2}{\int_0^a \rho r \left[\left| \frac{d\xi_r}{dr} \right|^2 r^2 + (m^2 - 1)|\xi_r|^2 \right] dr} \left| \frac{d\omega_A}{dr} \right|. \tag{31}$$

Notice that the ordering previously assumed is indeed satisfied. The expression of ω_i given in Eq. (31) differs from the one derived in Ref[5] by a factor 2. Eq. (31) gives the damping rate as function of the regular part of the eigenfunction and the factor B. In Appendix C, we derive an expression for B as a function of the regular part of the eigenfunction and we suggest an easy way to compute it. It is important to note that there is no small parameter in the problem and therefore the assumption of small B can be derived only a posteriori. From Eq. (C.13) in Appendix C it follows that for an Alfvén wave of the continuum spectrum, the assumption is true only when the following condition is satisfied

$$\left| r_0 \frac{d \ln \omega_A^2}{dr_0} \right| >> 1$$

This condition requires equilibrium configurations with large density or magnetic field gradients or steep q profiles.

2.5 The Global Alfvén Eigenmode

In this section we show that when the function $\omega_A^2(r)$ has a minimum located within the plasma column, a global mode exists whose frequency lies below the minimum of the Alfvén continuum spectrum. The properties of these global modes (Global Alfvén Eigenmodes) have been exensively investigated in connection with Alfvén wave heating . During heating experiments in the Lausanne tokamak, a large plasma impedance is observed at a specific frequency that has been identified as the frequency of a GAE mode. In this section we focus our attention on the $n = 1$, $m = 1$ cylindrical GAE, and we refer the reader to Ref.[6] for the treatment of higher (n,m) modes. We emphasize that the GAE exists in a straight cylinder, and thus does not require toroidicity.

We start with Eq. (16) which is valid for arbitrary m, and note that the function $g(r)$ vanishes to lowest order when $m = 1$. It follows that the correction of order ϵ^4 given in Eq. (18) must then be retained. We rewrite the Alfvén wave equation for $m = 1$ in the following way

$$\frac{1}{r}\frac{d}{dr}r^3(\rho\omega^2 - k_\parallel^2 B_0^2)\frac{d\xi_m}{dr} = g_1(r)\xi_m \tag{32}$$

where

$$g_1 = \rho k_z^2 B_\theta^2[\frac{2\mu_0 r p'}{B_\theta^2} + (3q+1)(q-1)] \tag{33}$$

The appropriate boundary condition for ξ near the magnetic axis is

$$\xi(r \to 0) = \bar{\xi}[1 + const \cdot r^2] \tag{34}$$

where $\bar{\xi} = \xi(0)$. We are interested in an "internal" disturbance that does not displace the plasma boundary. Hence, we also require that $\xi(a) = 0$. The derivation of the eigensolution presented in this section is very similar to that of the ideal kink mode. Focusing on modes with frequency $\omega^2 \approx \omega_{Amin}^2(r_0)$, we consider first the "outer" region away from $r = r_0$, the radius where the Alfvén frequency assumes

its minimum value (see Fig.2). The solutions for ξ and ω^2 are expanded in powers of ϵ^2, $\xi = \xi_0 + \xi_1 + \ldots$, $\omega^2 = \omega_A^2(r_0) + \omega_1^2 + \ldots$. To leading order ξ_0 is given by

$$\xi_0(r) = \bar{\xi}\Theta(r_0 - r) \tag{35}$$

where Θ is the step function. Eq. (35) is one of the two independent solutions of Eq. (32) in the outer region. The other solution can be written as

$$\xi_0(r < r_0) = C_0^- \int_0^r \frac{dr}{\rho r^3(\omega^2 - \omega_A^2)}$$

$$\xi_0(r > r_0) = C_0^+ \int_r^a \frac{dr}{\rho r^3(\omega^2 - \omega_A^2)}$$

where C_0^- and C_0^+ are two integration constants. It is readely seen that $C_0^- = 0$ for the regularity of the solution at $r = 0$ and that $\xi_0(r > r_0)$ can never match the solution in the inner layer [Eq. (43)] that is derived in the following of this section. Thus, $C_0^- = C_0^+ = 0$.

To next order,

$$\xi_1 = \bar{\xi}\int_0^r dr' \frac{\int_0^{r'}(r'' g_1(r''))dr''\Theta(r_0 - r'')}{\rho(r')r'^3(\omega^2 - \omega_A^2(r'))} \tag{36}$$

and, in the neighborhood of r_0, the solution exhibits the following behaviour

$$\frac{1}{\bar{\xi}}\frac{d\xi_1}{dr} \simeq -\frac{\Sigma_H r_0}{\pi(r - r_0)^2} \tag{37}$$

where

$$\Sigma_H = \frac{\pi\int_0^{r_0} r g_1(r)dr}{\rho(r_0)r_0{}^2(\frac{d^2\omega_A^2}{dr_0{}^2})} \sim \epsilon^2. \tag{38}$$

Notice that since r_0 correspond to a minimum in ω_A^2, then $d^2\omega_A^2/dr_0^2 > 0$. It thus follows that $\Sigma_H \propto \lambda_H$, where λ_H is the internal kink stability parameter.

In this section we consider an MHD stable plasma, and therefore positive Σ_H, i.e. $\lambda_H < 0$. In the region about the point of minimum, $(r - r_0)/r_0 \sim \epsilon^2$, even small corrections to the eigenvalue play an important role. We define accordingly a new eigenvalue Ω as follows

$$\omega^2 = \omega_A^2(r_0) - \Omega^2 \tag{38}$$

with $\Omega/\omega_A \sim \epsilon^2$. This leads to a normal mode equation in the inner region

$$\frac{d}{d\hat{x}}(\hat{x}^2 + \hat{\Omega}^2)\frac{d\xi}{d\hat{x}} = 0 \tag{39}$$

where we have introduced the normalized quantities

$$\hat{x} = \frac{r - r_0}{r_0} \sim \epsilon^2$$

$$\hat{\Omega}^2 = \frac{\Omega^2}{r_0^2}\left(\frac{d^2\omega_A^2}{dr_0^2}\right)^{-1} \sim \epsilon^4. \tag{40}$$

Eq. (39) must be supplemented by appropriate boundary conditions provided by the outer solution in the limit $r \to r_0$

$$\xi_{in}(\hat{x} \to \infty) \to \xi_{out}(\hat{x} \to 0)\big|_{r \simeq r_0} \tag{41}$$

where

$$\xi_{out}(\hat{x} \to \infty)\big|_{r \simeq r_0} = \xi_0\left[\Theta(-\hat{x}) + \frac{\Sigma_H}{\pi\hat{x}} + \ldots\right].$$

The inner layer equation can be easily solved, yielding

$$\xi_{in} = C_0 + C_1 \arctan\left(\frac{\hat{x}}{\hat{\Omega}}\right) \tag{42}$$

where C_0 and C_1 are two free integration constants. It is straightforward to show that matching the inner and outer solution according to Eq. (41) leads to the eigenfuction

$$\xi = \frac{1}{2}\left[1 - \frac{2}{\pi}\arctan\left(\frac{x}{\Sigma_H}\right)\right] \tag{43}$$

and the eigenvalue condition

$$\hat{\Omega}^2 = \Sigma_H^2 \tag{44}$$

or alternatively

$$\omega^2 = \omega_{Amin}^2 - \Sigma_H^2 r_0^2 \frac{d^2\omega_A^2}{dr_0^2}. \tag{45}$$

Notice that for $\Sigma_H < 0$, the profile of the radial displacement turns in the "wrong" direction when approaching the singular layer from the outer region so that no regular eigenfunction can be constructed for negative values of Σ_H. We can refer to $\Sigma_H > 0$ as the condition for the existence of a global Alfvén eigenmode with $m = 1$. This leads to a mode frequency below the minimum of the continuum spectrum. Since $\Sigma_H \propto -\lambda_H$, the condition $\Sigma_H > 0$ guarantees that the $m = 1$ GAE is indeed a stable mode in the framework of the ideal MHD theory.

2.6 The Ellipticity Induced Alfvén Eigenmode

A The eigenvalue equation

The primary aim of this section is the investigation of global modes induced by the noncircularity of the plasma cross section. In many tokamaks the elongation is finite ($\kappa = 1.8$) and thus represents a very strong source of poloidal symmetry breaking. The main effect is the coupling of different poloidal harmonics that leads to frequency gaps in the Alfvén continuum spectrum and to discrete global modes whose frequency lies within each gap. The analysis of these modes, as described by Eq. (8), is significantly simplified by introducing a subsidiary expansion in which the ellipticity is assumed small, although not as small as toroidicity. Specifically, we focus attention on elongation and order κ as follows

$$\kappa - 1 \sim \epsilon^{1/2}. \tag{46}$$

This ordering reduces Eq. (8) to its noncircular, infinite aspect ratio form where all toroidal effects are ignored. (However, the toroidal expansion must be maintained when calculating resonant particle growth rates.) In terms of the original Lagrangian formulation $\mathcal{L} = \epsilon^2\mathcal{L}_2 + \epsilon^3\mathcal{L}_3$, the subsidiary expansion neglects $\mathcal{L}_3$ and assumes $\epsilon^2\mathcal{L}_2$ can be rewritten as $\epsilon^2\mathcal{L}_2 = \epsilon^2(\mathcal{L}_{20} + \epsilon^{1/2}\mathcal{L}_{21}\ldots)$. Equivalently, Eq. (8) neglecting toroidicity but including the full $\mathcal{L}_2$, reduces to Eq. (12), rewritten here for convinience

$$\mathbf{B}\cdot\nabla[\nabla_p^2(\mathbf{B}\cdot\nabla X)] + \nabla_p J_\phi \times e_\phi \cdot \nabla_p(\mathbf{B}\cdot\nabla X) + \omega^2\nabla_p\cdot(\rho\nabla_p X) = 0. \tag{47}$$

This equation is similar to that derived in Ref. [7] whose main concern is kink instabilities in elliptical plasmas.

The subsidiary expansion can be conveniently substituted into Eq. (47) by introducing a set of normalized flux coordinates as follows. The equilibrium flux function, satisfying the Grad-Shafranov equation, is written as $\psi = \psi_0(r) + \psi_1(r)\cos 2\theta$

where $\psi_1/\psi_0 \sim \epsilon^{1/2}$ and (r,θ) are the usual toroidal coordinates $R = R_0 + r\cos\theta, Z = r\sin\theta$. The flux coordinates (r',θ') are defined by

$$r' = r - \Delta(r)\cos 2\theta$$

$$\theta' = \theta + \frac{\Delta(r)}{r}\sin 2\theta \tag{48}$$

where $\Delta(r) \equiv -\psi_1/\psi_0' \sim \epsilon^{1/2}a$. It is important to recognize that in the new coordinate system, ψ is a function only of r'. The elliptical distortion Δ can be easily shown[8] to satisfy the perturbed Grad-Shafranov equation given by

$$\frac{d}{dr}\left(rB_{\theta 0}^2\frac{d\Delta}{dr}\right) - 3\frac{B_{\theta 0}^2}{r}\Delta = 0$$

$$\Delta(0) = 0, \quad \Delta(a) = -a(\kappa - 1)/2. \tag{49}$$

Here $B_{\theta 0}(r)$ is the zeroth order poloidal magnetic field, which is assumed to be specified as a free function. We shall assume that Eq. (49) has been solved either analytically or numerically and thus $\Delta(r)$ is hereafter treated as a known quantity.

From Eq. (48), it is straightforward to show that

$$\mathbf{B}\cdot\nabla = -iB_0k_{\|} - B_\theta\frac{d}{dr'}\left(\frac{\Delta}{r'}\right)\cos 2\theta'\frac{\partial}{\partial\theta'} \tag{50}$$

where $k_{\|}$ is the operator

$$k_{\|} = \frac{1}{R_0}(n + \frac{i}{q}\frac{\partial}{\partial\theta'}) \tag{51}$$

$q(r') = r'B_0/R_0B_\theta$ is the safety factor and for convenience the zero subscript is suppressed from $B_\theta(r') \equiv -\psi'(r')/R_0$. Similarly, the ∇^2 operator can be written as

$$\nabla^2 = \frac{1}{r'}\frac{\partial}{\partial r'}r'\frac{\partial}{\partial r'} + \frac{1}{r'^2}\frac{\partial^2}{\partial\theta'^2} - 2\frac{d\Delta}{dr'}\cos 2\theta'\frac{\partial^2}{\partial r'^2}. \tag{52}$$

The last terms in Eqs. (50) and (52) represent the $\epsilon^{1/2}$ corrections. Actually, in Eq. (52) there are additional $\epsilon^{1/2}$ terms involving first and zeroth order derivatives with respect to r'. In analogy with previous analysis of gap modes we anticipate that the $\epsilon^{1/2}$ corrections are only going to be important in a narrow region of physical

space corresponding to the frequency gap. Thus, it suffices to maintain only the highest derivative $\partial^2/\partial r'^2$ terms in the corrections to ∇^2. In contrast, the operator $\mathbf{B}\cdot\nabla$ has no radial derivative terms because of the introduction of flux coordinates.

The subsidiary expansion and the flux coordinates are now substituted into Eq. (47). After a short calculation we obtain

$$(L_0 + L_1)X = 0 \tag{53}$$

where the operators L_0 and L_1 have the form

$$L_0 X \equiv \omega^2 \nabla_0 \cdot (\rho \nabla_0 X) - B_0^2 k_{\|} (\nabla_0^2 k_{\|} X) + \frac{iB_0}{r}\frac{dJ}{dr} k_{\|} \frac{\partial X}{\partial \theta} \tag{54}$$

$$L_1 X \equiv -2\omega^2 \rho \frac{d\Delta}{dr} \cos 2\theta \frac{\partial^2 X}{\partial r^2} + 2B_0^2 \frac{d\Delta}{dr} k_{\|} \left(\cos 2\theta \; k_{\|} \frac{\partial^2 X}{\partial r^2} \right)$$

$$+ iB_0 B_\theta \frac{d}{dr}\left(\frac{\Delta}{r}\right) \left[\cos 2\theta \; k_{\|} \frac{\partial}{\partial \theta}\frac{\partial^2 X}{\partial r^2} + k_{\|} \left(\cos 2\theta \frac{\partial}{\partial \theta}\frac{\partial^2 X}{\partial r^2} \right) \right]. \tag{55}$$

In these expressions the primes have been suppressed from (r', θ') and

$$\begin{aligned} J &= \frac{1}{r}\frac{d}{dr} r B_\theta \\ \nabla_0^2 &= \frac{1}{r}\frac{\partial}{\partial r} r \frac{\partial}{\partial r} + \frac{1}{r^2}\frac{\partial^2}{\partial \theta^2}. \end{aligned} \tag{56}$$

Equation (53) can be solved by Fourier analyzing X in the angle θ:

$$X(r, \theta) = \sum_{\ell} X_p(r) e^{ip\theta}. \tag{57}$$

Here, $p = m + 2\ell$, m is the fundamental mode number, and the different ℓ harmonics represent the coupling due to noncircularity. Substituting into Eq. (53) yields the following equation for the p'th harmonic

$$D_p X_p + D_{p+2} X_{p+2} + D_{p-2} X_{p-2} = 0 \tag{58}$$

where the D operators have the form

$$D_p \equiv \frac{1}{r}\frac{d}{dr}r(\omega^2\rho - k_p^2 B_0^2)\frac{d}{dr} - \frac{1}{r^2}\left[p^2(\omega^2\rho - k_p^2 B_0^2) - rB_0^2\frac{dk_p^2}{dr}\right] \tag{59}$$

$$D_{p+2} \equiv -\left[(\omega^2\rho - k_p k_{p+2}B_0^2)\frac{d\Delta}{dr} + \frac{1}{2}(p+2)rB_0B_\theta(k_p + k_{p+2})\frac{d}{dr}\left(\frac{\Delta}{r}\right)\right]\frac{d^2}{dr^2}$$

$$D_{p-2} \equiv -\left[(\omega^2\rho - k_p k_{p-2}B_0^2)\frac{d\Delta}{dr} + \frac{1}{2}(p-2)rB_0B_\theta(k_p + k_{p-2})\frac{d}{dr}\left(\frac{\Delta}{r}\right)\right]\frac{d^2}{dr^2}$$

and $k_p = (1/R_0)(n - p/q)$.

Note that D_{p-2}, D_{p+2} are small by order $\epsilon^{1/2}$ compared to D_p. Thus, over most of the cross section the $D_{p\pm2}$ terms can be neglected. However, if these terms are neglected everywhere, then whenever $\omega^2\rho = k_p^2 B_0^2$ the coefficient of the highest derivative in D_p vanishes and $(D_p)^{-1}$ does not exist; that is, there are no discrete modes, only a continuum.

The regions where coupling is most important can be found by plotting curves of $k_p R_0$ vs q for various ℓ as shown in Fig. 3 (dashed curves) for the case $n = 1, m = 1$. Observe that the $\ell = 0$ and $\ell = 2$ curves intersect at the $q = 2$ surface where $k_1(q = 2) = -k_3(q = 2) = 1/2R_0$. For arbitrary m, n strong coupling occurs when $q_0 = (m+1)/n, k_m = -k_{m+2} = 1/q_0R_0$, and $\omega_0 = v_a(r_0)/q_0R_0$.

Consider now a mode with X_m, X_{m+2} as the two dominant harmonics and neglect all others. In the potentially singular region near $q = q_0$, the terms with the highest derivatives for the m and $m+2$ harmonics are given by

$$\begin{aligned}(\omega^2\rho - k_m^2 B_0^2)\frac{d^2X_m}{dr^2} - 2\omega^2\rho\frac{d\Delta}{dr}\frac{d^2X_{m+2}}{dr^2} + \ldots = 0 \\ (\omega^2\rho - k_{m+2}^2 B_0^2)\frac{d^2X_{m+2}}{dr^2} - 2\omega^2\rho\frac{d\Delta}{dr}\frac{d^2X_m}{dr^2} + \ldots = 0\end{aligned} \tag{60}$$

If the determinant of these terms vanishes for any value of r, the equations cannot be inverted and no discrete modes are possible. The frequencies for which the determinant vanishes are given by

$$\omega^2(r) = \frac{v_a^2}{2(1 - 4\Delta'^2)}\left\{k_m^2 + k_{m+2}^2 \pm \left[(k_m^2 - k_{m+2}^2)^2 + 16\Delta'^2 k_m^2 k_{m+2}^2\right]^{1/2}\right\}$$

(61)

$$\approx \frac{v_a^2}{q^2 R_0^2}\left\{1 \pm 2\left[(m+1)^2(1-\frac{q_0}{q})^2 + \Delta'^2\right]^{1/2}\right\}$$

where the second form is obtained by explicitly expanding about the $q = q_0$ surface. Observe that as r varies between $0 < r < a$, there is a narrow band of frequencies centered about $\omega = v_a/qR_0, q = q_0$, for which the determinant *does not* vanish. This is the frequency "gap" shown as the solid curve in Fig. 3. Its boundaries are determined by setting $q = q_0$, corresponding to the throat of the gap.

$$\frac{v_a}{q_0 R_0}(1 - |\Delta'|) < \omega < \frac{v_a}{q_0 R_0}(1 + |\Delta'|). \tag{62}$$

Within this range, the determinant does not vanish, and the differential operators in Eq. (60) can be inverted. Thus, if a discrete mode does exist, its frequency must satisfy Eq. (62). To determine the actual existence of such a mode, it is necessary to solve the full equations over the entire plasma $0 < r < a$. In this connection, note from Fig. 3 that for typical tokamaks satisfying $1 < q(r) < 3$, the frequency ω_0 does not intersect the $m = 1, m = 3$ or any $m = 1 + 2\ell$ continuum at any value of $r \leq a$. Thus continuum damping which has been shown to be important for the TAE is not expected to be so for the EAE.

A simplified form of the full equations is obtained by assuming the mode consists primarily of the X_m and X_{m+2} harmonics, and evaluating the small operators $D_{p\pm2}$ at r_0 corresponding to the $q = q_0$ surface. For simplicity the density $\rho(r)$ is assumed constant: $\rho = \rho_0$. It is also convenient to introduce new variables ξ_m and ξ_{m+2} defined by $X_m = r\xi_m, X_{m+2} = r\xi_{m+2}$. Equation (58) for the $(m, m+2)$ harmonics reduces to

$$D_m \xi_m + F\xi_{m+2} = 0 \tag{63a}$$

$$D_{m+2}\xi_{m+2} + F\xi_m = 0. \tag{63b}$$

The operator D_p is given by

$$D_p \equiv \frac{1}{r}\frac{d}{dr} r^3(\omega^2\rho_0 - k_p^2 B_0^2)\frac{d}{dr} - (p^2-1)(\omega^2\rho_0 - k_p^2 B_0^2). \tag{64}$$

The operator F is slightly subtle. Straightforward substitution yields

$$F\xi_p = -2\omega^2\rho_0\Delta'(r_0)(r^2\xi_p')'. \tag{65}$$

However, under our previous assumption that the correction terms are only important in a narrow layer where the highest derivatives dominate, we maintain consistency by writing

$$F\xi_p \approx -2\omega_0^2\rho_0\Delta'(r_0)r_0^2\xi_p''. \tag{66}$$

The errors made by this approximation are of the same order as those already neglected in the derivation of the $D_{p\pm2}$ operators.

Equations (63)-(66) describe gap modes in weak noncircular geometries.

B Asymptotic Matching Solutions

The gap mode equations can be solved by a standard asymptotic matching procedure. The analysis is similar but more general than that originally given by the Princeton group.[2]

The first step is to simplify Eq. (63) in the layer region. We introduce normalized quantities

$$\begin{aligned} x &= \frac{r - r_0}{r_0} \\ \omega^2 &= \omega_0^2(1 + 2\Omega) \end{aligned} \tag{67}$$

where r_0 is the layer radius and Ω is the new eigenvalue. Under our previous ordering assumptions $\Omega \ll 1$ and $x \ll 1$. It then follows that in the vicinity of the layer

$$\begin{aligned} \frac{1}{q} &\approx \frac{1}{q_0}(1 - sx) \\ k_m^2 &\approx \frac{1}{R_0^2 q_0^2}(1 + 2msx) \\ k_{m+2}^2 &\approx \frac{1}{R_0^2 q_0^2}\left[1 - 2(m+2)sx\right]. \end{aligned} \tag{68}$$

Here, $s = r_0 q'(r_0)/q(r_0)$ is the shear at the layer. Equation (63) reduces to

$$\begin{aligned} \frac{d}{dx}(\Omega - msx)\frac{d\xi_m}{dx} - \Delta_0' \frac{d^2\xi_p}{dx^2} = 0 \\ \frac{d}{dx}(\Omega + psx)\frac{d\xi_p}{dx} - \Delta_0' \frac{d^2\xi_m}{dx^2} = 0. \end{aligned} \tag{69}$$

In these equations $p = m + 2$ and $\Delta_0' \equiv d\Delta(r_0)/dr_0$ is dimensionless.

Equation (69) can be easily solved, yielding

$$\begin{aligned} \xi_m &= \frac{1}{m^{1/2}}\left[\frac{C_p + \lambda C_m}{(1-\lambda^2)^{1/2}}\alpha - C_m \ln\cos\alpha + A_m\right] \\ \xi_p &= \frac{1}{p^{1/2}}\left[\frac{C_m + \lambda C_p}{(1-\lambda^2)^{1/2}}\alpha + C_p \ln\cos\alpha + A_p\right] \end{aligned} \tag{70}$$

where A_m, A_p, C_m, C_p are four free integration constants,

$$\lambda = \frac{m+1}{(mp)^{1/2}}\frac{\Omega}{\Delta_0'} \tag{71}$$

is a new form of the normalized eigenvalue Ω, and

$$x = \frac{\Delta_0'}{s(mp)^{1/2}}\left[\frac{\lambda}{m+1} + (1-\lambda^2)^{1/2}\tan\alpha\right] \tag{72}$$

defines the new independent variable α. Equation (70) represents the desired solution in the layer region.

The second step in the analysis is to solve for the solutions in the exterior regions, which satisfy

$$\begin{aligned} \frac{1}{r}\frac{d}{dr}r^3 f_m \frac{d\hat{\xi}_m}{dr} - (m^2-1) f_m \hat{\xi}_m = 0 \\ \frac{1}{r}\frac{d}{dr}r^3 f_p \frac{d\hat{\xi}_p}{dr} - (p^2-1) f_p \hat{\xi}_p = 0 \end{aligned} \tag{73}$$

where $f_m = \omega_0^2\rho_0 - k_m^2 B_0^2$, $f_p = \omega_0^2\rho_0 - k_p^2 B_0^2$ and the $\hat{}$ denotes exterior region. Near the layer, these equations reduce to

$$\frac{d}{dx}x\frac{d\hat{\xi}_m}{dx} = 0$$
$$\frac{d}{dx}x\frac{d\hat{\xi}_p}{dx} = 0. \tag{74}$$

The solutions to Eq. (74) are given by

$$\hat{\xi}_m^+ = K_m^+\left[\frac{1}{2}\ln x^2 + b_m^+\right] \qquad \hat{\xi}_m^- = K_m^-\left[\frac{1}{2}\ln x^2 + b_m^-\right]$$
$$\hat{\xi}_p^+ = K_p^+\left[\frac{1}{2}\ln x^2 + b_p^+\right] \qquad \hat{\xi}_p^- = K_p^-\left[\frac{1}{2}\ln x^2 + b_p^-\right]. \tag{75}$$

The superscripts $(+)$ and $(-)$ refer to the regions between the layer and $r = a$, and the layer and the origin respectively. The constants K_m and K_p are free integration constants. The coefficients b_m and b_p represent the fraction of "constant solution" to "logarithmic solution" near the layer. These coefficients are in principle known. For instance b_m^- can be obtained by integrating the exact exterior equation [Eq. (73)] from the origin towards the singular layer $r = r_0$, using the regularity boundary condition at $r = 0$. The coefficient b_m^- is found numerically by computing

$$b_m^- = \lim_{r\to r_0^-}\left[\frac{\hat{\xi}_m^-}{x\hat{\xi}_m^{-\prime}} - \frac{1}{2}\ln x^2\right]. \tag{76}$$

A similar calculation yields b_m^+. The only difference is that in this case Eq. (73) must be integrated inward from the boundary $r = a$, using $\hat{\xi}_m^+(a) = 0$. In this case

$$b_m^+ = \lim_{r\to r_0^+}\left[\frac{\hat{\xi}_m^+}{x\hat{\xi}_m^{+\prime}} - \frac{1}{2}\ln x^2\right]. \tag{77}$$

Equations (69) and (77) also yield b_p^- and b_p^+ by replacing m by p.

Another approach to calculate b_m and b_p is by variational techniques, as demonstrated in Appendix A. The result is a set of explicit integral expressions for these coefficients that can be easily evaluated for any given q profile.

Based on the above discussion we shall hereafter assume that $b_m^-, b_p^-, b_m^+, b_p^+$ are known quantities, and that the desired exterior solutions in the vicinity of the layer are given by Eq. (75).

C The Dispersion Relation

The eigenfrequency of the gap mode is obtained by asymptotically matching the solutions across the layer as follows,

$$\hat{\xi}_m^-(x \to -\infty)|_{r\simeq r_0} = \xi_m(x \to -\infty) \qquad \xi_m(x \to \infty) = \hat{\xi}_m^+(x \to \infty)|_{r\simeq r_0}$$
$$\hat{\xi}_p^-(x \to -\infty)|_{r\simeq r_0} = \xi_p(x \to -\infty) \qquad \xi_p(x \to \infty) = \hat{\xi}_p^+(x \to \infty)|_{r\simeq r_0}. \tag{78}$$

It is straightforward to show that in the limit $x \to \pm\infty$ the layer solutions given by Eq. (70) have the same functional form (i.e. $c_1 + c_2 \ln x^2$) as the exterior solutions. This is a direct consequence of Eq. (72): that is, as $x \to \pm\infty$ then $\alpha \to \pm\pi/2$ and $\cos\alpha \to \pm\eta/x$ where $\eta = \Delta_0'(1-\lambda^2)^{1/2}/s(mp)^{1/2}$.

The first step in the matching is to equate the coefficients of the logarithmic terms. This yields

$$K_m^+ = K_m^- = \frac{C_m}{m^{1/2}}$$
$$K_p^+ = K_p^- = \frac{C_p}{p^{1/2}}. \tag{79}$$

The second step in the matching is to equate the coefficients of the constant terms. After eliminating A_m and A_p from this set of relations we are left with two coupled equations for the coefficients C_m and C_p given by

$$\pi\frac{C_p + \lambda C_m}{(1-\lambda^2)^{1/2}} = C_m \Delta b_m$$
$$\pi\frac{C_m + \lambda C_p}{(1-\lambda^2)^{1/2}} = -C_p \Delta b_p \tag{80}$$

where $\Delta b_m = b_m^+ - b_m^-, \Delta b_p = b_p^+ - b_p^-$.

The dispersion relation for λ is obtained by setting the determinant to zero. A short calculation yields

$$\frac{\omega}{\omega_0} = 1 + \frac{m^{1/2}(m+2)^{1/2}}{m+1} \frac{\delta}{(1+\delta^2)^{1/2}} \Delta_0' \tag{81}$$

with

$$\delta = \frac{\pi^2 + \Delta b_{m+2} \Delta b_m}{\pi(\Delta b_{m+2} - \Delta b_m)}. \tag{82}$$

Note that δ can in general have either sign indicating that the frequency may be shifted in either direction with respect to ω_0. Also, note that for the special case of $m = 1$, Eq. (73) can be solved exactly, leading to the result that $b_m^- = \infty$. Thus, for $m = 1$, Eq. (82) simplifies to

$$\delta = -\frac{\Delta b_{m+2}}{\pi}. \tag{83}$$

The calculation of the asymptotically matched eigenfunctions and the corresponding eigenvalue ' .oves that an ellipticity induced gap mode does indeed exist.

2.7 The Toroidicity Induced Alfvén Eigenmode

Toroidicity, as well as noncircularity, leads to symmetry breaking and poloidal coupling. Unlike ellipticity, toroidicity couples neighboring poloidal harmonics. Following the work in Ref. [2], we show in this section that toroidal coupling induces gaps in the Alfvén spectrum. Within this gap a discrete mode (the Toroidicty Induced Alfvén Eigenmode) exists.

In order to simplify the problem, we consider a toroidal plasma with circular cross section satisfying the ohmic tokamak expansion, and order $\epsilon = a/R_0 << 1$. In an analogy with the previous analysis of the EAE, we anticipate that the ϵ corrections are only going to be important in a narrow layer corresponding to the frequency gap. It is sufficient to maintain the highest derivative terms $\partial^2/\partial r^2$

originating from the "weak" poloidal coupling ($\epsilon << 1$). It is readily shown that such a coupling effect comes from the inertia term in Eq (8), which can be rewritten in the simplified form

$$\mathbf{B} \cdot \nabla \left[\Delta^*(R^2 \mathbf{B} \cdot \nabla X)\right] + \omega^2 \nabla_p \cdot (\rho R^2 \nabla_p X) = 0. \tag{84}$$

We Fourier analyze X in the poloidal angle and substitute the usual toroidal coordinates $R = R_0 + r\cos\theta$, $Z = r\sin\theta$. Introducing the new variable $\xi_m = X_m/r$, we find the following eigenvalue equation in toroidal geometry in the limit of large aspect ratio

$$D_m \xi_m + F(\xi_{m+1} + \xi_{m-1}) = 0 \tag{85a}$$

$$D_{m+1} \xi_{m+1} + F(\xi_{m+2} + \xi_m) = 0. \tag{85b}$$

The operator D_p is given by

$$D_p \equiv \frac{1}{r}\frac{d}{dr} r^3 (\omega^2 \rho_0 - k_p^2 B_0^2) \frac{d}{dr} - (p^2 - 1)(\omega^2 \rho_0 - k_p^2 B_0^2). \tag{86}$$

The operator F is important only in a narrow layer where the highest derivatives dominate and can be written as

$$F\xi_p \approx -\omega_0^2 \rho_0 (\frac{r_0}{R_0}) r_0^2 \xi_p''. \tag{87}$$

The errors made by this approximation are of the same order as those already neglected in the derivation of the $D_{p\pm1}$ operators.

The degeneracy present in cylindrical geometry is now removed by the toroidal coupling. The regions where coupling is most important can be found by plotting curves of $k_p R_0$ vs q for m and $m+1$ as shown in Fig. 4 (dashed curves) for the case $n = 1, m = 1$. Observe that the $m = 1$ and $m = 2$ curves intersect at the $q = 1.5$ surface where $k_1(q = 1.5) = -k_2(q = 1.5) = 1/3R_0$. For arbitrary m, n strong coupling occurs when $q_0 = (2m+1)/2n, k_m = -k_{m+1} = 1/2q_0R_0$, and $\omega_0 = v_a(r_0)/2q_0R_0$. In the region about $r \simeq r_0$ only the m and $m+1$ harmonics

are important and the set of infinite equations reduces to the following two coupled equations for ξ_m and ξ_{m+1}

$$(\omega^2\rho - k_m^2 B_0^2)\frac{d^2\xi_m}{dr^2} + \omega^2\rho\epsilon\frac{d^2\xi_{m+1}}{dr^2} + \ldots = 0$$
$$(\omega^2\rho - k_{m+1}^2 B_0^2)\frac{d^2\xi_{m+1}}{dr^2} + \omega^2\rho\epsilon\frac{d^2\xi_m}{dr^2} + \ldots = 0 \tag{88}$$

If the determinant of these term vanishes for any value of r, the equations cannot be inverted and no discrete modes are possible. The frequencies for which the determinant vanishes belong to the continuum spectrum and they are given by

$$\omega^2(r) = \frac{v_a^2}{2}\left\{k_m^2 + k_{m+1}^2 \pm \left[(k_m^2 - k_{m+1}^2)^2 + 4\epsilon^2 k_m^2 k_{m+1}^2\right]^{1/2}\right\} \tag{89}$$

For $(r - r_0)/r_0 \sim 1$ the small coupling term of order ϵ under the square root sign can be neglected and the cylindrical continuum frequencies of the m and $m+1$ harmonics are recovered. In the limit of $(r - r_0)/r_0 \sim \epsilon$ the coupling term must be retained and a frequecy gap is generated. The gap is centered about the Alfvén frequency at r_0 ($\omega^2 = k_\parallel^2(r_0)v_A^2(r_0)$) and its width of order ϵ is given by

$$\frac{v_a}{2q_0R_0}(1 - \frac{\epsilon}{2}) < \omega < \frac{v_a}{2q_0R_0}(1 + \frac{\epsilon}{2}). \tag{90}$$

Within this range the determinant does not vanish and the differential operators in Eq (88) can be inverted. Thus, if a discrete mode does exist, its frequency must satisfy Eq (90). Since the structure of Eq. (88) is identical to that of Eq. (63), a discrete mode can be found by following the same procedure used in Sec. 2.6 to derive the EAE. We first define a new eigenvalue

$$\Omega \equiv (1 - \frac{\omega^2}{\omega_0^2}) \sim \epsilon \tag{91}$$

and we rewrite Eq. (88) in the layer region ($x = (r - r_0)/r_0 \sim \epsilon$) in the following way

$$\frac{d}{dx}(\Omega + 4msx)\frac{d\xi_m}{dx} - \hat{\epsilon}\frac{d^2\xi_p}{dx^2} = 0$$
$$\frac{d}{dx}(\Omega - 4psx)\frac{d\xi_p}{dx} - \hat{\epsilon}\frac{d^2\xi_m}{dx^2} = 0. \tag{92}$$

where $p = m + 1$, $x = (r - r_0)/r_0$ and $\hat{\epsilon} = r_0/R_0$. Since Eq. (92) is identical to Eq. (69) for the EAE, we readily derive the eigenvalue condition

$$\frac{\omega}{\omega_0} = 1 - \frac{m^{1/2}(m+1)^{1/2}}{2m+1} \frac{\delta}{(1+\delta^2)^{1/2}} \hat{\epsilon} \tag{93}$$

with

$$\delta = \frac{\pi^2 + \Delta b_{m+1} \Delta b_m}{\pi(\Delta b_m - \Delta b_{m+1})}. \tag{94}$$

and where the simbol Δb_m has the same meaning as in Eq. (82). Also for the TAE , δ can, in general, have either sign indicating that the frequency may be shifted in either direction with respect to ω_0.

2.8 Conclusions

Several discrete macroscopic shear Alfvén waves have been shown to exist in an axisymmetric torus with noncircular cross section. In particular we have demonstrated the existence of a new mode, the elliptically induced Alfvén eigenmode[9]. This mode is of the same general class as the toroidally induced Alfvén eigenmode. In configurations with finite ellipticity, the EAE has a global structure centered about the $q = (m + 1)/n$ surface. The region of "localization" is of order $\kappa - 1$ which is often much larger than ϵ. Thus, the EAE may be more "global" than the TAE in such configurations.

The most macroscopic EAE in a tokamak couples the $m = 1, n = 1$ and $m = 3, n = 1$ "cylindrical" eigenmodes. The region of strong coupling (i.e. the gap) occurs at the radius r_0 corresponding to $q(r_0) \equiv 2$ and the real frequency of the mode is approximately $\omega_0 = v_A(r_0)/R_0 q(r_0)$. The actual eigenfriquency is shifted from ω_0. The shift is proportional to the ellipticity and can in principle be positive or negative.

Within framework of ideal MHD, these waves are always stable. However when kinetic effects are considered, resonant particle effects can cause a destabilization of the mode. The EAE as well as the TAE and the GAE can be excited by resonance

with circulating alpha particles[10,11,12]. The details of the mode excitation for the TAE and the EAE have been investigated and are presented in Chapter 3 and 4. The GAE has been previously found to be stable in toroidal plasmas[10]. Thus it is not analyzed here.

The TAE and EAE studies indicate that growth or damping depends upon a competition between the alpha particle driver, electron Landau damping, ion Landau damping and continuum damping[13,14] (as first pointed out for the TAE mode). For typical tokamak profiles satisfying $1 < q(r) < 3$, the eigenfrequency ω_0 does not intersect the continua of $m = 1$, $m = 3$ or any other ellipticity induced m number, over the entire radius $0 < r < a$. Thus, the continuum damping does not directly affect the $m = 1, 3$ EAE. There is , however, a continuum damping when toroidicity is included, as this couples to the $m = 2$ continuum at the $q = 4/3$ surface. Even so, since the $m = 2$ coupling takes place near the center of the plasma (where electron Landau damping is small), this should not be a big effect. Our stability studies also show that perhaps unexpectedly, ion Landau damping may have a substantial stabilizing effect on the TAE and the electron Landau damping on the EAE.

Both the TAE and EAE need further investigation to determine how detrimental their effect may be on alpha particle confinement in ignited tokamaks.

CHAPTER 3.

A stability criterion for energetic particle-Alfvén modes: the Vlasov fluid model.

3.1 Introduction

In this chapter we show how an isotropic energetic particle population can destabilize fluid like MHD modes. We derive a general stability criterion for those modes that exist in the stable part of the ideal MHD spectrum, in particular Alfvén waves. We, therefore, consider a model in which the core plasma is treated as a single MHD fluid and the hot particles as a fully kinetic Vlasov species (Vlasov-fluid model) . By treating the core as a single fluid the effects of the electron Landau damping are ignored. Since this is usually a stabilizing influence for the modes under consideration, we obtain a conservative estimate for the stability threshold. However, a more complete treatment including the ion and the electron Landau damping in the limit of small gyroradius, small β in simple equilibrium configurations is carried out in the next chapter. The main new result derived here is an exact stability criterion valid for a general finite aspect ratio, finite β, noncircular axisymmetric torus. The simple form of the criterion suggests a powerful means for testing stability against resonant energetic particle driven Alfvén modes in realistic tokamak geometries using existing ideal MHD stability codes.

3.2 Model

Consider a plasma consisting of bulk ions, bulk electrons, and a hot kinetic species such as alpha particles, or neutral beam ions. The electrons are assumed massless and satisfy the following fluid equations

$$\frac{\partial n_e}{\partial t} + \nabla \cdot n_e \mathbf{v}_e = 0$$

$$e n_e (\mathbf{E} + \mathbf{v}_e \times \mathbf{B}) + \nabla p_e = 0 \tag{1}$$

$$p_e / n_e^\gamma = \text{ const.}$$

At stated, electron Landau damping is not included in the model. To the extent that the electron-electron collision time is short compared to the characteristic growth time, the neglect of electron Landau damping is justified. In many realistic situations, however, this is not the case. The use of fluid equations for electrons is thus primarily for simplicity, and leads to a conservative stability boundary, since electron Landau damping is usually a stabilizing effect for the class of modes under consideration.

The bulk ions are also modeled by fluid equations as follows

$$\frac{\partial n_i}{\partial t} + \nabla \cdot n_i \mathbf{v}_i = 0$$

$$n_i m_i \left(\frac{\partial \mathbf{v}_i}{\partial t} + \mathbf{v}_i \cdot \nabla \mathbf{v}_i \right) = e n_i (\mathbf{E} + \mathbf{v}_i \times \mathbf{B}) - \nabla p_i \tag{2}$$

$$p_i / n_i^\gamma = \text{ const.}$$

The ion model neglects Landau damping and finite Larmor radius effects. These are good approximations for many situations of interest satisfying $\omega / k_\| v_{ti} \gg 1$ and $\rho_i / a \ll 1$. In an additional calculation not presented here, finite Larmor radius effects have been included, and are shown to have virtually no effect on the conclusions deduced from the basic energy relation derived in Section V. Hence for simplicity they are not included in the analysis.

The hot particles are treated as a fully kinetic, collision free species satisfying the Vlasov equation

$$\frac{\partial f_\alpha}{\partial t} + \mathbf{u} \cdot \nabla f_\alpha + \frac{Ze}{m_\alpha} (\mathbf{E} + \mathbf{u} \times \mathbf{B}) \cdot \nabla_u f_\alpha = 0 \, . \tag{3}$$

This description is "more exact" (and more complicated) than the usual drift kinetic model. Even so, the details of the kinetic theory will not be required to deduce the basic stability criterion.

The model is completed by the addition of the low frequency Maxwell equations

$$\nabla \times \mathbf{E} = -\frac{\partial \mathbf{B}}{\partial t}$$

$$\nabla \times \mathbf{B} = \mu_0 \mathbf{J} = \mu_0 e \left[n_i \mathbf{v}_i - n_e \mathbf{v}_e + Z \int \mathbf{u} f_\alpha d\mathbf{u} \right] \tag{4}$$

$$n_e = n_i + Z n_\alpha$$

$$\nabla \cdot \mathbf{B} = 0$$

The overall model can be slightly simplified by introducing the MHD ordering at the outset of the analysis. By assuming $\omega \sim k_\| v_a$ and $\rho_i / a \sim n_\alpha / n_e \ll 1$, the model reduces to

$$\frac{\partial \rho}{\partial t} + \nabla \cdot \rho \mathbf{v} = 0 \tag{5}$$

$$\rho \frac{d\mathbf{v}}{dt} = \mathbf{J} \times \mathbf{B} - \nabla p - Ze \int (\mathbf{E} + \mathbf{u} \times \mathbf{B}) f_\alpha d\mathbf{u} \tag{6}$$

$$p / \rho^\gamma = \text{ const.} \tag{7}$$

$$\mathbf{E} + \mathbf{v} \times \mathbf{B} = 0 \tag{8}$$

$$\frac{df_\alpha}{dt} = 0 \tag{9}$$

$$\nabla \times \mathbf{E} = -\frac{\partial \mathbf{B}}{\partial t} \tag{10}$$

$$\nabla \times \mathbf{B} = \mu_0 \mathbf{J} \tag{11}$$

$$\nabla \cdot \mathbf{B} = 0 \tag{12}$$

where $\rho = m_i n_i$, $\mathbf{v} = \mathbf{v}_i$ and $p = p_e + p_i$ are the mass density, flow velocity, and particle pressure of the bulk plasma respectively. Note that the momentum equation is an exact consequence of the starting equations. Most of the simplifications arising from the MHD ordering occur in the Ohm's law which reduces to the well known perfect conductivity relation[18]. Also, while n_α is assumed small, the hot species pressure $n_\alpha T_\alpha$ is assumed comparable to the bulk pressure p.

The equilibrium and stability analysis that follows is based on the model given by Eqs. (5-12).

3.3 Equilibrium

The analysis begins with a description of the equilibrium. We consider a general finite aspect ratio, finite β, noncircular axisymmetric torus. The bulk plasma is assumed at rest (i.e. $\mathbf{v} = 0$) and most of the current is carried by electrons. The bulk pressure is confined primarily by the $\mathbf{J} \times \mathbf{B}$ force. This is the usual MHD regime.

Focusing on the hot species, we observe that there are several equilibrium forces: electric, magnetic, centrifugal, and thermal. While the Vlasov equation treats them all exactly, in most situations of practical interest the centrifugal and electric field forces are quite small. The hot species is confined by that portion of the $\mathbf{J} \times \mathbf{B}$ force arising from the single fluid $\mathbf{v}_\alpha \times \mathbf{B}$ force. In a purely collisionless plasma it is not possible to determine how this force is divided between $\mathbf{v}_{\alpha\phi} \times \mathbf{B}_p$ and $\mathbf{v}_{\alpha p} \times \mathbf{B}_\phi$ (where ϕ and p denote toroidal and poloidal respectively). A transport theory is needed to determine the apportionment. Neoclassical transport theory suggests that poloidal flow is strongly damped by viscosity while toroidal flow can persist for very long times in an axisymmetric geometry.[19]

These arguments indicate that a reasonable choice for the hot species equilibrium distribution function is

$$f_\alpha = f_\alpha(\epsilon, P_\phi)$$

$$\epsilon = \frac{m_\alpha u^2}{2} + Ze\Phi(R,Z) \tag{13}$$

$$P_\phi = m_\alpha R u_\phi + Ze\Psi(R,Z) \ .$$

Here the flux is related to the poloidal field by the usual relation $\mathbf{B}_p = \nabla\Psi \times \mathbf{e}_\phi / R$. Similarly, $\mathbf{E} = -\nabla\Phi$. In the MHD limit $\mathbf{E} = 0$ for static equilibria (from Ohm's law). Thus $\Phi = 0$. Since ϵ and P_ϕ are exact constants of the motion, Eq. (13) represents an exact solution to the Vlasov equation.

As a further simplification, it is assumed that f_α has the form of a rigid rotor

$$f_\alpha = f_\alpha(\epsilon + \Omega P_\phi) \tag{14}$$

where $-\Omega$ = const is the toroidal angular velocity of the hot species. (Note, with this sign convenction $\Omega > 0$.) This is an important assumption, critical in the derivation of the basic energy relation. The main justifications for rigid rotation are that (1) it produces plausible profiles and (2) it is probably the most stable form of distribution function. Any significant shear in the toroidal flow velocity represents an additional source of free energy, capable of driving new Kelvin-Helmholtz type instabilities and complicating the behavior of existing instabilities. The rigid rotor reduces hot particle plasma instabilities to their most basic form. Note that f_α is a general function of $\epsilon + \Omega P_\phi$, and not necessarily a Maxwellian.

From Eq. (14) it is straightforward to show that the hot species number density and current density can be written as

$$n_\alpha \equiv \int f_\alpha d\mathbf{u} = -\frac{1}{Ze\Omega}\frac{dp_\alpha}{d\chi} \tag{15}$$

$$\mathbf{J}_\alpha \equiv Ze\int \mathbf{u} f_\alpha d\mathbf{u} = R\frac{dp_\alpha}{d\chi}\mathbf{e}_\phi \ . \tag{16}$$

Here,

$$p_\alpha(\chi) = \int \frac{m_\alpha}{3}(\mathbf{u} + \Omega R\mathbf{e}_\phi)^2 f_\alpha d\mathbf{u} \tag{17}$$

is the hot species particle pressure and

$$\chi(R,Z) = \Psi - \frac{m_\alpha \Omega}{2Ze}R^2 \ . \tag{18}$$

Hereafter, we shall consider $p_\alpha(\chi)$, or equivalently $f_\alpha(\epsilon+\Omega P_\phi)$ to be a free function.

These relations are substituted into Maxwell's equation. After some simple manipulations we obtain an MHD-like set of equilibrium equations given by

$$\begin{aligned} \mathbf{J}\times\mathbf{B} - \nabla(p+p_\alpha) + m_\alpha n_\alpha \Omega^2 R\nabla R = 0 \\ \nabla\times\mathbf{B} = \mu_0\mathbf{J} \\ \nabla\cdot\mathbf{B} = 0\,. \end{aligned} \tag{19}$$

As expected, the hot species enters the momentum balance through an additional pressure gradient force and a centrifugal force. For many practical applications both of these contributions are small compared to the ∇p term of the bulk plasma.

Following standard procedures, it is possible to reduce Eq. (19) to a single Grad-Shafranov equation for the flux Ψ. This equation has the form

$$\begin{aligned} \Delta^*\Psi = -F\frac{dF}{d\Psi} - \mu_0 R^2\left(\frac{dp}{d\Psi}+\frac{dp_\alpha}{d\chi}\right) \\ \mathbf{B} = \frac{F}{R}\mathbf{e}_\phi + \frac{\nabla\Psi\times\mathbf{e}_\phi}{R}\,. \end{aligned} \tag{20}$$

In Eq. (20) $F(\Psi)$, $p(\Psi)$ and $p_\alpha(\chi)$ are free functions.

This completes the specification of the equilibrium problem. For the stability analysis we shall assume that a solution has been found to Eq. (19) or equivalently Eq. (20).

3.4 Stability

The stability analysis proceeds in a straightforward manner. In an axisymmetric torus all perturbed quantities can be written as $\tilde{Q}(R,Z)\exp(-i\omega t - in\phi)$. For convenience the analysis is separated into two parts, one involving the bulk plasma and the other the hot species.

A. Bulk plasma analysis. The stability of the bulk plasma is very MHD-like. We introduce the fluid displacement for the bulk plasma

$$\tilde{\mathbf{v}} \equiv -i\omega\xi \ . \tag{21}$$

From Eqs. (5)-(11), $\tilde{\mathbf{E}}, \tilde{\mathbf{B}}, \tilde{\mathbf{J}}, \tilde{\rho}$, and $\tilde{p}$ can be easily expressed in terms of ξ

$$\begin{aligned}
\tilde{\mathbf{E}} &= i\omega\xi \times \mathbf{B} && \text{Ohm's Law} \\
\tilde{\mathbf{B}} &= \nabla \times (\xi \times \mathbf{B}) && \text{Faraday's Law} \\
\tilde{\mathbf{J}} &= (1/\mu_0)\nabla \times \nabla \times (\xi \times \mathbf{B}) && \text{Ampere's Law} \\
\tilde{\rho} &= -\nabla \cdot (\rho\xi) && \text{Mass Conservation} \\
\tilde{p} &= -\xi \cdot \nabla p - \gamma p \nabla \cdot \xi && \text{Energy Equation}
\end{aligned} \tag{22}$$

With these substitutions, the momentum equation reduces to

$$-\omega^2 \rho \xi = \tilde{\mathbf{J}} \times \mathbf{B} + \mathbf{J} \times \tilde{\mathbf{B}} - \nabla\tilde{p} + \tilde{\mathbf{F}}_\alpha \tag{23}$$

where

$$\tilde{\mathbf{F}}_\alpha = -Ze \int (\tilde{\mathbf{E}} + \mathbf{u} \times \tilde{\mathbf{B}}) f_\alpha d\mathbf{u} - Ze \int \mathbf{u} \times \mathbf{B} \tilde{f}_\alpha d\mathbf{u} \ . \tag{24}$$

The close relationship to ideal MHD is apparent.

B. Hot species analysis. The one remaining quantity to be expressed in terms of ξ is the perturbed distribution function $\tilde{f}_\alpha$. Using the well known procedure of integrating back along the unperturbed particle orbits assuming $Im(\omega) > 0$, we find

$$\tilde{f}_\alpha = -\frac{Ze}{m_\alpha} \int_{-\infty}^{t} (\tilde{\mathbf{E}} + \mathbf{u} \times \tilde{\mathbf{B}}) \cdot \nabla_u f_\alpha dt' \ . \tag{25}$$

For the rigid rotor distribution function

$$\nabla_u f_\alpha = \frac{\partial f_\alpha}{\partial \epsilon} (m_\alpha \mathbf{u} + m_\alpha \Omega R \mathbf{e}_\phi) \ . \tag{26}$$

After a short calculation the integrand in Eq. (25) can be written as

$$(\tilde{\mathbf{E}} + \mathbf{u} \times \tilde{\mathbf{B}}) \cdot \nabla_u f_\alpha = m_\alpha \frac{\partial f_\alpha}{\partial \epsilon} \left[\Omega \frac{d}{dt'} (\xi_\perp \cdot \nabla\Psi) - i(\omega - n\Omega) \xi_\perp \cdot \mathbf{u} \times \mathbf{B} \right] \ . \tag{27}$$

This leads to the following expression for the perturbed distribution function

$$\tilde{f}_\alpha = -\frac{\partial f_\alpha}{\partial \epsilon}\left[Ze\Omega(\xi_\perp \cdot \nabla\Psi) - i(\omega - n\Omega)\tilde{S}\right] \tag{28}$$

where

$$\tilde{S} = Ze\int_{-\infty}^{t} \xi_\perp \cdot (\mathbf{u}\times\mathbf{B})dt' \ . \tag{29}$$

The first term in Eq. (28) is a simple fluid-like contribution. The second term is quite complicated, requiring an explicit integration along the complex unperturbed orbits.

The final form of the momentum equation is obtained by integrating the fluid-like contributions arising from the hot species. Substituting the first term in Eq. (28) into Eq. (24) yields

$$Z^2e^2\Omega(\xi_\perp \cdot \nabla\Psi)\int \mathbf{u}\times\mathbf{B}\frac{\partial f_\alpha}{\partial\epsilon}d\mathbf{u} = \frac{d^2p_\alpha}{d\chi^2}(\xi_\perp \cdot \nabla\Psi)\nabla\Psi \ . \tag{30}$$

Similarly, the first term in Eq. (24) is evaluated as follows

$$-Ze\int(\tilde{\mathbf{E}} + \mathbf{u}\times\tilde{\mathbf{B}})f_\alpha d\mathbf{u} = i(\omega - n\Omega)Zen_\alpha\xi_\perp\times\mathbf{B} + \frac{dp_\alpha}{d\chi}\nabla(\xi_\perp\cdot\nabla\Psi) \ . \tag{31}$$

Substituting into the momentum equation [Eq. (23)] gives

$$-\omega^2\rho\xi = \mathbf{F}_M(\xi) + \mathbf{F}_K(\xi) \ . \tag{32}$$

Here

$$\mathbf{F}_M(\xi) = \tilde{\mathbf{J}}\times\mathbf{B} + \mathbf{J}\times\tilde{\mathbf{B}} - \nabla(\tilde{p} + \tilde{p}_\alpha) + \tilde{\rho}_\alpha\Omega^2R\nabla R \tag{33}$$

with

$$\tilde{p}_\alpha = -\frac{dp_\alpha}{d\chi}(\xi_\perp\cdot\nabla\Psi)$$

$$\tilde{\rho}_\alpha = -m_\alpha\frac{dn_\alpha}{d\chi}(\xi_\perp\cdot\nabla\Psi) \ . \tag{34}$$

The quantity $\mathbf{F}_M(\xi)$ is the analog of the MHD force operator modified by fluid-like contributions to the pressure and centrifugal force arising from the hot species. The quantity $\mathbf{F}_K(\xi)$ is a hot species kinetic addition to the force given by

$$\mathbf{F}_K(\xi) = -i(\omega - n\Omega)Ze\left[n_\alpha\xi_\perp\times\mathbf{B} + \int \mathbf{u}\times\mathbf{B}\frac{\partial f_\alpha}{\partial\epsilon}\tilde{S}d\mathbf{u}\right] \ . \tag{35}$$

The kinetic complications are contained within the trajectory integral $\tilde{S}$.

Equation (32) is the desired form of the momentum equation, expressed entirely in terms of ξ.

3.5 The General Energy Relation

Because of the rigid rotor form of the equilibrium distribution function, it is possible to derive a simple and useful energy relation from the basic stability equation [Eq. (32)] by multiplying by $-\xi^*/2$ and integrating over the plasma volume. The left hand side becomes $\omega^2 K_M$ where

$$K_M(\xi^*, \xi) = \frac{1}{2}\int \rho|\xi|^2 d\mathbf{r} \,. \tag{36}$$

K_M is the familiar MHD kinetic energy normalization.

The first term on the right hand side can be written as

$$\delta W(\xi^*, \xi) = -\frac{1}{2}\int \xi^* \cdot \mathbf{F}_M(\xi) d\mathbf{r} \,. \tag{37}$$

δW is the MHD potential energy contribution modified by the fluid-like hot species contributions. Following well known procedures for mindless MHD algebra, it can be shown that the force operator $\mathbf{F}_M(\xi)$ is self-adjoint. One specific self-adjoint form is given by

$$\delta W = \frac{1}{2}\int d\mathbf{r}\Bigg[\gamma p|\nabla\cdot\xi|^2 + \frac{|\mathbf{B}\cdot\nabla\xi_\perp|^2}{\mu_0} + \frac{B^2}{\mu_0}|\nabla\cdot\xi_\perp + 2\xi_\perp\cdot\kappa|^2 - \frac{4B^2}{\mu_0}|\xi\cdot\kappa|^2 \tag{38}$$

$$- \frac{m_\alpha^2\Omega^2}{4Z^2e^2}\frac{d^2p_\alpha}{d\chi^2}|\xi_\perp\cdot\nabla R^2|^2 + \xi_\perp^*\xi_\perp : \nabla\nabla\left(p + p_\alpha + \frac{B^2}{2\mu_0}\right) - \frac{\rho_\alpha\Omega^2}{2}\xi_\perp^*\xi_\perp : \nabla\nabla R^2\Bigg]$$

where $\kappa = (\mathbf{B}/B)\cdot\nabla(\mathbf{B}/B)$ is the field line curvature. The self-adjointness property is important because it implies that $\delta W(\xi^*, \xi)$ is real even when ξ is complex. A more intuitive form of the potential energy can be obtained by a different sequence of algebra

$$\delta W = \frac{1}{2}\int d\mathbf{r}\Bigg\{\frac{|\mathbf{Q}_\perp|^2}{\mu_0} + \frac{B^2}{\mu_0}|\nabla\cdot\xi_\perp + 2\xi_\perp\cdot\kappa|^2 + \gamma p|\nabla\cdot\xi|^2 - \frac{J_\parallel}{B}\xi_\perp^*\times\mathbf{B}\cdot\mathbf{Q}_\perp$$

$$-\xi_\perp \cdot \nabla\psi \left[2\left(\frac{dp}{d\psi} + \frac{dp_\alpha}{d\chi} \right) \xi_\perp^* \cdot \kappa - \Omega^2 \frac{d\rho_\alpha}{d\chi} \xi_\perp^* \cdot \nabla \frac{R^2}{2} \right] \Bigg\} \tag{39}$$

where $\mathbf{Q}_\perp = [\nabla \times (\xi_\perp \times \mathbf{B})]_\perp$. In order, these terms represent line bending, magnetic compression, plasma compression, kink destabilization, curvature destabilization, and centrifugal destabilization.

The last term to evaluate for the energy relation is the kinetic modification denoted by T_K

$$T_K \equiv -\frac{1}{2} \int \xi^* \cdot \mathbf{F}_K(\xi) d\mathbf{r} \tag{40}$$

where $\mathbf{F}_K(\xi)$ is given by Eq. (35). The first part of T_K can be written as

$$T_K^{(1)} = (\omega - n\Omega) R_1 \tag{41}$$

with

$$R_1 = \frac{iZe}{2} \int n_\alpha \xi_\perp^* \cdot (\xi_\perp \times \mathbf{B}) d\mathbf{r} \; . \tag{42}$$

R_1 is clearly a real quantity. The second part of T_K has the form

$$T_K^{(2)} = \frac{i(\omega - n\Omega)Ze}{2} \int \xi_\perp^* \cdot (\mathbf{u} \times \mathbf{B}) \frac{\partial f_\alpha}{\partial \epsilon} \tilde{S} \;\; d\mathbf{u} \;\; d\mathbf{r} \; . \tag{43}$$

This expression can be simplified by noting that from the definition of $\tilde{S}$

$$Ze\xi_\perp^* \cdot (\mathbf{u} \times \mathbf{B}) = \frac{d\tilde{S}^*}{dt} = i\omega^* \tilde{S}^* + D\tilde{S}^* \tag{44}$$

where

$$D\tilde{S}^* \equiv \left(\mathbf{u} \cdot \nabla + \frac{Ze}{m_\alpha} \mathbf{u} \times \mathbf{B} \cdot \nabla_u \right) \tilde{S}^* \; . \tag{45}$$

$T_K^{(2)}$ becomes

$$T_K^{(2)} = -\frac{(\omega - n\Omega)}{2} \int \frac{\partial f_\alpha}{\partial \epsilon} \left[\omega^* |\tilde{S}|^2 - i\tilde{S} D\tilde{S}^* \right] d\mathbf{u} \;\; d\mathbf{r} \; . \tag{46}$$

The last term in Eq. (46) can be further simplified by writing the complex quantity $\tilde{S}$ as $\tilde{S} = \tilde{A} + i\tilde{C}$. Then,

$$i\tilde{S} D\tilde{S}^* = \frac{i}{2} D(\tilde{A}^2 + \tilde{C}^2) - (\tilde{C} D\tilde{A} - \tilde{A} D\tilde{C}) \; . \tag{47}$$

Since $D(\partial f_\alpha/\partial\epsilon) = 0$ from the equilibrium relations, the contribution to $T_K^{(2)}$ from the first term on the right hand side of Eq. (47) is an exact differential which integrates to zero over the phase space volume. Thus, the integration of $i\tilde{S}D\tilde{S}^*$ yields a real quantity. $T_K^{(2)}$ can now be written as

$$T_K^{(2)} = (\omega - n\Omega)\left[R_2 - \frac{\omega^*}{2}\int \frac{\partial f_\alpha}{\partial\epsilon}|\tilde{S}|^2 d\mathbf{u}\ \ d\mathbf{r}\right] \tag{48}$$

where

$$R_2 = \frac{1}{2}\int \frac{\partial f_\alpha}{\partial\epsilon}(\tilde{C}D\tilde{A} - \tilde{A}D\tilde{C})d\mathbf{u}\ \ d\mathbf{r}\ . \tag{49}$$

Combining the contributions from Eqs. (36), (37), (41) and (48), we obtain the following energy relation

$$\omega^2 K_M = \delta W + (\omega - n\Omega)\left[\overline{R} - \frac{\omega^*}{2}\int \frac{\partial f_\alpha}{\partial\epsilon}|\tilde{S}|^2 d\mathbf{u}\ \ d\mathbf{r}\right] \tag{50}$$

and $\overline{R} = R_1 + R_2$ is a real quantity. The final form of the energy relation is obtained by writing $\omega = \omega_r + i\omega_i$ with $\omega_i > 0$, and setting the real and imaginary parts of Eq. (50) to zero.

$$\omega_i\left[2\omega_r K_M - \overline{R} + \frac{n\Omega}{2}\int \frac{\partial f_\alpha}{\partial\epsilon}|\tilde{S}|^2 d\mathbf{u}\ \ d\mathbf{r}\right] = 0 \tag{51}$$

$$(\omega_r^2 - \omega_i^2)K_M - \delta W - (\omega_r - n\Omega)\overline{R} + \frac{1}{2}\left[(\omega_r - n\Omega)\omega_r + \omega_i^2\right]\int \frac{\partial f_\alpha}{\partial\epsilon}|\tilde{S}|^2 d\mathbf{u}\ \ d\mathbf{r} = 0\ .$$

Eliminating $\overline{R}$ yields

$$|\omega - n\Omega|^2 = \frac{K_M}{K_M + K_\alpha}\left(n^2\Omega^2 - \frac{\delta W}{K_M}\right) \tag{52}$$

where

$$K_\alpha = -\frac{1}{2}\int \frac{\partial f_\alpha}{\partial\epsilon}|\tilde{S}|^2 d\mathbf{u}\ \ d\mathbf{r}\ . \tag{53}$$

Equation (52) is the desired form of the general energy relation.

3.6 Discussion

A. General comments. Several interesting conclusions can be extracted from Eq. (52). For simplicity, consider first the case with no hot kinetic species; that is, an ideal MHD plasma. Equation (52) reduces to

$$|\omega|^2 = -\frac{\delta W}{K_M} \,. \tag{54}$$

If $\delta W > 0$ for all allowable perturbations, then Eq. (54) exhibits an obvious contradiction that is only resolved by recognizing that the original assumption $\omega_i > 0$ must be violated. In other words, when $\delta W > 0$, the plasma is stable, consistent with standard MHD analysis.

The next point to note is that if a trial function is found that produces a minimum in $\delta W/K_M$ whose value $(\delta W/K_M)_{min} = 0$, then the self-adjointness of $\mathbf{F}_M(\xi)$ implies that this trial function is an actual eigenfunction of the system with eigenvalue $\omega_r = \omega_i = 0$. This too is consistent with the well established stability analysis of ideal MHD.

Based on the above information it is tempting to conclude that $\omega = 0$ represents the true stability transition. While this is a consequence of the standard analysis, it does not follow from Eq. (54) alone. Specifically, if a trial function is found which makes $\delta W < 0$, there is no guarantee that Eq. (54) cannot be satisfied by $\omega_r \neq 0$, $\omega_i \leq 0$. Some additional physics is required to establish this conclusion. In ideal MHD this physics is related to the conservation of energy and the Energy Principle. In the case of a hot kinetic species, the additional physics is related to the presence of resonant particles.

The conclusions for the general case including a hot kinetic species follow in an analogous manner. We consider equilibrium distribution functions satisfying

$$\frac{\partial f_\alpha}{\partial \epsilon} < 0 \tag{55}$$

so that $K_\alpha > 0$. If δW (including the hot species fluid-like contributions) is greater

than $n^2\Omega^2 K_M$ for all allowable trial functions, then Eq. (52) exhibits a contradiction, implying that the assumption $\omega_i > 0$ is violated; that is

$$\frac{\delta W}{K_M} > n^2\Omega^2 \tag{56}$$

is a sufficient condition for stability. Note that Eq. (56) implies that there are no unstable modes in the equivalent ideal MHD model without hot particles.

Continuing, for a trial function that minimizes $\delta W/K_M$ with $(\delta W/K_M)_{min} = n^2\Omega^2$, then the self-adjointness of $\mathbf{F}_M(\xi)$ again guarantees that this is a true eigenfunction of the system with eigenvalue $\omega_r = n\Omega$, $\omega_i = 0$.

Therefore

$$\left(\frac{\delta W}{K_M}\right)_{min} = n^2\Omega^2 \tag{57}$$

is a marginal stability point. In a system with resonant particles, the eigenvalues are in general complex, $\omega_r \neq 0, \omega_i \neq 0$. When $(\delta W/K_M)_{min} > n^2\Omega^2$, the contradiction in Eq. (52) implies that $\omega_i < 0$. When $(\delta W/K_M)_{min} = n^2\Omega^2$, we have determined that $\omega_i = 0$; the eigenvalue is purely real. It is then plausible that when resonant particle effects are included, a trial function which makes $(\delta W/K_M)_{min} < n^2\Omega^2$ will lead to $\omega_i > 0$. We conjecture that modes stable in ideal MHD (e.g. Alfvén waves) become unstable in the presence of a kinetic species when $(\delta W/K_M)_{min} < n^2\Omega^2$. This conjecture has been explicitly proven for a related, but slightly simpler system consisting of fluid electrons and fully kinetic ions.[20] In terms of the standard terminology, the unstable mode has $\omega_r \gg \omega_i$ with $\omega_r^2 \approx \delta W/K_M$ corresponding to a positive energy MHD wave. The stability boundary $\omega_r = n\Omega$, represents a transition from positive ($\omega_r > n\Omega$) to negative ($\omega_r < n\Omega$) dissipation, the latter giving rise to instability.

Assuming the validity of this conjecture, then the condition

$$\frac{\delta W}{K_M} \geq n^2\Omega^2 \tag{58}$$

is sufficient for stability in general and also necessary for Alfvén wave stability.

It is important to recognize that our criterion does not obviously apply to modes which lie in the unstable part of the ideal MHD spectrum, $(\delta W/K_M)_{min} < 0$, such as the $m = 1$ internal kink mode with $q(0) < 1$. In many cases these modes exist *only* in the unstable part of the spectrum, never exhibiting a discrete eigenmode with $\omega^2 > 0$ for any set of plasma parameters. Thus our description of the transition from a stable to unstable phase through the critical point $(\delta W/K_M)_{min} = n^2\Omega^2 > 0$ is not applicable. For this reason one cannot recover the energetic-particle kink stability window at high β_α[21,22] from the basic energy relation.

Observe that δW appearing in Eq. (58) can be larger or smaller than δW for pure MHD because of the inclusion of the fluid-like hot particle contributions. In the interesting limit where the hot species β_α is small compared the bulk β, these terms are negligible and both forms of δW coincide. In this regime, Eq. (58) implies that a hot kinetic species is always destabilizing. An ideal plasma requires $\delta W > 0$, whereas the addition of a hot kinetic species, raises the lower limit on δW to $\delta W > n^2\Omega^2 K_M$. This result is in qualitative agreement with a related calculation by J. F. Krall[23] who performed a stability analysis of interchange modes in an axisymmetric mirror with an energetic ion component. In that work, the background plasma is described by MHD equations and the energetic ions by the Vlasov equation. By using a rigid rotor equilibrium distribution function and numerically solving for the dispersion relation, Krall found that the already unstable mirror equilibria was significantly further destabilized by the energetic ions.

If finite Larmor radius effects of the bulk ions are introduced, the conclusions remain unchanged. This can be seen heuristically by replacing ω^2 with $\omega(\omega+\omega_{*i})$ in Eq. (32). Here $\omega_{*i} = \mathbf{k}\cdot\mathbf{V}_{Di}$ is the ion diamagnetic drift frequency. If ω_{*i} is constant in space, the general stability criterion can be rewritten as $\delta W/K_M \geq n^2\Omega^2 + n\Omega\omega_{*i}$. Since $n\Omega \sim \omega_{*\alpha} \gg \omega_{*i}$ the additional term has virtually no effect on the threshold condition.

There is an important practical consequence that follows from Eq. (58). If one is primarily interested in accurate threshold conditions rather than growth rates,

then Eq. (58) implies that these conditions can be determined in realistic geometries using pure fluid codes. The complicated particle orbits do not explicitly enter the threshold conditions. For example, in the regime $\beta_\alpha \ll \beta$, one can run, with perhaps some modifications, one of the well established ideal MHD stability codes such as PEST, ERATO, or GATO. The lowest eigenvalue ω^2_{min} can be calculated (and may be positive or negative) and then compared to the value of $n^2\Omega^2$. The threshold condition occurs when $\omega^2_{min} = n^2\Omega^2$.

B. Applications. The stability criterion given by Eq. (58) can be applied to the problems of the GAE and the gap modes (see Sec. 2.5,2.6 and 2.7). To make comparisons with the existing literature, we must determine the relationship between Ω and $\omega_{*\alpha}$ (the perpendicular diamagnetic drift frequency). We define $\omega_{*\alpha} \equiv \mathbf{k} \cdot \mathbf{V}_D$ where

$$\mathbf{V}_D = \frac{1}{Ze n_\alpha B^2}\mathbf{B} \times (\nabla p_\alpha - m_\alpha n_\alpha R \nabla R) = \frac{\mathbf{B} \times \nabla \Psi}{Ze n_\alpha B^2}\frac{dp_\alpha}{d\chi}$$

$$\mathbf{k} = n\nabla\left[-\phi + \int_{\theta_0}^{\theta} \frac{FJ}{R^2} d\theta'\right] , \tag{59}$$

$F(\Psi) = RB_\phi$, and θ is an orthogonal poloidal angle. The Jacobian J is related to $\mathbf{B}_p$ and θ by the usual relation $J = 1/(\mathbf{B}_p \cdot \nabla\theta)$. Note that $\mathbf{k}$ is defined for any value of n but can only be unambiguously intepreted as the wavenumber for localized modes. A short calculation yields

$$\omega_{*\alpha} = n\Omega \, . \tag{60}$$

Perhaps unexpectly, we see that $\omega_{*\alpha}$, which is proportional to the perpendicular diamagnetic drift velocity, is related to the macroscopic angular velocity Ω which is predominantly in the parallel (i.e. toroidal) direction. This result is reconciled by observing that the momentum equation for the hot particles implies that the macroscopic fluid velocity and diamagnetic drift velocity are related by $\mathbf{v}_\alpha = \mathbf{V}_D + (v_{||}/B)\mathbf{B}$ where $v_{||}$ is a free function. For the rigid rotor distribution function it can be shown that $v_{||} = -\Omega F(\Psi)/B$. This leads to $\mathbf{v}_p = 0$ and $v_\phi = -\Omega R$.

According to Eq. (60) the instability condition for energetic particle Alfvén waves has the folllowing form

$$|\omega_r| < \omega_{*\alpha}. \tag{61}$$

In the absence of electron Landau damping, (which is often not the dominant stabilizing effect), Van Dam et al[20] have derived a similar instability threshold in a finite aspect ratio circular tokamak: $\omega_{*\alpha} > K\omega_A$ where $\omega_A = k_{\|}(r_0)v_a(r_0)$ and r_0 is the radius corresponding to the gap. The constant K is of order unity and depends upon the choice of the equilibrium alpha distribution function. For a Maxwellian and a slowing down distribution $K = 1$ and $K = 1/2$ respectively. This threshold is in general agreement with our basic stability criterion if we note that $\omega_A^2 = \delta W/K_M$ for the gap mode. However, our criterion predicts $K = 1$ for all distribution functions. The discrepancy is due to different definitions of $\omega_{*\alpha}$. In our criterion the critical $\omega_{*\alpha}$ is always given by $\omega_{*\alpha}^2 = \delta W/K_M$. However, the value of $n\Omega = \omega_{*\alpha}$ varies as the alpha particle distribution function changes while holding certain macroscopic quantities fixed (e.g. total number of alphas, total alpha energy, width of the alpha profile, etc.).

Van Dam et al show that the TAE mode may be of serious concern to the ITER project. Their initial calculations predict that ITER will be stable for a slowing down distribution. However, the safety margin is quite small. Other distribution functions, as well as finite aspect ratio, finite β, and noncircularity could quantitatively change the threshold. This suggests that an accurate threshold calculation, based on Eq. (58) and the procedure described immediately thereafter would indeed be a worthwhile endeavor.

CHAPTER 4

Stability of Alfvén gap modes in burning plasmas: The drift kinetic model

4.1 Introduction

In the previous chapter it has been shown[2] that MHD Alfvén waves whose frequency ω_A is lower than the alpha diamagnetic frequency $\omega_{*\alpha}$ can be driven unstable via transit resonance with alpha particles. The conventional wisdom is that Toroidal Alfvén Eigenmodes (TAE)[4-7] pose the most serious threat to alpha confinement. In this chapter we show that two other global Alfvén modes, the Ellipticity Induced Alfvén Eigenmode (EAE)[8] and the Noncircular Triangularity Induced Alfvén Eigenmode (NAE) can be excited via resonant interaction with alpha particles and that their stabilty threshold can be lower than that of the TAE in high density regimes and for toroidal wavenumber $n > 1$.

Recall that the TAE[4] results from toroidicity which couples neighboring poloidal harmonics. Its frequency lies in gaps in the Alfvén contiuum generated by the toroidal coupling. In the limit of large aspect ratio (calculated at the gap position, $\epsilon_{gap} \ll 1$), the mode is localized in a narrow region of thickness $\sim \epsilon_{gap} a$ about the $q = (2m+1)/2n$ surface.

The EAE[8] is a global mode resulting from two elliptically coupled harmonics. Its frequency lies in the Alfvén continuum gaps generated by elliptical coupling. In the limit of small ellipticity ($\kappa - 1 \ll 1$) the mode is localized in a narrow region of thickness $\sim (\kappa - 1)a/2$ about the $q = (m+1)/n$ surface.

The NAE results from the coupling induced by the triangularity of the plasma cross section. The mode consists primarily of two triangularly coupled harmonics, localized in a region of thickness $\sim \delta a/4$ about the $q = (2m+3)/2n$ surface, and its real frequency lies in the Alfvén continuum gaps generated by the triangular coupling.

In particular since many tokamaks have finite ellipticity $(\kappa - 1)/2 \simeq 0.5$, as compared to small toroidicity and triangularity ($\epsilon_{gap} \ll 1$, $\delta/4 \ll 1$) the EAE may be a potentially more dangerous mode than either the TAE or NAE.

In this section we derive the growth rates of the three gap modes in the presence of circulating alpha particles, taking into account the stabilizing effects of the ion and electron Landau damping. Unlike the energy relation derived in the previuos chapter, the evaluation of the growth rates requires the perturbed Vlasov equation to be solved. A small Larmor radius assumption ($\rho/a << 1$) and an gyrophase average technique will be used to calculate $\tilde{f}$ for low-(m,n) numbers. The procedure is extremely simple compared to the high-n derivation available in the literature.

4.2 The Model

A The basic moment equations

Consider a plasma consisting of bulk electrons and ions and a species of energetic particles, each described by the Vlasov equation

$$\frac{\partial f_j}{\partial t} + \mathbf{v} \cdot \nabla f_j + \frac{q_j}{m_j}(\mathbf{E} + \mathbf{v} \times \mathbf{B}) \cdot \nabla_v f_j = 0. \tag{1}$$

Here, j denotes particle species. Taking the zeroth order moment leads to the well known conservation of mass relation

$$\frac{\partial n_j}{\partial t} + \nabla \cdot n_j \mathbf{u}_j = 0. \tag{2}$$

Similarly, the first order moment yields the momentum equation

$$m_j \frac{\partial}{\partial t}(n_j \mathbf{u}_j) + \nabla \cdot \overleftrightarrow{\Pi}_j = q_j n_j (\mathbf{E} + \mathbf{u}_j \times \mathbf{B}) \tag{3}$$

where

$$\overleftrightarrow{\Pi}_j \equiv m_j \int \mathbf{v}\mathbf{v} f_j d\mathbf{v}. \tag{4}$$

Note that $\overleftrightarrow{\Pi}_j$ contains both thermal and inertial effects.

The desired form of the momentum equation is obtained by summing Eq. (3) over species and using the quasineutral condition. This gives

$$\mathbf{J} \times \mathbf{B} = \sum_j \left(\nabla \cdot \overleftrightarrow{\Pi}_j + m_j \frac{\partial}{\partial t} n_j \mathbf{u}_j \right). \tag{5}$$

Our approach is to solve the Vlasov equation and evaluate $n_j, \mathbf{u}_j$ and $\overleftrightarrow{\Pi}_j$ in terms of the electric and magnetic fields. The model is closed by the addition of the low frequency Maxwell equations

$$\begin{aligned} \nabla \times \mathbf{E} &= -\frac{\partial \mathbf{B}}{\partial t} \\ \nabla \times \mathbf{B} &= \mu_0 \mathbf{J} \\ \nabla \cdot \mathbf{B} &= 0. \end{aligned} \tag{6}$$

Equations (2), (5) and (6) represent the basic moment description of the problem.

B Equilibrium

The equilibrium distribution function for a finite β, finite aspect ratio, non-circular axisymmetric Vlasov plasma is assumed to be an arbitrary function of the constants of motion ϵ and p_ϕ; that is

$$f_{0j} = F_j(\epsilon, p_\phi) \tag{7}$$

where

$$\begin{aligned} \epsilon &= \frac{m_j v^2}{2} + q_j \Phi \\ p_\phi &= m_j R v_\phi + q_j \Psi \end{aligned} \tag{8}$$

and $\Phi(R,Z), \Psi(R,Z)$ are the equilibrium electric potential and poloidal flux function respectively. For low frequency phenomena f_0 could also be a function of the adiabatic invariants μ and $\sigma = v_{||}/|v_{||}|$.

We now make a number of simplifying assumptions that minimizes the volume of algebra required while maintaining the essential physics. First we assume that the ions and energetic species can carry only a toroidal current, so that Eq. (7) is the exact form of equilibrium distribution function. The electrons are allowed to carry both toroidal and poloidal current. Their distribution function is of the form $f_{0e} = F_e(\epsilon, p_\phi) + \tilde{F}_e(\epsilon, p_\phi, \mu, \sigma)$ where $\tilde{F}_e/F_e \sim r_{Le}/a$. The quantity $\tilde{F}_e$, which generates poloidal current, does not explicitly enter the evaluation of $\overleftrightarrow{\Pi}_e$ in the small gyroradius limit and makes inertial contributions of order m_e/m_i smaller than for the ions. Thus, $\tilde{F}_e$ never explicitly enters the calculation and is hereafter suppressed from the analysis.

Second, observe that in the small gyroradius limit

$$F_j(\epsilon, p_\phi) \approx F_j(\epsilon, \Psi) + \frac{m_j R v_\phi}{q_j} \frac{\partial F_j}{\partial \Psi} + \ldots \tag{9}$$

The dominant contribution to $\overleftrightarrow{\Pi}_j$ arises from the first term whose form implies that the equilibrium pressure is isotropic. This is a good assumption for most tokamaks. Anisotropic pressure would require finite μ dependence in F_j.

The third simplification arises from the assumption that the equilibrium electric field is zero: $\Phi(R,Z) = 0$. In practice small electric fields do exist, but as is shown in Appendix B, they do not alter the dispersion relation in any substantial manner.

Under these assumptions the equilibrium momentum balance equation reduces to

$$\mathbf{J} \times \mathbf{B} = \nabla p \tag{10}$$

where $\overleftrightarrow{\Pi}_j = p_j \overleftrightarrow{\mathbf{I}}$,

$$p(\Psi) = \sum_j p_j(\Psi) \tag{11}$$

and

$$p_j(\Psi) = \int \frac{m_j v^2}{3} F_j(\epsilon, \Psi) d\mathbf{v}. \tag{12}$$

Equation (10) implies that any ideal MHD equilibrium solution is also a solution to the more general model considered here. Using Ampere's law and following standard procedures, it is possible to reduce Eq. (10) to a single Grad-Shafranov equation for Ψ given by

$$\Delta^* \Psi = -\mu_0 R^2 \frac{dp}{d\Psi} - F\frac{dF}{d\Psi} \tag{13}$$

$$\mathbf{B} = \frac{F}{R}\mathbf{e}_\phi + \frac{1}{R}\nabla\Psi \times \mathbf{e}_\phi$$

where $p(\Psi)$ and $F(\Psi)$ are free functions.

Finally, note that the assumption $\Phi = 0$ implies that the ions and energetic species are held in macroscopic equilibrium primarily by the $\mathbf{u}_j \times \mathbf{B}$ force. In the small gyroradius limit the toroidal fluid velocity for these species can be written as

$$u_{\phi j} = \frac{R}{q_j n_j}\frac{dp_j}{d\Psi}. \tag{14}$$

This completes the specification of the equilibrium problem. For the stability analysis it is assumed that a solution has been found to Eq. (10) or equivalently Eq. (13).

C Stability

The stability analysis proceeds in the standard manner. All perturbed quantities are written as

$$Q_1 = Q_1(R, Z)\exp(-i\omega t - in\phi). \tag{15}$$

The perturbed distribution function is found by the method of characteristics

$$f_{1j} = -\frac{q_j}{m_j}\int_{-\infty}^{t} (\mathbf{E}_1 + \mathbf{v} \times \mathbf{B}_1) \cdot \nabla_v F_j dt'. \tag{16}$$

Using the equilibrium relation $F_j = F_j(\epsilon, p_\phi)$, it can easily be shown that f_{1j} has the form

$$f_{1j} = -\frac{q_j}{\omega}\left[i\frac{\partial F_j}{\partial p_\phi}RE_{1\phi} + \left(\omega\frac{\partial F_j}{\partial \epsilon} - n\frac{\partial F_j}{\partial p_\phi}\right)\int_{-\infty}^{t}\mathbf{E}_1\cdot\mathbf{v}dt'\right] \tag{17}$$

Equation (17) can be further simplified by making the assumption $E_{1\|} = 0$. This is a good approximation for MHD Alfvén waves although a small portion of the overall electron Landau damping is neglected. The condition $E_{1\|} = 0$ allows us to define

$$\mathbf{E}_{1\perp} \equiv i\omega\boldsymbol{\xi}_\perp \times \mathbf{B} \tag{18}$$

where $\boldsymbol{\xi}_\perp$ represents the perturbed $\mathbf{E}\times\mathbf{B}$ displacement. Using Eq. (18) we can rewrite the quantity $\mathbf{E}_1\cdot\mathbf{v}$ (evaluated along the unperturbed orbit) as follows

$$\mathbf{E}_1\cdot\mathbf{v} = -i\omega\boldsymbol{\xi}_\perp\cdot(\mathbf{v}\times\mathbf{B}) = -i\omega\frac{m_j}{q_j}\boldsymbol{\xi}_\perp\cdot\frac{d\mathbf{v}}{dt} = -i\omega\frac{m_j}{q_j}\left[\frac{d}{dt}(\boldsymbol{\xi}_\perp\cdot\mathbf{v}) - \mathbf{v}\cdot\frac{d\boldsymbol{\xi}_\perp}{dt}\right]. \tag{19}$$

The desired form of the perturbed distribution function becomes

$$f_{1j} = -q_j\frac{\partial F_j}{\partial p_\phi}(\boldsymbol{\xi}_\perp\cdot\nabla\Psi) + im_j\left(\omega\frac{\partial F_j}{\partial\epsilon} - n\frac{\partial F_j}{\partial p_\phi}\right)\left[\boldsymbol{\xi}_\perp\cdot\mathbf{v} - \int_{-\infty}^{t}\mathbf{v}\cdot\frac{d\boldsymbol{\xi}_\perp}{dt'}dt'\right]. \tag{20}$$

Equation (20) is exact. In principle we want to utilize this equation to calculate the perturbed $n_j, \mathbf{u}_j$, and $\overleftrightarrow{\mathbf{\Pi}}_j$ in terms of $\boldsymbol{\xi}_\perp$ by taking appropriate moments. Observe that most of the terms represent simple fluid-like contributions whose moments can be easily evaluated. The difficulty of course lies with the last term which involves a complicated integral along the unperturbed orbits. It is here that the substitution given by Eq. (19) proves useful. The form of the integral in Eq. (20) is smaller by r_{Lj}/a than that appearing in Eq. (17). It can be easily evaluated in the small gyroradius limit using only the *zeroth* order guiding center orbits. This calculation is carried out in the next section in the interesting regime corresponding to finite wavelength, macroscopic modes.

D The drift kinetic expansion

The last step in the simplification of f_{1j} is the substitution of the small gyroradius, drift kinetic expansion into Eq. (20). The explicit transformation is given by

$$\begin{aligned} \mathbf{v} &= v_{\|}\mathbf{b}(\mathbf{R}) + v_{\perp}\left[\mathbf{n}(\mathbf{R})\cos\varsigma - \boldsymbol{\tau}(\mathbf{R})\sin\varsigma\right] \\ \mathbf{x} &= \mathbf{R} + \frac{v_{\perp}}{\Omega_j(\mathbf{R})}\left[\mathbf{n}(\mathbf{R})\sin\varsigma + \boldsymbol{\tau}(\mathbf{R})\cos\varsigma\right] \end{aligned} \tag{21}$$

where $\Omega_j = q_j B/m_j$, $\mathbf{b} = \mathbf{B}/B$, $\mathbf{R}$ is the guiding center of the particle, and $(\mathbf{n}, \boldsymbol{\tau}, \mathbf{b})$ are a right-handed set of locally orthogonal unit vectors in physical space. The quantity ς is the gyrophase angle of the particle while $v_{\|}$ and $v_{\perp}$ are the parallel and perpendicular particle velocities. The variables $v_{\|}$ and $v_{\perp}$ actually represent an intermediate step in the transformation. In the final step $v_{\|}$ and $v_{\perp}$ are related to the energy and magnetic moment by the usual relations

$$\begin{aligned} \epsilon &= \frac{m_j}{2}\left(v_{\perp}^2 + v_{\|}^2\right) \\ \mu &= \frac{m_j v_{\perp}^2}{2B(\mathbf{R})}. \end{aligned} \tag{22}$$

Along the unperturbed orbits, the guiding center variables satisfy the following equations of motion

$$\begin{aligned} \frac{d\epsilon}{dt} &= 0 \\ \frac{d\mu}{dt} &\approx 0 \\ \frac{d\varsigma}{dt} &\approx \Omega_j \\ \frac{d\mathbf{R}}{dt} &\approx v_{\|}\mathbf{b} + \mathbf{v}_D \end{aligned} \tag{23}$$

where

$$\mathbf{v}_D = \mathbf{v}_{\nabla B} + \mathbf{v}_\kappa$$

$$\mathbf{v}_{\nabla B} = \frac{v_\perp^2}{2\Omega_j}\mathbf{b} \times \nabla \ln B \tag{24}$$

$$\mathbf{v}_\kappa = \frac{v_\parallel^2}{\Omega_j}\mathbf{b} \times \boldsymbol{\kappa}$$

and $\boldsymbol{\kappa} = \mathbf{b} \cdot \nabla \mathbf{b}$. The equations for $\dot{\mu}, \dot{\zeta}$, and $\dot{\mathbf{R}}$ are correct to leading order in $\delta_j \equiv r_{Lj}/a$. The higher order corrections are not explicitly needed. Note also that the $\mathbf{E} \times \mathbf{B}$ drift velocity vanishes in the expression for $\mathbf{v}_D$ since $\mathbf{E}_0 = 0$.

The next step is to substitute the drift kinetic expansion into the expression for $\mathbf{v} \cdot (d\boldsymbol{\xi}/dt)$ in Eq. (20). A simple calculation shows that $\mathbf{v} \cdot (d\boldsymbol{\xi}/dt)$ has the form

$$\mathbf{v} \cdot \frac{d\boldsymbol{\xi}}{dt} = a_0 + a_1 e^{i\zeta} + a_2 e^{2i\zeta} \tag{25}$$

with $a_j = a_j(\epsilon, \mu, \mathbf{R}, t')$. The last two terms are rapidly oscillating and nearly average to zero. It can be easily shown that their contributions to f_{1j} are smaller by δ_j than those already appearing. The quantity a_0 represents the resonant particle effects. It produces a larger contribution competitive with the fluid contribution and is dissipative in nature. This is the only term that need be maintained. A short calculation shows that

$$a_0(\epsilon, \mu, \mathbf{R}, t') = \frac{v_\perp^2}{2}\nabla \cdot \boldsymbol{\xi}_\perp + \left(\frac{v_\perp^2}{2} - v_\parallel^2\right)\boldsymbol{\xi}_\perp \cdot \boldsymbol{\kappa}. \tag{26}$$

The final form for f_{1j} is obtained by substituting Eq. (26) into Eq. (20) and introducing the drift kinetic expansion into the fluid-like terms. The result is

$$f_{1j} \approx -\frac{\partial F_j}{\partial \Psi}(\boldsymbol{\xi}_\perp \cdot \nabla \Psi) + i m_j(\omega - \hat{\omega}_{*j})\frac{\partial F_j}{\partial \epsilon}\left[\boldsymbol{\xi}_\perp \cdot \mathbf{v} - \int_{-\infty}^{t} a_0 dt'\right]. \tag{27}$$

In this expression $F_j = F_j(\epsilon, \Psi)$ and

$$\hat{\omega}_{*j}(\epsilon, \Psi) \equiv \frac{n}{q_j}\frac{\partial F_j/\partial \Psi}{\partial F_j/\partial \epsilon}. \tag{28}$$

It is important to notice that a_0 is a function of the invariants of motion ϵ, μ, the time t and the guiding center position R. Since the guiding center trajectories are much simpler than the full particle orbits, an analytic approximation can be used to obtain explicit evaluations.

4.3 Application to Energetic Particle-Alfvén Waves

A The moment equations

By focussing attention on energetic particle-Alfvén waves, the basic stability equation is obtained by linearizing the moment equation [Eq. (5)] and Maxwell's equations [Eq. (6)], and then substituting the expression for f_{1j} [Eq. (27)] to evaluate the perturbed $\overleftrightarrow{\Pi}_j$ and $n_j \mathbf{u}_j$. From the definition $\mathbf{E}_1 = i\omega \boldsymbol{\xi}_\perp \times \mathbf{B}$, Maxwell's equations yield

$$\begin{aligned} \mathbf{B}_1 &= \nabla \times (\boldsymbol{\xi}_\perp \times \mathbf{B}) \\ \mu_0 \mathbf{J}_1 &= \nabla \times \nabla \times (\boldsymbol{\xi}_\perp \times \mathbf{B}). \end{aligned} \tag{29}$$

The linearized form of the momentum equation is given by

$$\mathbf{J}_1 \times \mathbf{B} + \mathbf{J} \times \mathbf{B}_1 = \sum_j \left[\nabla \cdot \overleftrightarrow{\Pi}_{1j} - i\omega m_j (n_{1j} \mathbf{u}_j + n_j \mathbf{u}_{1j}) \right]. \tag{30}$$

For simplicity, zero subscripts have been omitted from equilibrium quantities. Recall that at this point we have introduced the small gyroradius approximation in deriving the perturbed distribution function, but have made no assumptions regarding the size of β or ϵ. For Alfvén waves this is formally equivalent to introducing the gyroradius parameter $\delta \equiv r_{Li}/a$ and assuming that

$$\begin{aligned} \frac{\omega}{k_\parallel v_a} &\sim 1 \qquad & \frac{\omega}{\Omega_i} &\sim \delta \\ \frac{n_\alpha}{n_i} &\sim \delta \qquad & \frac{T_\alpha}{T_i} &\sim \frac{1}{\delta} \\ \frac{\omega_{*i}}{\omega} \sim \frac{\omega_{*e}}{\omega} &\sim \delta \qquad & \frac{\omega_{*\alpha}}{\omega} &\sim 1 \end{aligned} \tag{31}$$

where the subscripts e, i, α denote electrons, ions, and alphas, respectively.

On the basis of Eq. (31) it follows that the ion contribution dominates the inertial effects:

$$\sum_j m_j(n_{1j}\mathbf{u}_j + n_j\mathbf{u}_{1j}) = \sum_j m_j \int \mathbf{v} f_{1j} d\mathbf{v} \approx \omega^2 \rho \boldsymbol{\xi}_\perp. \tag{32}$$

For simplicity the subscript i has been omitted from ρ, the ion mass density.

Similarly, a straightforward calculation shows that the $\overleftrightarrow{\Pi}_{1j}$ tensor has the form

$$\begin{aligned} \overleftrightarrow{\Pi}_{1j} &= \int m_j \mathbf{v}\mathbf{v} f_{1j} d\mathbf{v} \\ &= \begin{bmatrix} p_{1\perp j} & 0 & 0 \\ 0 & p_{1\perp j} & 0 \\ 0 & 0 & p_{1\parallel j} \end{bmatrix} \end{aligned} \tag{33}$$

The elements $p_{1\perp j}$ and $p_{1\parallel j}$ are given by

$$\begin{aligned} p_{1\perp j} &= -\boldsymbol{\xi}_\perp \cdot \nabla p_j - i \int (\omega - \hat{\omega}_{*j}) \frac{m_j v_\perp^2}{2} \frac{\partial F_j}{\partial \epsilon} s_j d\mathbf{v} \\ p_{1\parallel j} &= -\boldsymbol{\xi}_\perp \cdot \nabla p_j - i \int (\omega - \hat{\omega}_{*j}) m_j v_\parallel^2 \frac{\partial F_j}{\partial \epsilon} s_j d\mathbf{v} \end{aligned} \tag{34}$$

where

$$s_j = m_j \int_{-\infty}^{t} \left[\frac{v_\perp^2}{2} \nabla \cdot \boldsymbol{\xi}_\perp + \left(\frac{v_\perp^2}{2} - v_\parallel^2 \right) \boldsymbol{\xi}_\perp \cdot \boldsymbol{\kappa} \right] dt'. \tag{35}$$

Combining these results leads to a single vector equation for the unknown $\boldsymbol{\xi}_\perp$

$$-\rho\omega^2 \boldsymbol{\xi}_\perp = \mathbf{F}_\perp(\boldsymbol{\xi}_\perp) + i\mathbf{D}_\perp(\boldsymbol{\xi}_\perp). \tag{36}$$

Here

$$\mathbf{F}_\perp(\boldsymbol{\xi}_\perp) = \mathbf{J}_1 \times \mathbf{B} + \mathbf{J} \times \mathbf{B}_1 + \nabla(\boldsymbol{\xi}_\perp \cdot \nabla p) \tag{37}$$

is the ideal MHD force operator for incompressible displacements (and as implied, $\mathbf{F}_\perp \cdot \mathbf{b}$ can be easily shown to vanish). The operator $\mathbf{D}_\perp$ contains the dissipative effects associated with resonant particles and can be written as

$$\mathbf{D}_\perp(\boldsymbol{\xi}_\perp) = \sum_j m_j \int \left[\frac{v_\perp^2}{2} \nabla_\perp + (v_\parallel^2 - \frac{v_\perp^2}{2}) \boldsymbol{\kappa} \right] \left[(\omega - \hat{\omega}_{*j}) \frac{\partial F_j}{\partial \epsilon} s_j \right] d\mathbf{v}. \tag{38}$$

Equations (36)–(38) describe the low frequency, finite wavenumber stability of energetic particle-Alfvén waves in an axisymmetric torus.

It is now convenient to introduce a subsidiary expansion in β. We assume $\delta \ll \beta \ll 1$, but note that no ordering is required for the inverse aspect ratio, the deviation from circularity, or the safety factor: $\epsilon \sim \kappa - 1 \sim q \sim 1$.

The low β assumption is useful because the dissipation operator becomes small compared to the inertial effects. This can be seen by recognizing that the orbit integral s_j scales as

$$s_j \sim \frac{m_j v_\perp^2 \xi_\perp}{R(\omega - k_\| v_\|)}. \tag{39}$$

Equation (38) implies that

$$D_j \sim \frac{p_j \xi_\perp}{R^2} x_j Z(x_j) \tag{40}$$

where D_j is the j'th particle contribution to $|\mathbf{D}_\perp|$, $x_j = \omega/k_\| v_{Tj}$, and $Z(x)$ is the plasma dispersion function. The function $xZ(x)$ is in general complex, but $|xZ(x)| \lesssim 1$ for all x assuming $\omega_i > 0$. By noting that $F_\perp \sim k_\|^2 B^2 \xi_\perp/\mu_0$ and $k_\| R \sim n/q \sim 1$ for Alfvén waves it follows that

$$|\mathbf{D}_\perp/\mathbf{F}_\perp| \lesssim \beta. \tag{41}$$

This scaling result is important because in the low β limit it implies that the kinetic effects make only a small modification to the ideal MHD wave. In particular, the real part of $i\mathbf{D}_\perp$ leads to a small β correction in the basic dispersion relation $\omega \approx k_\| v_a$. The imaginary part of $i\mathbf{D}_\perp$ produces the kinetic dissipation effects that determine the growth rate and stability boundaries. Since $Im(i\mathbf{D}_\perp)$ is also small, it can be calculated perturbatively.

B General expression for the growth rate

In this section we make use of the low β ordering to derive a general expression for the growth rate of energetic particle Alfvén waves. The derivation is based on an energy relation obtained by multiplying Eq. (36) by $\boldsymbol{\xi}_\perp^*/2$ and integrating over the plasma volume. We assume $\delta \ll 1$ but temporarily treat $\beta \sim 1$. Using Eq. (32) we obtain

$$\omega^2 K_M = \delta W_M + \delta W_K \tag{42}$$

where

$$K_M = \frac{1}{2}\int \rho |\boldsymbol{\xi}_\perp|^2 d\mathbf{r} \tag{43}$$

is the plasma kinetic energy normalization,

$$\delta W_M = -\frac{1}{2}\int \boldsymbol{\xi}_\perp^* \cdot \mathbf{F}_\perp(\boldsymbol{\xi}_\perp) d\mathbf{r} \tag{44}$$

is the ideal MHD perpendicular potential energy and

$$\delta W_K = -\frac{i}{2}\int \boldsymbol{\xi}_\perp^* \cdot \mathbf{D}_\perp(\boldsymbol{\xi}_\perp) d\mathbf{r} \tag{45}$$

is the kinetic contribution to the energy. After a simple integration by parts, δW_K can be rewritten as

$$\delta W_K = \frac{i}{2}\sum_j \int (\omega - \hat{\omega}_{*j}) \frac{\partial F_j}{\partial \epsilon} s_j \frac{ds_j^*}{dt} d\mathbf{v} d\mathbf{r}. \tag{46}$$

The next step is to recognize that s_j is an integral along the unperturbed particle orbits as a function of the guiding center coordinates. Therefore,

$$\frac{ds_j^*}{dt} = i\omega^* s_j^* + D s_j^*. \tag{47}$$

where

$$D \equiv \mathbf{v}\cdot\nabla + \frac{q_j}{m_j}\mathbf{v}\times B_0 \cdot \nabla_v \tag{48}$$

If we write the complex quantity s_j as $s_j = a_j + ic_j$ and make use of Eq. (47), we obtain

$$s_j \frac{ds_j^*}{dt} = i\omega^* |s_j|^2 + i(c_j D a_j - a_j D c_j) + \frac{1}{2} D\left(a_j^2 + c_j^2\right). \tag{49}$$

Since F and $\hat{\omega}_*$ are functions of the constants of motion ϵ and p_ϕ, the contribution to δW_K from the last term in Eq. (49) is an exact differential that integrates to zero over the phase space volume. The quantity δW_K can thus be rewritten as

$$\delta W_K = \frac{1}{2}\sum_j \int (\omega - \hat{\omega}_{*j})\frac{\partial F_j}{\partial \epsilon}(\overline{R}_j + i\omega_i |s_j|^2) d\mathbf{v} d\mathbf{r} \tag{50}$$

where $\overline{R}_j$ is a real quantity given by

$$\overline{R}_j = c_j D a_j - a_j d c_j - \omega_r |s_j|^2. \tag{51}$$

Consider now the limit $\omega_i \ll \omega_r$ corresponding to either marginal stability or the low β assumption. A straightforward dimensional analysis using Eq. (39) shows that

$$\int \frac{\partial F_j}{\partial \epsilon}|s_j|^2 d\mathbf{v} d\mathbf{r} \lesssim \frac{\epsilon p_j \xi_\perp^2}{k_\parallel v_{Tj} \omega_i} \sim \frac{1}{\omega_i}. \tag{52}$$

Thus, the term $i\omega_i |s_j|^2$ in Eq. (50) leads to a finite contribution in δW_K as $\omega_i \to 0$. More subtlely, the $\overline{R}_j$ term in Eq. (50) also leads to a finite contribution of order $\beta_j \delta W_M$. This is a direct consequence of Eq. (41) and the discussion therein. The subtlety is that each of the separate terms in $\overline{R}_j$ diverge as $1/\omega_i$, but because of the general scaling argument associated with Eq. (41), these singularities must cancel identically.

The desired expression for the growth rate is obtained by setting the real and imaginary parts of Eq. (42) to zero and introducing the low β expansion. The real part yields

$$\omega_r^2 = \frac{\delta W_M}{K_M} + O(\beta). \tag{53}$$

The real frequency and eigenfunction correspond to the ideal MHD Alfvén wave.

In the limit $\omega_i \ll \omega_r$ consistent with low β, the imaginary part of Eq. (42) yields

$$\omega_i = \frac{W_K}{K_M + K_K} \tag{54a}$$

$$\approx \frac{W_K}{K_M} \tag{54b}$$

where

$$W_K = \lim_{\omega_i \to 0} \frac{-L}{\omega_i} \left[\frac{1}{4\omega_r} \sum_j \int (\hat{\omega}_{*j} - \omega_r) \frac{\partial F_j}{\partial \epsilon} \omega_i |s_j|^2 \right] d\mathbf{v} d\mathbf{r}$$

$$K_K = -\frac{1}{4\omega_r} \sum_j \int \frac{\partial F_j}{\partial \epsilon} \overline{R}_j d\mathbf{v} d\mathbf{r}. \tag{55}$$

Note that K_K is neglected in the second expression for ω_i since $K_K \sim \beta K_M$. Also, for rigid rotor distribution functions $\hat{\omega}_{*j} = \omega_{*j} = \text{const.}$

Equation (54b) is a general expression for the growth rate. It is valid for arbitrary aspect ratio and noncircularity but requires $\delta \ll \beta \ll 1$. Its evaluation requires a knowledge of the trajectory integral s_j along the unperturbed guiding center orbits. This can be carried out "exactly" numerically for realistic tokamak geometries, or evaluated approximately analytically using the additional assumption of large aspect ratio. For the usual case of $\partial F_j / \partial \epsilon < 0$, we see that a given species produces a stabilizing contribution to the dispersion relation when its diamagnetic frequency is less that the real frequency of the mode: $\hat{\omega}_{*j} < \omega_r$. The converse situation applies when $\hat{\omega}_{*j} > \omega_r$. The point of equality $\hat{\omega}_{*j} = \omega_r$ represents the transition from the positive to negative dissipation for the j'th species.

C The TAE growth rate

The general expression for the growth rate given by Eq. (54b) is now applied to the TAE instability. To proceed analytically we assume large aspect ratio as well as low β. Specifically, we assume a circular cross section tokamak satisfying the ohmic scaling expansion $\beta \sim \epsilon^2$, $q \sim 1$.

The analysis begins with the evaluation of the unperturbed particle orbits and the trajectory integral s_j. Consistent with the ohmic expansion, the leading order guiding center orbits are given by

$$r(t') = r(t)$$

$$\theta(t') = \frac{v_{\|} B_\theta}{r B_0}(t' - t) \qquad (56)$$
$$\phi(t') = \frac{v_{\|}}{R_0}(t' - t).$$

The particles lie on circular flux surfaces and move parallel to $\mathbf{B}$.

Next, note that within the tokamak expansion $\nabla \cdot \boldsymbol{\xi}_\perp + 2\boldsymbol{\xi}_\perp \cdot \boldsymbol{\kappa} \sim O(\epsilon^2)$ and $\boldsymbol{\kappa} = \mathbf{e}_R/R_0 + O(\epsilon^2/a)$ for Alfvén waves. Thus, to leading order ϵ, s_j reduces to

$$s_j = -m_j \int_{-\infty}^{t} \left(v_{\|}^2 + \frac{v_\perp^2}{2} \right) \frac{\xi_R}{R_0} dt'. \qquad (57)$$

Also note that both $v_{\|}$ and $v_\perp$ are constant to leading order in ϵ.

The integral s_j is evaluated by expanding the eigenfunction $\xi_r \equiv \xi$ as a general Fourier series

$$\xi = \sum_m \xi_m(r) e^{im\theta}$$
$$\xi_\theta = i \sum \frac{(r\xi_m)'}{m} e^{im\theta} \qquad (58)$$

where the second expression follows from the relation $\nabla \cdot \boldsymbol{\xi}_\perp \sim O(\epsilon)$. Substituting into Eq. (58) and focussing on circulating particles we obtain

$$s_j = \frac{i m_j}{2R_0} \left(v_{\|}^2 + \frac{v_\perp^2}{2} \right) \sum_m \left[\xi_{m-1} + \xi_{m+1} - \frac{(r\xi_{m-1})'}{m-1} + \frac{(r\xi_{m+1})'}{m+1} \right] \frac{e^{-i\omega t - in\phi + im\theta}}{\omega - \omega_m} \qquad (59)$$

where

$$\omega_m = \left(\frac{m}{q} - n \right) \frac{v_{\|}}{R_0}. \qquad (60)$$

Equation (59) is valid for both the TAE and EAE instabilities.

Consider now the TAE instability. This perturbation consists primarily of two toroidally coupled harmonics ξ_m and ξ_{m+1}. All other harmonics are essentially zero. Furthermore, the strongest coupling occurs in a narrow region of thickness $\sim \epsilon a$ localized about the surface $r = r_0$ corresponding to $q_0 \equiv q(r_0) = (2m+1)/2n$. The

mode localization implies that the $\xi'_{m\pm1}$ terms dominate in Eq. (59). Substituting these results into the expression for s_j and maintaining only those terms which do not average to zero in θ, leads to the following expression for $|s_j|^2$:

$$|s_j|^2 = \frac{m_j^2 r_0^2}{4R_0^2}\left(v_\parallel^2 + \frac{v_\perp^2}{2}\right)^2 \left[\frac{|\xi'_m|^2}{m^2} + \frac{|\xi'_{m+1}|^2}{(m+1)^2}\right]\left[\frac{1}{|\omega-\omega_{m-1}|^2} + \frac{1}{|\omega-\omega_m|^2}\right]. \tag{61}$$

In this expression all equilibrium quantities are evaluated on the surface $r = r_0$.

At this point the general expression for the growth rate [Eq. (54b)] can be simplified significantly by noting that for localized perturbations, the kinetic energy normalization reduces to

$$K_M \approx \frac{r_0^2\rho_0}{2}\int\left[\frac{|\xi'_m|^2}{m^2} + \frac{|\xi'_{m+1}|^2}{(m+1)^2}\right]dr \tag{62}$$

where $\rho_0 = \rho_i(r_0)$. Observe that K_M and $|s_j|^2$ have the same combination of ξ'_m and ξ'_{m+1} terms which thus cancel when evaluating ω_i. Using the fact that $\omega_r \approx k_\parallel v_a$ with $k_\parallel = 1/2R_0q_0$ for the TAE instability, we obtain the following expression for the growth rate

$$\frac{\omega_i}{k_\parallel v_a} = \lim_{\omega_i\to 0} L\sum_j \frac{\mu_0 m_j^2 q_0^2}{2B_0^2}\int\left(v_\parallel^2 + \frac{v_\perp^2}{2}\right)^2\left(\omega_r\frac{\partial F_j}{\partial\epsilon} - \frac{n}{q_j}\frac{\partial F_j}{\partial\Psi}\right)\left[\frac{\omega_i}{|\omega-\omega_{m-1}|^2} + \frac{\omega_i}{|\omega-\omega_m|^2}\right]dv. \tag{63}$$

In the limit of small ω_i, the $v_\parallel$ integral can be carried out analytically. A short calculation yields

$$\frac{\omega_i}{k_\parallel v_a} = \sum_j\left[\frac{2\pi^2\mu_0 m_j^2 R_0 q_0^3}{B_0^2}\int\left(v_\parallel^2 + \frac{v_\perp^2}{2}\right)^2\left(\omega_r\frac{\partial F_j}{\partial\epsilon} - \frac{n}{q_j}\frac{\partial F_j}{\partial\Psi}\right)v_\perp dv_\perp\right]\Bigg|_{v_\parallel=v_a} + \Bigg|_{v_\parallel=v_a/3}. \tag{64}$$

Equation (64) gives the TAE growth rate for arbitrary distribution functions $F_j(\epsilon,\Psi)$.

The growth rate can be easily evaluated for a Maxwellian distribution function

$$F_j = n_j\left(\frac{m_j}{2\pi T_j}\right)^{3/2}\exp(-m_j v^2/2T_j). \tag{65}$$

Here $n_j = n_j(\Psi)$ and $T_j = T_j(\Psi)$. Some straightforward algebra leads to

$$\left(\frac{\omega_i}{k_\| v_a}\right)_j = -q_0^2 \beta_j \left[G^T_{mj} - n q_0 \delta_j \frac{(H^T_{mj} + \eta_j J^T_{mj})}{1+\eta_j} \right] \tag{66}$$

where $\beta_j = 2\mu_0 n_j T_j / B_0^2$, $\delta_j = -r_{L\theta}(dp_j/dr)/p_j$, $r_{L\theta} = v_{Tj}/\Omega_{\theta j}$, $\Omega_{\theta j} = q_j B_p / m_j$ and $\eta_j = d\ln T_j / d\ln n_j$. Each of these quantities is evaluated at $r = r_0$. The functions G_j^T, H_j^T and J_j^T are functions of the single parameter $\lambda_j = v_a / v_{Tj}$ and are given by

$$\begin{aligned}
G^T_{mj} &= g_m(\lambda_j) + g_m(\lambda_j/3) \quad g(\lambda_j) = \frac{\pi^{1/2}}{2}\lambda_j(1+2\lambda_j^2+2\lambda_j^4)e^{-\lambda_j^2} \\
H^T_{mj} &= h_m(\lambda_j) + \frac{1}{3}h_m(\lambda_j/3) \quad h_m(\lambda_j) = \frac{\pi^{1/2}}{2}(1+2\lambda_j^2+2\lambda_j^4)e^{-\lambda_j^2} \\
J^T_{mj} &= j_m(\lambda_j) + \frac{1}{3}j_m(\lambda_j/3) \quad j_m(\lambda_j) = \frac{\pi^{1/2}}{2}(3/2+2\lambda_j^2+\lambda_j^4+2\lambda_j^6)e^{-\lambda_j^2}.
\end{aligned} \tag{67}$$

The Maxwellian distribution function is a good approximation for electrons and ions. For these species the parameter δ_j (the ratio of poloidal gyroradius to pressure scale length) satisfies $\delta_j \ll 1$. Consequently only the G_j^T term need be maintained.

For the alpha particles it is more reasonable to assume a slowing down distribution. A simple model that has the correct asymptotic behavior and allows a simple evaluation of the integrals is as follows

$$F_\alpha = \frac{A}{(v^2+v_0^2)^{3/2}} \qquad 0 < v < v_\alpha \tag{68}$$

where $A = A(\Psi)$ and $v_0^2 = v_0^2(\Psi)$ are two free functions that are easily related to the density and temperature. The quantity v_0^2 represents the low velocity transition to the bulk plasma. Typically $m_\alpha v_0^2/2 \approx 2T(\Psi)$ where T is the bulk plasma temperature. The cutoff velocity v_α is defined by $m_\alpha v_\alpha^2/2 \equiv E_\alpha = 3.5$ MeV. Clearly $v_\alpha^2 \gg v_0^2$. After another straightforward calculation we obtain an analogous expression for the alpha particle contribution to the growth rate

$$\left(\frac{\omega_i}{k_\| v_a}\right)_\alpha \approx -q_0^2 \beta_\alpha (G^T_{s\alpha} - n q_0 \delta_\alpha H^T_{s\alpha}) \tag{69}$$

with $\beta_\alpha = 2\mu_0 n_\alpha T_\alpha / B_0^2$, $\delta_\alpha = -(2/3) r_{L\theta}(dp_\alpha/dr)/p_\alpha$, $r_{L\theta} = v_\alpha/\Omega_{\theta\alpha}$, and $\Omega_{\theta\alpha} = q_\alpha B_p / m_\alpha$. The functions G and H are functions of the parameter $\lambda_\alpha = v_a/v_\alpha$ and can be written as

$$G^T_{s\alpha} = g_s(\lambda_\alpha) + g_s(\lambda_\alpha/3) \quad g_s(\lambda_\alpha) = \left(\frac{3\pi}{16}\right)\lambda_\alpha(3 + 4\lambda_\alpha - 6\lambda_\alpha^2 - \lambda_\alpha^4)H(1-\lambda_\alpha)$$
$$H^T_{s\alpha} = h_s(\lambda_\alpha) + \frac{1}{3}h_s(\lambda_\alpha/3) \quad h_s(\lambda_\alpha) = \left(\frac{3\pi}{16}\right)(1 + 6\lambda_\alpha^2 - 4\lambda_\alpha^3 - 3\lambda_\alpha^4)H(1-\lambda_\alpha). \tag{70}$$

Here H is the Heaviside step function.

The final form of the growth rate is obtained by combining these expressions and assuming $n_i \approx n_e \equiv n$, $T_e \approx T_i \equiv T$

$$\frac{\omega_i}{k_\parallel v_a} = -q_0^2\left[\frac{\beta_c}{2}(G^T_{mi} + G^T_{me}) + \beta_\alpha(G^T_{s\alpha} - n q_0 \delta_\alpha H^T_{s\alpha})\right]. \tag{71}$$

where $\beta_c = 4\mu_0 nT/B_0^2$ is the core beta. Equation (71) is a more accurate expression of the TAE growth rate than that given in the original work of Fu and Van Dam,[5] where the effect of the ion Landau damping was not included. Applications of Eq. (71) are discussed shortly.

D The EAE growth rate

We consider the EAE in the limit of small ellipticity ($\kappa - 1 \ll 1$). The strongest coupling occurs about the $q \simeq q_0 = (m+1)/n$ surface and the perturbation consists primarily of two elliptically coupled harmonics m and $m+2$. Following the same procedures used for the TAE, the expression for $|s_j|^2$ becomes

$$|s_j|^2 = \frac{m_j^2 r_0^2}{4R_0^2}\left(v_\parallel^2 + \frac{v_\perp^2}{2}\right)^2 \left\{\left[\frac{|\xi'_m|^2}{m^2} + \frac{|\xi'_{m+2}|^2}{(m+2)^2}\right]\frac{1}{|\omega - \omega_{m-1}|^2} + \left|\frac{\xi'_{m+2}}{m+2} - \frac{\xi'_m}{m}\right|^2 \frac{1}{|\omega - \omega_{m+1}|^2}\right\}.$$

Notice that, unlike the TAE, K_M and $|s_j|^2$ do not have the same combination of ξ'_m and ξ'_{m+2}. Thus, the lowest order eigenfunctions given in Ref. [8] are needed. As for

the TAE, the largest contribution comes from the resonant layer about the $q = q_0$ surface. In the limit of small ω_i and using a slowing down distribution function for the alphas, the growth rate has the following form

$$\frac{\omega_i}{k_{\|} v_a} = -\left(\frac{q_0}{2}\right)^2 \left[\frac{\beta_e}{2}\left(G^E_{mi} + G^E_{me}\right) + \beta_\alpha \left(G^E_{s\alpha} - \frac{nq_0}{2}\delta_\alpha H^E_{s\alpha}\right)\right] \qquad (72)$$

where

$$G^E_{mj} = g_m(\lambda_j/2) + \int dx g_m(u_{nj}/|y|)F(\xi')$$

$$G^E_{s\alpha} = g_s(\lambda_\alpha/2) + \int dx g_s(u_{n\alpha}/|y|)F(\xi')$$

$$H^E_{s\alpha} = \frac{1}{2}h_s(\lambda_\alpha/2) + \int dx \frac{u_{n\alpha}/|y|}{\lambda_\alpha} h_s(u_{n\alpha}/|y|)F(\xi')$$

$$F(\xi') = \left|\frac{\xi'_{m+2}}{m+2} - \frac{\xi'_m}{m}\right|^2 \Bigg/ \int \left(\left|\frac{\xi'_{m+2}}{m+2}\right|^2 + \left|\frac{\xi'_m}{m}\right|^2\right) dx$$

$$u_{nj} = \frac{2n}{q_0\Delta'}\lambda_j \quad u_{n\alpha} = \frac{2n}{q_0\Delta'}\lambda_\alpha \quad dx = 2\pi^2 \frac{R_0 r_0^2 \Delta'}{s_0} dy$$

$$y = \frac{2s_0}{\Delta'}\left(\frac{r - r_0}{r_0}\right) \quad s_0 = \frac{r_0 q_0'}{q_0} \qquad \Delta' = \left(r\frac{\kappa(r) - 1}{2}\right)'\Bigg|_{r_0}$$

Applications of Eq. (72) are also discussed shortly.

E The NAE growth rate

The Noncircular Triangularity Induced Alfvén Eigenmode (NAE) which results from triangular coupling is localized about the $q \simeq q_0 = (2m+3)/2n$ surface and consists primarily of the two harmonics m and $m+3$. The procedure to calculate the growth rate is identical to that used for the TAE and in the limit of small triangularity, the mode is highly localized so that the growth rate is independent of the eigenfunction (as for the TAE). It is easy to show that using a slowing down distribution function for the alphas, the NAE growth rate has the form

$$\frac{\omega_i}{k_{\|} v_a} = -\left(\frac{q_0}{3}\right)^2 \left[\frac{\beta_e}{2}\left(G^N_{mi} + G^N_{me}\right) + \beta_\alpha \left(G^N_{s\alpha} - \frac{nq_0}{3}\delta_\alpha H^N_{s\alpha}\right)\right] \qquad (73)$$

where

$$G^N_{mj} = g_m(3\lambda_\alpha) + g_m(3\lambda_j/5)$$

$$G^N_{s\alpha} = g_s(3\lambda_j) + g_s(3\lambda_\alpha/5)$$

$$H^N_{s\alpha} = 3h_s(3\lambda_\alpha) + (3/5)h_s(3\lambda_\alpha/5)$$

F The growth rate of a continuum Alfvén wave

In this section we calculate the growth of an Alfvén wave of the continuum spectrum. A detailed derivation can be easily found in the literature[9,10]. The purpose of this treatment is to make the reader familiar with the analysis of the continuum Alfvén waves that will be used later to estimate the so called "continuum damping" on gap modes. The stability analysis of the Alfvén wave of the continuum spectrum is inherently more complicated of that of a global mode. In the latter case the kinetic effects do not affect the lowest order eigenfunction, and therefore, can be treated in a perturbative fashion. In contrast, an Alfvén wave of the continuous spectrum is highly localized in a narrow region $\Delta r \sim (\omega_i/\omega_r)r_0$ about the $\omega_A(r_0) = \omega_r$. Since ω_i is related to the kinetic effects, then the eigenfunction itself must be derived retaining the lowest order kinetic terms. A rigorous derivation of the eigenvalue equation for Kinetic-MHD modes will be given in Chapter 5. We now present a very simple way to derive an approximate form of the eigenvalue equation starting from the energy relation given in Eq. (42) which was derived by assuming a continuous eigenfunction. The derivation is greatly simplified by assuming apriori that the mode is localized about the $r = r_0$ surface. In particular, we postulate that in the neighborhood of the resonant surface the eigenfunction assumes a logarithmic behavior, as in the ideal MHD treatment. Following the procedure of Sec. 2.4, we define the singular part of the eigenfunction ξ_s as a function with a logarithmic behavior at $r = r_0$ and that satisfies the boundary conditions at $r = 0$ and $r = a$. Furthermore, we define the regular part as $\xi_r = \xi - \xi_s$. As stated, ξ_s is going to be important only in a narrow layer of thickness $\delta = r_0\omega_i/\omega_r << 1$.

The next step is to rewrite the energy relation to lowest order in δ. Consider the real part first. Notice from Eq. (41) that $Real[\delta W_k] \sim \beta \delta W_M$, and therefore only the fluid contribution must be retained. The kinetic energy normalization can be simplified maintaining only those terms which do not average to zero in θ. To lowest order in δ,

$$K_M \simeq \frac{1}{2} r_0^2 \rho_0 \int \frac{|\xi'_{sm}|^2}{m^2} d\mathbf{r}. \tag{77}$$

We then consider the imaginary part of the energy relation and notice that to calculate $Im[\delta W_K]$ we need to perform the integration along the orbits in the term s_j. Following the procedure developed in Sec. C , s_j can be written in the following form,

$$|s_j|^2 = \frac{m_j^2 r_0^2}{4R_0^2} (v_{\|}{}^2 + \frac{v_\perp{}^2}{2}) \frac{|\xi'_{sm}|^2}{m^2} \Big[\frac{1}{|\omega - \omega_{m-1}|^2} + \frac{1}{|\omega - \omega_{m+1}|^2} \Big]. \tag{78}$$

In these expressions all equilibrium quantities are evaluated at the surface $r = r_0$ and $\omega_m = k_{\|m} v_{\|}$. The integration over the phase space in $Im[\delta W_K]$ is now split into an integration over the real space of a function of $\mathbf{r}$ and an integration over the velocity space of a function of $\mathbf{v}$ only

$$Im[\delta W_K] \simeq K_M(\xi_s)(2\omega_r \gamma_k) \tag{79}$$

where

$$\gamma_k = \lim_{\omega_i \to 0} \frac{1}{8\omega_r R_0^2 \rho_0} \sum_j \int d\mathbf{v} (v_{\|}{}^2 + \frac{v_\perp{}^2}{2})^2 \frac{\partial F_j}{\partial \epsilon} (\omega - \hat{\omega}_{*j}) \Big[\frac{1}{|\omega - \omega_{m-1}|^2} + \frac{1}{|\omega - \omega_{m+1}|^2} \Big]. \tag{80}$$

To lowest order in δ, the energy relation can be written in the following form

$$(\omega^2 - i2\omega_r \gamma_k) K_M(\xi_s) = \delta W_M + O(\delta). \tag{81}$$

As previously mentioned, δW_M is a real quantity. The growth rate of the mode easily follows

$$\omega_i = \gamma_k + O(\delta). \tag{82}$$

In order to find the eigenfunction of the mode, we derive the Euler-Lagrangian equation from Eq. (81). To leading order in δ, we obtain

$$\frac{d}{dx}(\omega^2 - \omega_A^2(r_0) - i2\omega_r\gamma_k)\frac{d\xi_s}{dx} = 0$$

where we have introduced the normalized coordinate $x = (r - r_0)/r_0$. Away from the singular layer, the kinetic effects do not play an important role and the Alfvén wave equation reduces to

$$\frac{d}{dx}(\omega^2 - \omega_A^2(r_0))\frac{d\xi_s}{dx} = 0 \tag{83}$$

An approximate form of the Alfvén wave equation, valid in the whole domaine $[0, a]$, can be written in the following form

$$\frac{d}{dr}\rho r_0^3(\omega^2 - \omega_A^2(r) - i2\omega_r\gamma_k)\frac{d\xi}{dr} - (m^2 - 1)\rho r(\omega^2 - \omega_A^2(r) - i2\omega_r\gamma_k)\xi = 0. \tag{84}$$

Eq.(84) is identical to the eigenvalue equation given in Ref.[9-11] in the limit of zero ion Larmor radius. In the narrow layer $r \simeq r_0$ of thickness δ, Eq. (84) yields the following solution

$$\xi_s = A + B\ln(i\hat{x} + \hat{\gamma}) \tag{85}$$

where we have introduced the two dimensionless variables

$$\hat{x} = sgn(\omega_r\frac{d\ln\omega_A^2}{dr})\frac{d\ln\omega_A^2}{dr}(r - r_0)$$

$$\hat{\gamma} = 2(\omega_i - \gamma_k)/|\omega_r|. \tag{86}$$

According to the expression for the growth rate given in Eq. (82), it follows that $\hat{\gamma} \simeq 0$ and the eigenfunction become dicontinuous at $r = r_0$ contradicting the initial assumption used in the derivation of the energy relation that the eigenfunction be continuous. In order to solve the problem correctly, the fourth order FLR effects should be retained and the discontinuity be removed. Such a problem has been investigated in Ref.[9] where the fourth order eigenvalue equation is numerically solved leading to a continuous eigenfunction and to a growth rate almost identical

to the one given by Eq. (82). The differences in the growth rate is due to the higher order terms in ρ_{Li}/a, to the sideband coupling induced by toroidicity and to the inclusion of the parallel electron Landau damping.

4.4 The continuum damping of gap modes

In this section we investigate an additional physical mechanism that is usually, but not always, stabilizing for Alfvén gap modes. In the previous chapter we considered gap modes whose frequency does not intersect the Alfvén continuum. For realistic density profiles or for modes with $m > 1$, an Alfvén wave of the continuum can have the same frequency as a gap mode with the same m number. Fig. 5 shows the continuum spectrum of an elliptic plasma column for $n = 2, m = 2 - 4$. The intersection with the continuum of an $(n = 2, m = 2-4)$ EAE is also shown. In this case, one can think of the gap mode as a global mode except near the resonance with the continuum where the eigenfunction exhibits a logarithmic singularity, and therefore, is highly localized. Two important effects occur when this resonance takes place; first, the electric field in the narrow region about the resonant point is so large that the contribution to the plasma inertia from the $E \times B$ drift originating in the layer considerably slows the mode down. Second, the Alfvén wave of the continuum spectrum can be damped (or excited); and consequently, it can further stabilize (or destabilize) the global gap mode. We show in this section that the overall effect is always stabilizing.

We consider a gap mode induced by the coupling of the two harmonics m and p, and we assume that the continuum spectrum of the mth harmonic intersects with the real frequency of the gap mode at the surface $r = r_0$. As shown in Sec. (2.3), the eigenfunction of the mth harmonic has a logarithmic behavior about $r = r_0$. We decompose the eigenfunction in a regular and a singular part ξ_s such that

$$\xi_{sm} \simeq A + B \ln(\hat{x} + \hat{\gamma}) \tag{87}$$

$$\xi_r = \xi - \xi_s \tag{88}$$

where $\hat{x}$ is the normalized radial coordinate

$$\hat{x} = sgn(\omega_r \frac{d \ln \omega_A^2}{dr_0}) \frac{d \ln \omega_A^2}{dr_0} (r - r_0) \tag{89}$$

and $\hat{\gamma} \sim \omega_i/\omega_r$ is a parameter which will be defined later. Because of the poloidal coupling, the eigenfunction of the pth harmonic is also expected to have a logarithmic singularity at $r \simeq r_0$. However, for small coupling ($\epsilon << 1$), the singular part of ξ_p will be of order ϵ with respect to the singular part of ξ_m.

We also introduce the parameter γ_g which represents the growth rate of the gap mode in the absence of continuum resonance as derived in Sec. 4.3. It is very important to order the constant B in Eq. (87) such that the new effects give a contribution to the growth rate of the same order of γ_g. There is no obvious small parameter that characterizes the solution in the neighborhood of the continuum damping. Even so, we introduce a maximal ordering

$$\frac{B}{\xi_r} \sim (\frac{\hat{\gamma}}{\epsilon})^{1/2} << 1 \tag{90}$$

where $\xi_r = \xi - \xi_s$, ϵ is the small poloidal coupling parameter and $\hat{\gamma} << \epsilon$. Only a posteriori, we will derive the condition on the equilibrium configuration that guarantees the inequality in Eq. (90). The next step is to rewrite the energy relation [Eq.(42)] in terms of ξ_r and ξ_s. Since the interaction occurs with the continuum spectrum of the mth harmonic, we expect the contribution coming from the coupled harmonic p in the neighborhood of the continuum resonance to be negligible. According to the previous ordering, the kinetic energy normalization and the imaginary part of the δW_K can be written as

$$K_M(\xi) = K_M(\xi_r) + K_M(\xi_{sm}) + O(\epsilon) \tag{91}$$

$$Im[\delta W_K] = 2\omega_r \gamma_g K_M(\xi_r) + 2\omega_r \gamma_k K_M(\xi_{sm}) + O(\epsilon) \tag{92}$$

where

$$K_M(\xi_r) = \frac{1}{2} \int d\mathbf{r} \rho |\xi_r|^2 \tag{93}$$

$$K_M(\xi_s) = \frac{1}{2}\int dr\rho|\xi_{sm}|^2$$

and γ_k is the growth rate of a continuum Alfvén wave located at $r = r_0$ given in Eq. (80). The cross terms in Eq. (93) have been neglected because they contribute through a term of order $(\hat{\gamma}\epsilon)^{1/2}$. As previously shown, the real part of the δW_K can be neglected with respect to the fluid potential energy. To lowest order in ϵ the energy relation can be written in the following form.

$$L(\xi_r) = -L(\xi_{sm}) \tag{94}$$

with

$$L(\xi_r) = (\omega^2 - i2\omega_r\gamma_g)K_M(\xi_r) + \delta W_M(\xi_r) \tag{95}$$

$$L(\xi_s) = (\omega^2 - i2\omega_r\gamma_k)K_M(\xi_s) + \delta W_M(\xi_s) \tag{96}$$

This form of the energy relation also includes higher order terms in ϵ, that we keep only for convenience. Notice that to lowest order in ϵ the singular and the regular part of the eigenfunction give separate contributions. It is important to remember that ξ_s and ξ_r represent the solution of the eigenvalue equation in the two regions; i.e., inside the singular layer ($|r - r_0|/r_0 \sim \hat{\gamma}$) and outside ($|r - r_0|/r_0 > \hat{\gamma}$) respectively. The two functionals $L(\xi_r)$ and $L(\xi_s)$ are quadratic forms of ξ_r and ξ_s. Taking the variations of the functional, with respect to ξ_r and ξ_s, and setting it to zero for arbitrary $\delta\xi_s$ and $\delta\xi_r$, leads to two equations valid in different regions. For $|r - r_0|/r_0 > \hat{\gamma}$ the minimization of $L(\xi_r)$ yields the following equation for ξ_r

$$D(\gamma_g)\xi_{rm} - \epsilon F\xi_{rp} = 0$$

$$D(\gamma_g)\xi_{rp} - \epsilon F\xi_{rm} = 0 \tag{97}$$

where

$$D(\Gamma) = \frac{d}{dr}\rho r^3(\omega^2 - i2\omega_r\Gamma - \omega_A^2)\frac{d}{dr} - (m^2 - 1)\rho r(\omega^2 - i2\omega_r\Gamma - \omega_A^2) \tag{98}$$

$$F = r_g^3\rho(r_g)\omega^2\frac{d^2}{d^2r} \tag{99}$$

and r_g is the gap location. For $|r - r_0|/r_0 \sim \hat{\gamma}$ the minimization of $L(\xi_{sm})$ yields the following singular layer equation for ξ_{sm}

$$D(\gamma_k)\xi_{sm} = 0. \tag{100}$$

The solution of Eq. (100) in the narrow layer around the continuum resonance surface can be readily derived, yielding

$$\xi_{sm}(r \simeq r_0) = A + B\ln(i\hat{x} + \hat{\gamma}) \tag{101}$$

where

$$\hat{\gamma} = 2\frac{\omega_i - \gamma_k}{\omega_r}. \tag{102}$$

If $\gamma_k < 0$ then $\hat{\gamma} > 0$ readily follows. If $\gamma_k > 0$, assuming $\hat{\gamma} > 0$ implies that the growth rate is larger than that of a continuum Alfvén wave localized at $r = r_0$. In order to keep the eigenfunction continuous through the continuum resonance surface, we assume $\hat{\gamma} > 0$. The derivation of the parameter B will be given in Appendix C. Assuming $\gamma_g << \epsilon$, the solution of Eq. (97) gives the gap mode eigenfunction without interaction with the continuum that was derived in Sec. 2.5 and 2.6. The next step is to explicitly calculate the imaginary part of the energy relation [Eq. (94)], by substituting the expression for the eigenfunction. To lowest order in $\hat{\gamma}$ the kinetic energy contribution coming from ξ_{sm} gives

$$K_M(\xi_{sm}) = \frac{1}{2}\rho_0 r_0^2 \int dr \frac{|\xi'_{sm}|^2}{m^2}. \tag{103}$$

The integration over the singular layer $r - r_0/r_0 \sim \hat{\gamma}$ can be easily carried out yielding

$$K_M(\xi_{sm}) \simeq \frac{4\pi^3 R_0 \rho_0}{|\omega_i - \gamma_k|} r_0^3 |B|^2 |\frac{d\omega_A}{dr}|_{r_0} \tag{104}$$

Sustituting into Eq. (94) leads to the following form of the gap mode growth rate

$$\omega_i = \gamma_g - \Gamma \tag{105}$$

where

$$\Gamma = \frac{4\pi^3 R_0 r_0^3 \rho_0 |B|^2}{K_M(\xi_r)} |\frac{d\omega_A}{dr}|. \tag{106}$$

In the case of $\hat{\gamma} < 0$, the eigenfunction is discontinuous and a procedure similar to the one developed in Sec. (2.4) can be applied. It is easy to show that the growth rate of the gap mode would be identical to the one given in Eq. (105) derived for $\hat{\gamma} > 0$. It is important to notice that the interaction with the continuum always leads to a damping, despite the destabilizing nature of the kinetic effects in the continuum resonance layer. This result is consistent with the one obtained in Ref. [12] where the limit $\gamma_k = 0$ was considered. It can be easily seen that setting $\gamma_k = 0$, the result remains unchanged.

In Appendix C we derive an easy way to evaluate the term B in Eq. (106) and we show that an appropriate ordering is $\Gamma \sim \epsilon^3$. Since $\gamma \sim \beta\omega_A$ with $\beta \sim \epsilon^2$ we will neglect the continuum damping effect in the remainder of this Chapter. Although the continuum damping appears to be a small effect, a more carefull investigation of its effect is certainly needed.

4.5 Discussion

In this section we analyze in detail the dispersion relations for gap modes given in Eqs. (71), (72) and (74). Marginal stability conditions can be easily evaluated by setting $\omega_i = 0$. In order to find the parameter $\beta_\alpha = 2\mu_0 n_\alpha T_\alpha / B_0^2$, we first calculate T_α from the α equilibrium distribution function

$$n_\alpha T_\alpha = \frac{1}{3} m_\alpha \int v^2 f_\alpha d^3\mathbf{v}.$$

For an isotropic slowing down distribution function with a cutoff energy E_α, the temperature is approximately constant and is given by $T_\alpha \simeq E_\alpha/6$. The α particle density can be obtained by balancing the production with the slowing down rate

$$\langle \sigma v \rangle \frac{n_e^2}{4} = \frac{n_\alpha}{\tau_s}.$$

where $\tau_s = 1.17\ 10^{12}[T_e(keV)]^{3/2}/n_e(cm^{-3})$ is the slowing down time. If we assume that $T_e \simeq T_i$, then the marginal stability condition for the TAE and NAE can be written in the form

$$n_e^{T.N} = n_e^{T.N}(T_e, B_0, q(r), a, R_0, m, n). \tag{75}$$

Since the growth rate of the EAE depends on the mode eigenfunctions, the dependence on the plasma elongation must be included and the EAE marginal stability condition becomes

$$n_e^E = n_e^E(T_e, B_0, q(r), \kappa(r), a, R_0, m, n). \tag{76}$$

Stability domains in the (n_e, T) space, for typical ignition experiment parameters ($B_0 = 8$ T, $q_0 \simeq 1$, $q_a \simeq 3.5, \kappa(a) = 1.8, a = .78, R_0 = 2.4$) are illustrated in Fig. 6. Instability occurs in a well defined range $n_{min} < n < n_{max}$. The lower boundary occurs when the Alfvén velocity becomes so high that there are no resonant α particles, while the higher limit occurs when the ion or the electron Landau damping becomes dominant. For the BPX operational density of $n_0 \simeq 5 \times 10^{20}$ m^{-3} and

temperature of $T_0 \simeq 20$ keV the $m = 1, n = 1$ gap modes seem to be stable. Modes with $m > 1, n > 1$ show a lower instability threshold and therefore are more likely to be destabilized in a burning plasma. In particular the EAE $m = 3, n = 3$ seems to pose a potential threat to a BPX-like device.

Several interesting conclusions can be extracted from Eqs. (71), (72) and (73). First, we observe that for large β, the resonance $v_{||} = v_a/3$ of the TAE strongly enhances the ion Landau damping. This explains the stability domain of the TAE at high plasma densities as shown in Fig. 7.

The next point to note is that the electron Landau damping in highly elongated plasmas strongly stabilizes low-n EAEs. Figure 8 shows the EAE $(m = 1, n = 1)$ stability boundaries for different values of the plasma elongation.

Finally we observe that for all three gap modes the destabilizing terms is proportional to the product nq_0. Therefore, we expect the high-m modes to be the most unstable as shown in Fig. 6.

In the derivation of the gap mode growth rates, the effects of continuum damping and trapped particle resonance have not been included. The latter is expected to be important for high-n modes. Finally, because of the limits of validity $\epsilon \ll 1, \kappa - 1 \ll 1, \delta \ll 1$, low (m, n) the expressions (71), (72) and (73) can only be considered as an approximate criterion to test stability against Alfvén gap modes.

4.6 Conclusions

We have demonstrated that two new global Alfvén modes, the Ellipticity and Triangularity Induced Alfvén Eigenmodes, can be destabilized via transit resonance with energetic alpha particles. The growth or damping of these modes depends upon a competition between the alpha particle driver, electron and ion Landau damping. The electron Landau damping turns out to be particularly important for the $m = 1$, $n = 1$ EAE in highly elongated plasmas ($\kappa \sim 2$). We have also

shown that ion Landau damping can stabilize the TAE at high density regimes. For sufficiently high densities and $n > 1$ the EAE can have a stability threshold lower than that of the TAE. Both the EAE and TAE need further investigation to determine how detrimental their effects can be on alpha particle confinement in ignited tokamaks. In particular, the behavior of higher n modes which have lower thresholds, but greater localization needs to be addressed[12]. For these modes the effect of continuum damping becomes very important beacuse of the multiple interactions with the continuum spectrum. Although the procedure to calculate the continuum damping given in this Chapter is restricted to the case of one interaction only, a more general theory can be developed starting from the results obtained in Sec. 4. For a more detailed theory on the continuum damping effects on the TAE modes we refer the reader to Refs [12-13].

CHAPTER 5.

The eigenvalue problem of the kinetic-MHD. Internal kink.

5.1 Introduction

Since the original discovery [1] of "sawtooth" oscillations in the ST tokamak, there has been considerable interest in the theory of $m = 1$ modes. These modes are believed to constitute the initial trigger for the observed crash in the central plasma temperature that is the signature of the sawtooth (the temperature rises in time to a maxiumum value at which point it crashes abruptly; the process is repeated in a cyclical fashion giving rise to a time-trace resembling the teeth of a saw). Following the intital [2] description of the physics of the sawtooth, much work has been done to put the modelling on a firmer foundation. The basic picture involves a central portion of the plasma column where the inverse rotational transform $q(r) = rB_\phi/RB_\theta$ is below unity (we consider circular magnetic flux surfaces, at first, for simplicity; B_ϕ and B_θ are the toroidal and poloidal components of the magnetic field, respectively, while r is the variable along the minor radius of the tokamak, $r \leq a$, and R is the major radius). This central portion is subjected to a rigid body displacement with toroidal and primary poloidal mode numbers $n = 1$ and $m = 1$. At the boundary, $r = r_s$ where $q(r_s) = 1$, the mode has its greatest spatial variation and is subject to non-ideal MHD effects, namely tearing and reconnection of magnetic field lines. This reconnection process leads to a re-arrangement of magnetic flux and concomitant expulsion of the hot plasma core (in the case of a

"full sawtooth crash"). The re-arrangement leads to a situation where $q(r=0) \geq 1$ (thereby removing the condition that permitted the instability in the first place) while the expulsion of the core is detected as a drop in the central temperature (the "crash").

Much numerical work has been devoted to the modelling of the nonlinear phase of the instability, a necessary process if one is to understand the crash itself. This work has, for the most part, been based on a set of reduced resistive MHD equations. On the other hand, recent experiments in high temperature plasmas [3]-[4] have resulted in sawtooth-free operation for periods of several seconds. The only acceptable explanation, to date, has involved the kinetic response of a population of energetic trapped particles (e.g., ions energized by Ion Cyclotron Resonant Heating whose precession drift frequency is greater than the mode frequency) [5]-[10]. This population of energetic particles tends to act as a "rigid anchor" against the motion imposed by the perturbation, hence providing the necessary stabilizing effect. Thus, interest has been focussed on kinetic effects within the $q(r) \leq 1$ region.

Also, in the frame of ideal MHD the $m=1, n=1$ ideal kink mode is predicted to be stable in most of the discharges where sawtooth activity has been observed. The resistive kink has been initially proposed as the only possible candidate to explain the experimental results. Only recently, experiments in JET have shown that in most of the sawtooth crashes there is no reconnection occuring and the mode resembles the characteristics of an ideal mode. The so-called quasi-interchange mode (which is an ideal mode) was then proposed by J. Wesson to be responsable for the sawtooth oscillations. In order to match the experimental data with the theory of the quasi-interchange, the value of the safety factor on axis had to be only few percent less the unity. Later on, experimental measurements of $q(0)$ have shown that $q(0)$ is well below unity during the whole sawtooth period.

Because of the strong disagreement between fluid theory and experiments, in this Chapter we investigate whether the kinetic response of bulk ions and electrons can lead to new developments in the linear theory of $n=1, m=1$ modes and

eventually to be usefull to explain experimental obervations. We address this issue of the kinetic response of the plasma ions and electrons (although the theory is valid for any particle species), within the $r \leq r_s$ region, where toroidal effects are of importance. We show how the kinetic response of trapped ions can destabilize the high frequency ($\omega \simeq \omega_{*i}$) branch of the kink mode. This instability , denoted as Kinetic Kink Mode is driven by both the resonant and nonresonant trapped particle response within the $q(r) < 1$ surface.

Although we are mostly concern with the interanl kink, the general eigenvalue problem of kinetic-MHD is treated in this Chapter. Its applications are of interest to high frequency Alfvén waves ($\omega \sim \omega_A$) as well as low frequency perturbations ($\omega \sim \omega_{*i}$). We include the effects of an equilibrium electric field and a parallel perturbed electric field which we derive from the electron momentum conservation equation. After the general derivation we derive the eigenvalue equation for gap modes and for the $m = 1$ internal kink. In the region away from the singular layer (about the $q = 1$ surface for the internal kink, and about the gap region for the gap modes) the MHD gauge $A_{||} = 0$ will be adopted and the electron inertia will be neglected. In the inner region (about the singular layer) the effect of the $A_{||}$ will be retained only for the $m = 1, n = 1$ kink mode and not for the gap modes. Neglecting $A_{||}$ in the gap region is usually a good assumption only when the width of the inner layer is large enough so that no large parallel currents are present, i.e. when the gap mode has a global structure. The dispersion relation derived in Sec. 8 for the $m = 1$ mode including the effects of $A_{||}$ through the retention of a finite resistivity, will only be solved in the "ideal case" ($\eta \rightarrow 0$). The hard task of numerically solving the dispersion relation in the resistive kink and reconnecting mode regimes represents important work for the future.

An outline of this Chapter can be given as follows. In Sec. 5.2-5.6 , we derive a general form of the momentum conservation equation for the outer region ($A_{||} = 0$) , including the kinetic response of trapped and circulating particles. In Sec. 5.7 we consider the high frequency limit ($\omega > \omega_{*i}$) and derive the eigenvalue equation

for shear Alfvén waves in toroidal geometry. In Sec.5.8 the low frequency limit is studied ($\omega \simeq \omega_{*i}$) and the stability of the $m = 1$ internal kink is investigated (Sec. 5.9). The conclusions are given in Sec. 5.10.

5.2 Model

Consider a plasma consisting of bulk ions, bulk electrons, and an energetic ion species such as alpha particles or neutral beam ions. Each component is treated as a fully kinetic collision-free species satisfying the Vlasov equation

$$\frac{\partial f}{\partial t} + \mathbf{v} \cdot \nabla f + \frac{Ze}{m} (\mathbf{E} + \mathbf{v} \times \mathbf{B}) \cdot \nabla_v f \; = \; 0. \tag{1}$$

The total current can be expressed in terms of the distribution function of each species in the following form:

$$\mathbf{J} = \sum_j Z_j e \int d\mathbf{v} \mathbf{v} f_j. \tag{2}$$

We denote with j the particle species and with $Z_j e$ the particle charge. The electric field can be written in terms of a scalar and vector potential in the following way:

$$E = i\omega \mathbf{A} - \nabla \Phi \tag{3}$$

where A is the vector potential. In the outer region, far from the rational surface, we are free to use the MHD gauge $A_{||} = 0$. Close to the rational $q = m/n$ surface where reconnection phenomena take place, the $A_{||}$ plays an important role and cannot be eliminated by a guage condition. From the parallel electron momentum balance equation (derived by taking the $m\mathbf{v}$ moment of the Vlasov equation) , neglecting the electron inertia, one obtains

$$e n_e E_{||} = -\nabla_{||} p_{e||}. \tag{4}$$

where we denote with p_e and n_e the electron pressure and density respectively. Note that $p_{e||}$ has to be calculated using the distribution function f_e

$$p_{e||} = m_e \int d\mathbf{v} v_{||}^2 f_e.$$

The model is completed by the addition of the low frequency Maxwell equations and quasineutrality condition

$$\nabla \times \mathbf{E} = -\frac{\partial \mathbf{B}}{\partial t} \tag{5}$$

$$\nabla \times \mathbf{B} = \mu_0 \mathbf{J} \tag{6}$$

$$\sum_j Z_j n_j = 0 \tag{7}$$

$$\nabla \cdot \mathbf{B} = 0 \tag{8}$$

The energetic particle density is usually assumed small, but its pressure is considered comparable to the bulk plasma pressure.

5.3 Equilibrium

The analysis begins with a description of the equilibrium. We consider a large aspect ratio ($\epsilon << 1$), low β, circular axisymmetric torus. For each species, we observe that there are several equilibrium forces: electric, magnetic, centrifugal and thermal. In most situations of practical interest, the centrifugal forces are quite small, and the pressure gradient is balanced by the electric field and by the $\mathbf{v} \times \mathbf{B}$ force. The $\mathbf{v} \times \mathbf{B}$ force induces a plasma flow that can either be in the toroidal or poloidal direction. As already mentined in Chapter 3, in a purely collisionless plasma, it is not possible to determine how the magnetic force is divided between $\mathbf{v}_\phi \times \mathbf{B}_\mathbf{p}$ and $\mathbf{v}_\mathbf{p} \times \mathbf{B}_\phi$ (where ϕ and p denote toroidal and poloidal respectively). A transport theory is needed to determine the apportionment. Neoclassical transport theory suggests that poloidal flow is strongly damped by viscosity, while toroidal flow can persist for very long times in an axisymmetric geometry. These arguments indicate that a reasonable choice for the distribution function is the "so called" rigid-rotor distribution,

$$F = F(\mathcal{E} + \Omega P_\phi) \tag{9}$$

here $\mathcal{E} = mv^2/2 + Ze\Phi$ is the particle energy, $P_\phi = mRv_\phi + Ze\Psi(R,Z)$ is the canonical angular momentum, Ω is a constant angular velocity (this equilibrium distribution function yields a flow velocity, $\mathbf{u} = -R\Omega\hat{e}_\phi$. Also Φ and Ψ denote the equilibrium electrostatic potential and poloidal magnetic flux. The poloidal magnetic flux is defined via the expression for the unperturbed magnetic field: $\mathbf{B} = B_T\hat{e}_\phi + \mathbf{B}_p$ where $\mathbf{B}_p = \nabla\Psi \times \hat{e}_\phi/R$. The standard cylindrical coordinate system (R,ϕ,Z) is adopted here, with R denoting the horizontal coordinate from the symmetry axis of the tokamak. This form of the distribution function leads to a great simplification in the derivation of the finite larmor radius effects on the plasma inertia without altering the essential physics in the kinetic resonant and nonresonant particle response. The fluid behavior of the plasma remains completely unaffected by this choice of the distribution function. Thus, a more general theory, removing the rigid rotor assumption, can be carried out, and we would expect the final result to be almost unchanged.

From Eq. (9) it is straightforward to show that the jth species number density and current density can be written as

$$n_j = \int d^3v F_j = -\frac{1}{Ze\Omega}\frac{dp_j}{d\chi} \tag{10}$$

$$\mathbf{J}_j = Ze\int d^3v \mathbf{v} F_j = R\hat{e}_\phi \frac{dp_j}{d\chi} \tag{11}$$

where p_j is the plasma pressure

$$p_j \equiv \frac{1}{3}m_j \int d^3v(\mathbf{v} + \Omega R\hat{e}_\phi)^2 F_j \tag{12}$$

while

$$\chi_j(R,Z) \equiv \Psi + \frac{\Phi}{\Omega} - \frac{m_j}{2Z_j e}R^2\Omega_j \tag{13}$$

is a generalized potential function. Hereafter, we shall consider $p_j(\chi_j)$ or equivalently $f_j(\epsilon + \Omega P_\phi)$ to be free functions.

These relations are substituted into Maxwell's equation. After some simple manipulation, we obtain an MHD-like set of equilibrium equations given by

$$\mathbf{J}\times\mathbf{B} - \sum_j \nabla p_j + m_j n_j \Omega_j^2 R\nabla R = 0 \tag{14}$$

$$\nabla \times \mathbf{B} = \mu_0 \mathbf{J} \tag{15}$$

$$\nabla \cdot \mathbf{B} = 0. \tag{16}$$

As expected, each species enters the momentum balance through a pressure gradient force and a centrifugal force. For many practical applications, the centrifugal forces are small compared to the ∇p term.

Following standard procedures, it is possible to reduce Eq. (14) to a single Grad-Shafranov equation for the flux Ψ. This equation has the form

$$\Delta^* \Psi = -F\frac{dF}{d\Psi} - \mu_0 R^2 \sum_j \frac{dp_j}{d\chi_j} \tag{17}$$

$$\mathbf{B} = \frac{F}{R}\mathbf{e}_\phi + \frac{\nabla\Psi \times \mathbf{e}_\phi}{R} \tag{18}$$

In Eq. (17) $F(\Psi)$ and $p_j(\chi_j)$ are free functions.

This completes the specification of the equilibrium problem. For the stability analysis we shall assume that a solution has been found to Eq. (17) or equivalently Eq. (18).

5.4 Stability

The stability analysis proceeds in straightforward manner. In an axisymmetric torus all perturbed quantities can be written as $\tilde{Q}(R,Z)\exp(-i\omega t - in\phi)$.

Perturbing the force operator $\mathbf{F} = \mathbf{J} \times \mathbf{B}$ using the definition of the current in terms of the distribution function given in Eq. (2) we obtain:

$$\left(\mathbf{J} \times \tilde{\mathbf{B}} + \tilde{\mathbf{J}} \times \mathbf{B}\right) = \sum_j \left[n_j Z_j e \tilde{\mathbf{E}} + R\frac{dp_j}{d\chi}\hat{e}_\phi \times \tilde{\mathbf{B}} + Z_j e \int d^3v (\mathbf{E} + \mathbf{v} \times \mathbf{B}) \tilde{f}_j \right] \tag{19}$$

where the quasineutrality condition has been used. We also define the perturbed $\tilde{\mathbf{E}} \times \mathbf{B}$ displacement in the following way:

$$\xi_\perp = i\frac{\tilde{\mathbf{E}} \times \mathbf{B}}{\omega B^2}. \tag{20}$$

The linearization of the parallel electron fluid equation [Eq. (4)] gives the linearized parallel electric field (see Appendix B)

$$\tilde{E}_{\|} = -\mathbf{b}\cdot\nabla\left[\xi_{\perp}\cdot\mathbf{E}_0 + \frac{1}{n_{e0}}(\tilde{p}_{e\|} + \xi_{\perp}\cdot\nabla p_{e\|0})\right]. \tag{21}$$

We consider Eq. (21) and notice that from the the electron equilibrium condition it follows that $E_0 \sim (\nabla p_{e\perp 0})/en_{e0}$. In Eq. (21) the term $\tilde{p}_{e\|} + \xi_{\perp}\cdot\nabla p_{e\|0}$ is usually small. Therefore assuming an isotropic equilibrium pressure, $p_{e\perp 0} = p_{e\|0}$, we can neglect the pressure terms with respect to the electrostatic term in Eq. (21).

The linearized Ohm's law in the outer region easily follow

$$\tilde{\mathbf{E}} = i\omega\xi_{\perp}\times\mathbf{B} - \nabla(\xi_{\perp}\cdot\mathbf{E}_0). \tag{22a}$$

Note the Eq. (22) leads to the standard MHD form of the perturbed magnetic field

$$\tilde{\mathbf{B}} = \nabla\times(\xi_{\perp}\times\mathbf{B}). \tag{22b}$$

We refer to the two terms in the right side of Eq. (19) as T_1 and T_2, respectively.

To compute T_1, we use Eq. (22b), (7) and (18) and obtain:

$$T_1 = \sum_j i(\omega - n\Omega_j)n_j Z_j e\,(\xi_{\perp}\times\mathbf{B}) - \frac{dp_j}{d\chi_j}\nabla\left(\xi_{\perp}\cdot\nabla\bar{\Psi}_j\right) \tag{23}$$

where $\bar{\Psi}_j = \Psi + \Phi/\Omega_j$.

In order to calculate T_2, we need an expression for the perturbed distribution function which can be found in Appendix B:

$$\tilde{f} = -\frac{\partial F}{\partial \mathcal{E}}\left[Ze\Omega(\xi_{\perp}\cdot\nabla\bar{\Psi}) - i(\omega - n\Omega)\tilde{S}\right] \tag{24}$$

where

$$\tilde{S} = Ze\int_{-\infty}^{t}\xi_{\perp}\cdot(\mathbf{E} + \mathbf{v}\times\mathbf{B})dt'. \tag{25}$$

Notice that $\tilde{S}$ is simply the integral of the Lorentz force dotted into the displacement along the unperturbed orbit of the particle. Following the procedure used in Chapter 4 we can write $\tilde{S}$ in the following form:

$$\tilde{S} = m(\xi_\perp \cdot \mathbf{v}) - m \int d^3\mathbf{v}\ (\mathbf{v} \cdot \frac{d\xi_\perp}{dt'})dt' \qquad (26).$$

We shall denote by $\hat{S}$ the last term in Eq. (26). Hence:

$$T_2 = \sum_j Z_j e \int d^3v \left[-Z_j e \Omega_j \frac{\partial F}{\partial \mathcal{E}} (\mathbf{E} + \mathbf{v} \times \mathbf{B})(\xi_\perp \cdot \nabla \bar{\Psi}_j) \right]$$
$$+ i \sum_j Z_j e(\omega - n\Omega_j) \int d^3v (\mathbf{E} + \mathbf{v} \times \mathbf{B}) \tilde{S} \frac{\partial F}{\partial \mathcal{E}} \qquad (27)$$

Of the terms within the first integral, only those proportional to v_ϕ contribute ($\mathbf{v}_\perp$ vanishes upon integration over gyrophase). Now, using the fact that $n = \int d^3v F(\mathcal{E} + \Omega P_\phi)$, equating $\mathcal{E} + \Omega P_\phi = m(\mathbf{v} + \hat{e}_\phi R\Omega)^2 + (Ze)\Omega\chi$, we obtain: $\partial n/\partial \chi = -(Ze/R) \int d^3v v_\phi \, \partial F/\partial \mathcal{E}$. Thus, using the relation between n and p (see Eq. (10)), we write:

$$T_2 = -\sum_j (\xi_{\perp\perp} \cdot \nabla \bar{\Psi}_j) \nabla \bar{\Psi}_j \frac{d^2 p_j}{d\chi^2} + i \sum_j Z_j e(\omega - n\Omega_j) \int d^3v (\mathbf{E} + \mathbf{v} \times \mathbf{B}) \tilde{S} \frac{\partial F_j}{\partial \mathcal{E}} \qquad (28)$$

Summing the contributions from T_1 and T_2, using Eq. (13), and defining the fluid-like density and pressure perturbations,

$$\tilde{\rho}_j = -m \frac{dn_j}{d\chi_j} (\xi_\perp \cdot \nabla \bar{\Psi}_j) \qquad (29)$$

$$\tilde{p}_j = -\frac{dp_j}{d\chi_j} (\xi_\perp \cdot \nabla \bar{\Psi}_j) \qquad (30)$$

we find:

$$\left(\tilde{\mathbf{J}} \times \mathbf{B} + \mathbf{J} \times \tilde{\mathbf{B}} \right) = T_1 + T_2$$
$$= \sum_j \left(\nabla \tilde{p}_j + \tilde{\rho}_j \Omega_j^2 R \nabla R \right) + i \sum_j Z_j e(\omega - n\Omega_j) \Big[n_j \xi_\perp \times \mathbf{B}$$
$$+ \int d^3v (\mathbf{E} + \mathbf{v} \times \mathbf{B})\ \tilde{S} \frac{\partial F_j}{\partial \mathcal{E}} \Big] \qquad (31)$$

The last term can manipulated, using Eq. (26), so that part of it cancels against $n_j \xi_\perp \times \mathbf{B}$. Then,

$$\left(\tilde{\mathbf{J}} \times \mathbf{B} + \mathbf{J} \times \tilde{\mathbf{B}} \right) = \sum_j \left(\nabla \tilde{p}_j + \tilde{\rho}_j \Omega_j^2 R \nabla R \right)$$
$$+ i \sum_j Z_j e(\omega - n\Omega_j) \int d\mathbf{v} (\mathbf{E} + \mathbf{v} \times \mathbf{B})\ \hat{S} \frac{\partial F_j}{\partial \mathcal{E}} \qquad (32)$$

where

$$\hat{S} \equiv \int_{-\infty}^{t} dt' \mathbf{v} \cdot \frac{d\xi_{\perp}}{dt'} \tag{32a}$$

We now focus on the integral over the velocity space in Eq. (32),

$$I = \int d\mathbf{v} Ze(\mathbf{E} + \mathbf{v} \times \mathbf{B}) \hat{S} \frac{\partial F}{\partial \mathcal{E}}$$

and notice that according to the particle equation of motion

$$Z_j e(\mathbf{E} + \mathbf{v} \times \mathbf{B}) = m \frac{d\mathbf{v}}{dt}. \tag{34}$$

Substituting Eq. (34) into Eq. (33), and integrating by-parts yields

$$I = m \int d\mathbf{v} \left[\frac{d}{dt} (\mathbf{v} \hat{S} \frac{\partial F}{\partial \mathcal{E}}) - \mathbf{v} \frac{\partial F}{\partial \mathcal{E}} \frac{d\hat{S}}{dt} \right] \tag{35}$$

where

$$\frac{d\hat{S}}{dt} = \mathbf{v} \cdot \frac{d\xi_{\perp}}{dt} \tag{36}$$

$$\frac{d}{dt} = -i\omega + \mathbf{v} \cdot \nabla + Ze(\mathbf{E} + \mathbf{v} \times \mathbf{B}) \cdot \nabla_v. \tag{37}$$

Using the fact that

$$\mathbf{v} \cdot \nabla (= \nabla \cdot (\mathbf{v}$$

and

$$(\mathbf{E} + \mathbf{v} \times \mathbf{B}) \cdot \nabla_v (= \nabla_v \cdot ((\mathbf{E} + \mathbf{v} \times \mathbf{B})$$

leads to the following simplified expression for I

$$I = m \int d\mathbf{v} \left[-i\omega \hat{S} - \mathbf{v} \cdot \frac{d\xi_{\perp}}{dt} \right] \frac{\partial F}{\partial \mathcal{E}} \mathbf{v} + \nabla \cdot m \int d\mathbf{v} (\mathbf{v} \mathbf{v} \hat{S} \frac{\partial F}{\partial \mathcal{E}}). \tag{38}$$

Because of the rigid rotor assumption, the distribution function dependence on the velocity can be simplified by using the new variables $\mathbf{w}$ and $\mathcal{E}_w$ with $\mathbf{w} = \mathbf{v} + \Omega R \hat{e}_{\phi}$ the relative velocity, and $\mathcal{E}_w = (1/2) m w^2$ the relative kinetic energy. The spatial and velocity dependence in F are now separated

$$F(\mathcal{E} + \Omega P_{\phi}) = F(\mathcal{E}_w + Ze\Omega\chi). \tag{39}$$

In order to perform the integration over the velocity space in Eq. (38), we introduce the gyroangle ς through the following definition

$$\mathbf{v} = v_{||}\mathbf{b} + v_{\perp}(\mathbf{e_2}\cos\varsigma + \mathbf{e_3}\sin\varsigma) \tag{40}$$

where $\mathbf{b} = \mathbf{B}/B$ and $(\mathbf{b}, \mathbf{e_2}, \mathbf{e_3})$ are an orthogonal triplet. Looking at low frequency modes, we order $\Omega_j < \omega << \Omega_c$, with Ω_c the cyclotron frequency, and in I, we retain all terms up to first order in ω/Ω_c and Ω_j/Ω_{cj}. One has to be very careful in using this ordering because the rotational frequency of an energetic species, Ω_h, is usually large and can sometimes make the previous assumption invalid. It easy to show that the relevant parameter is $(n_h\Omega_h/n_i\Omega_{ci}$, where n_h is the hot particle density which is usually small. Thus, we shall adopt the ordering $n_h\Omega_h < n_i\Omega_i \simeq n_e\Omega_e$.

As shown in Chapter 4, $\hat{S}$ is to lowest order in ρ_L/a, independent of ς. Therefore, the first term on the RHS of Eq. (38) vanishes because it is odd in $v_{||}$ and $\mathbf{v}_{\perp}$. In order to perform the integration in the second term of Eq. (38), we note that in a large aspect ratio tokamak, $v_{||} \simeq w_{||} - \Omega R$ and $\mathbf{v}_{\perp} = \mathbf{w}_{\perp}$. We also make use of Eq. (40) and of the gyrophase average procedure that gives

$$< \mathbf{w}\cdot(\mathbf{w}\cdot\nabla\xi_{\perp}) >_{\varsigma} = \frac{w_{\perp}^2}{2}\nabla\cdot\xi_{\perp} + (\frac{w_{\perp}^2}{2} - w_{||}^2)\kappa\cdot\xi_{\perp} \tag{41}$$

where $\kappa \simeq -\mathbf{e_R}/R$ is the magnetic field curvature and $(\mathbf{e_R}, \mathbf{e}_\phi, \mathbf{e_Z})$ is the standard cylindrical triplet. Substituting into Eq. (38), we find

$$-m\int d\mathbf{v}\mathbf{v}\cdot\frac{d\xi_{\perp}}{dt}\frac{\partial F}{\partial\mathcal{E}} \simeq -i(\omega - n\Omega)n_0\xi_{\perp} - \Omega(2\xi_R + R(\nabla\cdot\xi_{\perp}))\hat{e}_{\phi} \tag{42}$$

where $\xi_R = \xi_{\perp}\cdot\mathbf{e_R}$.

The derivation of the FLR effects in the third term on the RHS of Eq. (38) requires a somewhat lengthy calculation that we summarize in the following steps:

First we compute $\hat{S}$ with the first order FLR correction

$$\hat{S} = < \hat{S} > + \hat{S}_{\varsigma} \tag{43}$$

where

$$< \hat{S} >= \int_{-\infty}^{t} dt' \left[\frac{v_\perp^2}{2} \nabla \cdot \xi_\perp + \left(\frac{v_\perp^2}{2} - v_\parallel^2 \right) \kappa \cdot \xi_\perp \right] \tag{44}$$

$$\hat{S}_\varsigma = \frac{v_\perp^2}{2\Omega_c} (s_1 \cos 2\varsigma + s_2 \sin 2\varsigma) \tag{45}$$

and the cyclotron frequency has entered the calculation through the change of variable $dt \simeq d\varsigma/\Omega_c$. In the $(\mathbf{e_R}, \mathbf{e_\phi}, \mathbf{e_Z})$ frame of reference and to lowest order in $\epsilon = a/R_0$, the two terms s_1 and s_2 can be written in the following form:

$$s_1 = \left(\frac{\partial \xi_R}{\partial R} - \frac{\partial \xi_Z}{\partial Z} \right) \tag{46}$$

$$s_2 = \left(\frac{\partial \xi_R}{\partial Z} + \frac{\partial \xi_Z}{\partial R} \right). \tag{47}$$

Substituting into Eq. (38) and after some manipulations, the third term on the RHS yields

$$\nabla \cdot \int d\mathbf{v} \mathbf{v} \mathbf{v} \hat{S} \frac{\partial F}{\partial \mathcal{E}} \simeq \nabla \cdot \overleftrightarrow{\pi}^{nf} + \rho \mathbf{\Omega}_*(\xi_\perp). \tag{48}$$

The first term on the RHS of Eq. (48) derives from the gyrophase independent terms and contains all the resonant particle effects. To lowest order in small parameters such as the ratio of the particle gyro radius (ρ) to the minor radius a, this tensor has only two components, we write:

$$\nabla \cdot \overleftrightarrow{\tilde{\pi}}^{nf} = \nabla_\perp \tilde{\eta}_\perp^{nf} + \nabla_\parallel \tilde{\eta}_\parallel^{nf} + (\tilde{\eta}_\parallel^{nf} - \tilde{\eta}_\perp^{nf}) [\vec{\kappa} + \hat{e}_\parallel (\nabla \cdot \hat{e}_\parallel)] \tag{49}$$

where $\vec{\kappa} = (\hat{e}_\parallel \cdot \nabla) \hat{e}_\parallel$ is the magnetic curvature. The kinetic pressure terms are of the form:

$$\tilde{p}_{\perp,\parallel}^{nf} = -i(\omega - n\Omega) \eta_{\perp,\parallel}$$

$$\begin{aligned} \tilde{\eta}_{\perp,\parallel}^{nf} =& m^2 \int d^3v \left(\frac{v_\perp^2}{2}, v_\parallel^2 \right) \hat{S} \frac{\partial F}{\partial \mathcal{E}} \\ =& 4\pi \int_0^\infty d\mathcal{E}\ \mathcal{E} \int_0^h d\Lambda \frac{1}{h|v_\parallel|} \left(\frac{v_\perp^2}{2}, v_\parallel^2 \right) \hat{S} \frac{\partial F}{\partial \mathcal{E}} \end{aligned} \tag{50}$$

where the velocity space integral has been written in terms of the energy, $\mathcal{E}$, the pitch angle variable, $\Lambda = \mu B_0/\mathcal{E}$ (where $\mu = m v_\perp^2/2B$ is the magnetic moment),

and the magnetic field line element, $h(\psi,\theta) = B_0/B$. The term denoted as Ω_* is the FLR operator coming from the gyrophase average of the off diagonal terms of the pressure tensor. To lowest order in ϵ, it can written in the following form:

$$\Omega_*(\xi_\perp) = \frac{1}{2}\left[\mathbf{v_D}\cdot\nabla\xi_\perp + \mathbf{b}\times\mathbf{v_D}\cdot\nabla(\mathbf{b}\times\xi_\perp) - \frac{p}{\Omega_c}\hat{\nabla}_p^2(\mathbf{b}\times\xi_\perp)\right] \tag{51}$$

where $\mathbf{v_D}$ is the diamagnetic drift velocity

$$\mathbf{v_D} \equiv \frac{1}{Zen_0B^2}\mathbf{B}\times\nabla p \tag{52}$$

and $\hat{\nabla}_p^2$ is a poloidal operator given by

$$\hat{\nabla}_p^2 \equiv \frac{\partial^2}{\partial R^2} - \frac{\partial^2}{\partial Z^2} \tag{53}$$

Thus, we can rewrite Eq. (32) in a convenient form of the linearized momentum conservation equation:

$$-\sum_j \rho_j(\omega - n\Omega_j)(\omega - n\Omega_j - i\Omega_{*j})\xi_\perp = (\tilde{\mathbf{J}}\times\mathbf{B} + \mathbf{J}\times\tilde{\mathbf{B}}) - \sum_j[\nabla\tilde{p}_j + \tilde{\rho}_j\Omega_j^2 R\nabla R + i(\omega - n\Omega_j)\nabla\cdot\overset{\leftrightarrow}{\tilde{\pi}}{}_j^{nf}] \tag{54}$$

Eq. (54) is suitable to study kinetic effects on high frequency ($\omega \sim \omega_A$), as well low frequency ($\omega \sim \omega_{*i}$) ideal MHD modes. Eq. (54) consists of two scalar equations for the two components of the displacement vector $\xi_\perp$ and can be numerically solved once the boundary conditions are specified.

5.5 The large aspect ratio expansion

We now proceed to the derivation of a simplified eigenvalue equation by means of an asymptotic expansion. In order to include the effects of trapped particles, which are a small fraction of the total particle population ($n_T/n \propto \epsilon^{1/2}$), we introduce $\epsilon^{1/2} << 1$ as an expansion parameter. According to standard MHD analysis of

the internal kinks, the perturbed total pressure (magnetic+fluid plasma) is expected to be small, and using Faraday's law it can be written as

$$\tilde{P} \equiv B\tilde{B}_{||} + \tilde{p}^f = -B^2[\nabla \cdot \xi_\perp + 2\kappa \cdot \xi_\perp]. \tag{55}$$

An equation for $\tilde{P}$ can be easily derived by taking the $\hat{e}_\phi \times \nabla\Psi$ component of Eq. (54). Expanding the eigenfunction $\xi_\perp$ in powers of $\epsilon^{1/2}$ and solving order by order, one finds

$$\begin{aligned} \nabla \cdot \xi_{\perp 0} &= 0 \\ \nabla \cdot \xi_{\perp 1} &= 0 \\ \nabla \cdot \xi_{\perp 2} &= -2\kappa \cdot \xi_{\perp 0} \\ \nabla \cdot \xi_{\perp 3} &= -2\kappa \cdot \xi_{\perp 1} \end{aligned} \tag{56}$$

where

$$\xi_\perp = \xi_{\perp 0} + \xi_{\perp 1} + \xi_{\perp 2} + \xi_{\perp 3} + \ldots \tag{57}$$

has been expanded up to order $\epsilon^{3/2}$ and $\xi_{\perp n} \sim \epsilon^{n/2}$. In deriving the previous set of equations, the low-β ohmic tokamak ordering has also been employed. A simple solution of Eqs. (56) can be found, yielding

$$\xi_\perp = R\nabla U \times \hat{e}_\phi + O(\epsilon^2) \tag{58}$$

and the number of unknowns is reduced to one, the stream function U.

We now apply the "annihilation operator," $\mathbf{e}_{||} \cdot \nabla\times$ to Eq. (54) and notice that the perturbed total pressure is eliminated from the problem. Focussing on the term

$$\mathbf{e}_{||} \cdot \nabla \times [(\tilde{\mathbf{B}} \cdot \nabla)\mathbf{B} + (\mathbf{B} \cdot \nabla)\tilde{\mathbf{B}}] \tag{59}$$

we collect all terms containing $\tilde{B}_{||}$ and find exactly

$$\begin{aligned} \mathbf{e}_{||} \cdot \nabla \times [\mathbf{B} \cdot \nabla\tilde{\mathbf{B}}_{||} + (\tilde{\mathbf{B}}_{||} \cdot \nabla)\mathbf{B}] = \\ -2\mathbf{e}_{||} \times \kappa \cdot \nabla(B\tilde{B}_{||}) + 2B\tilde{B}_{||}\mathbf{e}_{||} \cdot \nabla(\frac{J_{||}}{B}). \end{aligned} \tag{60}$$

To the required order, the last term on the RHS of Eq. (60) can be neglected, and the first term can be rewritten in terms of the components of the perpendicular displacement by using the $\mathbf{e}_{\|} \times \kappa$ component of Eq. (54), yielding

$$\mathbf{e}_{\|} \times \kappa \cdot \nabla(B\tilde{B}_{\|}) = \sum_j \rho\bar{\omega}_j(\bar{\omega}_j + \Omega_{*j})(\mathbf{e}_{\|} \times \kappa \cdot \xi_{\perp}) - \mathbf{e}_{\|} \times \kappa \cdot [\nabla\tilde{p}_{\perp} - \tilde{\kappa}B^2] \quad (61)$$

where $\bar{\omega}_j \equiv \omega - n\Omega_j$ and $\tilde{\kappa}$ is the perturbed curvature which depends on $\xi_{\perp}$ only. Using Eq. (58) and after a somewhat lengthy calculation, the eigenvalue equation for the stream function U can be written in the following form:

$$-\sum_j \nabla_p \rho\bar{\omega}_j(\bar{\omega}_j + \omega_{*j})R^2\nabla_p U = \mathbf{B}\cdot\nabla[\Delta^*(R^2\mathbf{B}\cdot\nabla U)] + \frac{1}{R}\nabla_p(RJ_\phi)\times$$

$$\hat{e}_\phi \cdot \nabla_p(R^2\mathbf{B}\cdot\nabla U) - 2R^2\frac{\partial}{\partial Z}(p'\mathbf{B}_\mathbf{p}\cdot\nabla U) + \mathbf{e}_{\|}\times\kappa\cdot\nabla(\tilde{p}_{\|}^{nf} + \tilde{p}_{\perp}^{nf}) + O(\epsilon^{7/2}) \quad (62)$$

where we have used the relation

$$\mathbf{e}_{\|}\cdot\nabla\times\Omega_*(\xi_{\perp}) = \mathbf{e}_{\|}\cdot\nabla\times(\mathbf{v_D}\cdot\nabla\xi_{\perp}) \simeq \mathbf{v_D}\cdot\nabla(\mathbf{e}_{\|}\cdot\nabla\times\xi_{\perp}) \quad (63)$$

The parameter ω_* is the diamagnetic drift frequency

$$\omega_* = \mathbf{k}_{\perp}\cdot\mathbf{v_D} = -\frac{n}{Zen_0}\frac{dp}{d\Psi}$$

with $\mathbf{k}_{\perp}$ defined as in Sec. 4.3.6. Using the equilibrium equation for each species,

$$\mathbf{E} + \mathbf{v}\times\mathbf{B} = \frac{1}{Zen}\nabla p \quad (64)$$

and setting $\mathbf{v} = -\Omega R\hat{e}_\phi$, yields

$$\Omega = -\frac{d\Phi}{d\Psi} - \frac{1}{Zen}\frac{dp}{d\Psi} \quad (65)$$

where Φ is the electrostatic potential. After substituting Eq. (65) into the definition of $\bar{\omega}$ and defining $\hat{\omega} = \omega + n\omega_E$ with $\omega_E = d\Phi/d\Psi$, we can rewrite the inertia term as follows:

$$\rho\bar{\omega}(\bar{\omega} + \omega_*) = \rho\hat{\omega}(\hat{\omega} - \omega_*). \quad (66)$$

Note that $n\omega_E$ is just the $\mathbf{E}\times\mathbf{B}$ drift frequency, $\mathbf{k}_\perp \cdot \mathbf{v}_{\mathbf{E}\times\mathbf{B}}$. Comparing Eq. (62) with the standard MHD eigenvalue equation derived in Sec. 2.2 we notice the presence of two new terms in Eq. (62): (1) the FLR effects in the plasma inertia given in Eq. (66), (2) the resonant and nonresonant kinetic particle response in the non-fluid pressure terms $\tilde{p}_{\|}^{nf}$, $\tilde{p}_{\perp}^{nf}$. Eq. (62) contains all terms up to order $\epsilon^{7/2}$ (remember that the highest order term in Eq. (62) is of order ϵ^2).

5.6 Kinetic pressure terms

We now proceed with the detailed consideration of the kinetic pressure terms defined in Eq. (50). For convenience we consider separately the trapped and circulating particle contribution. We rewrite the perturbed nonfluid pressure in the following form:

$$\tilde{p}_{\perp,\|}^{nf} = \tilde{p}_{\perp,\|}^{T} + \tilde{p}_{\perp,\|}^{C} \tag{67}$$

where

$$\tilde{p}_{\perp,\|}^{C,T} = -i(\omega - n\Omega)\eta_{\perp,\|}^{C,T} \tag{68}$$

$$\eta_{\perp,\|}^{C,T} = m^2 \int_{C,T} d\mathbf{v}\left(\frac{v_\perp^2}{2}, v_\|^2\right)\frac{\partial F}{\partial \mathcal{E}}\hat{S}^{C,T} \tag{69}$$

We denote with T and C the trapped and circulating particle respectively. Note that the integration along the particle orbits in $\hat{S}$ must be performed accordingly. As has been shown in Chapter 4:

$$\begin{aligned}\int_{-\infty}^{t} dt' \mathbf{v}\cdot\frac{d\xi_\perp}{dt'} &\approx \int_{-\infty}^{t} dt'\left[\frac{v_\perp^2}{2}\nabla\cdot\xi_\perp + \left(\frac{v_\perp^2}{2} - v_\|^2\right)\kappa\cdot\xi_\perp\right] \\ &\approx -\int_{-\infty}^{t} dt'\left(\frac{v_\perp^2}{2} + v_\|^2\right)\kappa\cdot\xi_\perp\end{aligned} \tag{70}$$

where we have made use of the properties of low-β equilibria [Eq. (56)]: $\nabla\cdot\xi_\perp + 2\kappa\cdot\xi_\perp = 0$ (to lowest order in ϵ).

A Trapped particles

Denoting by $Q(\mathcal{E},\mu,\psi,\theta,\phi,t)$ the integrand of (70), we can Fourier transform in time and ϕ (we consider axisymmetric systems) and expand in θ:

$$Q(\mathcal{E},\mu,\psi,\theta,\phi,t) = \sum_{m=-\infty}^{\infty} Q_m(\mathcal{E},\mu,\psi)\exp(-in\phi + im\theta - i\omega t) \tag{71}$$

Considering the orbit of the particle guiding center, we write (to lowest order in ρ/a):

$$\phi(t') - \phi(t) = \int_{\theta(t)}^{\theta(t')} q(\psi,\theta)d\theta - \omega_D(\theta)(t'-t) + \omega_E(t'-t) \tag{72}$$

where ω_E is given in Eq.(65), $q \equiv JB_\phi/R$ and $J \equiv 1/(\mathbf{B}\cdot\nabla\theta)$ is the Jacobian of the ψ,θ,ϕ coordinate system. The first term of Eq. (72) is simply a statement that the particle follows the sheared magnetic field line, the second represents the precession drift of the particle guiding center due to grad-B and field line curvature (see, e.g., Eq. (7)-(8) in Ref. [18]), and the last represents the $\mathbf{E}\times\mathbf{B}$ drift. Considering trapped particles, we expand the θ dependence of the orbit integrals in terms of the periodic bounce motion of the guiding center [19]:

$$\exp\{-in\int qd\theta'' - i[\omega_D^0 - \omega_D(\theta)](t'-t) + im(\theta'-\theta)\} = \sum_p A_p \exp[ip\omega_b(t'-t)] \tag{73}$$

where $\omega_b = 2\pi/\tau_b$ and the bounce period is defined as

$$\tau_b \equiv \oint d\theta \frac{JB}{v_\parallel(\theta)} = 2\int_{-\theta_0}^{\theta_0} d\theta \frac{JB}{|v_\parallel(\theta)|} \tag{75}$$

Here $\pm\theta_0$ are the turning points of the particle orbit ($v_\parallel(\pm\theta_0) = 0$). The orbit integrations of Eq. (70) now are quite simple, and considering low frequency perturbations, we obtain:

$$\int_{-\infty}^{t} dt' Q \approx i\exp\left[-in\left(\phi - \int_{\theta_0}^{\theta} d\theta' q\right)\right]\frac{Q_m\sigma_{0m}}{\hat{\omega} - n\omega_D^{(0)}}$$

where $\omega_D^{(0)} \equiv \oint \omega_D$ is the orbit-averaged precession drift frequency, $\hat{\omega} = \omega - n\omega_E$ and

$$\sigma_{0m} \equiv \frac{1}{\tau_b} \oint d\theta \frac{JB}{v_{||}} \exp\left(+im\theta - in \int_{\theta_0}^{\theta} d\theta' JB/v_{||} \right) \tag{76}$$

By low frequency perturbations, we mean $|\hat{\omega}| << \omega_b$, which is valid for low-n modes satisfying $|\hat{\omega}| \leq \omega_*$ (the diamagnetic frequency, defined in the next section), and $\omega_*/\omega_b \sim (\rho/r_p)(r_s/R)^{-3/2}$. Here ρ is the particle gyro radius (of the order of 1 mm for 1 KeV ions in a 4 T magnetic field), $r_p \sim$ 10–50 cm is the pressure scale length, while $r_s/R \sim 0.1$. We also take this opportunity to remember that a similar analysis has been carried out by Coppi and Rewoldt [16] studying trapped particles' effects on electrostatic modes.

Considering the two components of the kinetic pressure (non fluid contribution) (cf. Eq. (69)), we can write the trapped particle (T) contribution in the following form:

$$\tilde{\eta}^T_{\perp,||} = 4i\pi \exp[-in(\phi - \int_{-\theta_0}^{\theta} d\theta' q)] \sum_m \int_0^{\infty} d\mathcal{E}\ \mathcal{E} \int_0^h d\Lambda \frac{1}{h^2|v_{||}|} \left(\frac{v_\perp^2}{2}, v_{||}^2 \right) \frac{Q_m \sigma_{0m}}{\hat{\omega} - n\omega_D^{(0)}} \frac{\partial F}{\partial \mathcal{E}} \tag{77}$$

Expanding $\tilde{\eta}^T$ into harmonics in θ, and inverting the order of the θ and λ integrals, we obtain the expression for the k-th harmonic:

$$\left(\tilde{\eta}^T_{\perp,||} \right)_k = 4i\pi \exp(in\phi) \sum_m \int_0^{\infty} d\mathcal{E}\ \mathcal{E} \int_0^h d\Lambda \frac{1}{h^2|v_{||}|} \left(\frac{v_\perp^2}{2}, v_{||}^2 \right) \frac{\sigma^*_{0k} \sigma_{0m}}{\hat{\omega} - n\omega_D^{(0)}} \frac{\tau_b Q_m}{qR} \frac{\partial F}{\partial \mathcal{E}} \tag{78}$$

The relevant term containing the trapped particle effects in Eq. (62), is given by

$$\mathbf{e}_{||} \times \boldsymbol{\kappa} \cdot \nabla (\tilde{p}^T_\perp + \tilde{p}^T_{||}). \tag{79}$$

Following the trapped particle ordering $v_{||} \sim \epsilon v_{\perp}$, we neglect the parallel pressure contribution in Eq. (79). Decomposing into harmonics in θ as was done previously, introducing the potential U via the relation $\xi_{\perp\perp} = R\nabla U \times \hat{e}_{\phi}$, we obtain:

$$R^{-1}\vec{\kappa}\times\hat{e}_{||}\cdot\nabla\tilde{\eta}_{\perp}^{T} = \sum_{k}\exp(ik\theta)\left[\frac{d}{dr}\left(\eta_{k+1}^{T}-\eta_{k-1}^{T}\right)+\frac{1}{r}\left((k+1)\eta_{k+1}^{T}+(k-1)\eta_{k-1}^{T}\right)\right] \tag{80}$$

where

$$\eta_{k}^{T} = \sum_{l}\left[\frac{d}{dr}\left(U_{l+1}-U_{l-1}\right)+\frac{1}{r}\left((l+1)U_{l+1}+(l-1)U_{l-1}\right)\right]\Gamma_{l,k}^{T} \tag{81}$$

$$\Gamma_{l,k} = \frac{\pi}{qR^{3}m^{2}}\int_{0}^{\infty}d\mathcal{E}\;\mathcal{E}^{3}\int_{hmin}^{hmax}d\Lambda\left(\frac{\Lambda}{h}\right)^{2}\tau_{b}\frac{\sigma_{0l}^{*}\sigma_{0k}}{\hat{\omega}-n\omega_{D}^{(0)}}\frac{\partial F}{\partial\mathcal{E}} \tag{82}$$

The kinetic terms involve trapped particles only and will be seen to be of order $(r_s/R)^{3/2}$ for low frequency modes satisfying $\hat{\omega} < n\omega_D$.

B Circulating particles

We now focus on circulating particles and follow the analysis presented in Chapter 4. However, the present analysis will be slightly different because of the presence of an equilibrium electric field. Therefore, we replace the first of Eqs. (4.56) with Eq. (72) which is formally also valid for circulating particles. In this chapter we define the transit frequency ω_t as the inverse of the poloidal orbit period. Note that this definition is different from the one used in the literature and in Chapter 4; and we apologize to the reader for this confusion. For passing particles the parallel and the perpendicular velocity are of the same order; hence, both the parallel and the perpendicular pressures must be retained. The relevant term containing the passing particle effects in Eq. (62) is given by

$$\mathbf{e}_{||}\cdot\kappa\times\nabla(\tilde{p}_{\perp}^{C}+\tilde{p}_{||}^{C}). \tag{83}$$

Performing the integration along the circulating particle orbits in $\hat{S}$ as shown in Eq. (4.59), decomposing into harmonics in θ and using Eq. (58) yields

$$R^{-1}\kappa \times \hat{e}_{\|} \cdot \nabla(\tilde{\eta}_{\|}^{C} + \tilde{\eta}_{\perp}^{C}) = \sum_{k} \exp(ik\theta) \left[\frac{d}{dr} \left(\eta_{k+1}^{C} - \eta_{k-1}^{C} \right) + \frac{1}{r} \left((k+1)\eta_{k+1}^{C} + (k-1)\eta_{k-1}^{C} \right) \right] \quad (84)$$

Here

$$\eta_{k}^{C} = \left[\frac{d}{dr} \left(U_{k+1} - U_{k-1} \right) + \frac{1}{r} \left((k+1)U_{k+1} + (k-1)U_{k-1} \right) \right] \Gamma_{k}^{C} \quad (85)$$

$$\Gamma_{k}^{C} = \frac{m^2}{4R^2} \int dv \left(\frac{v_{\perp}^2}{2} + v_{\|}^2 \right)^2 \frac{\partial F}{\partial \mathcal{E}} \frac{1}{\hat{\omega} - \omega_k - n\omega_D^{(0)}} \quad (86)$$

and $\omega_k = (nq - m)\omega_t$ where ω_t is the transit frequency and $q(r)$ is the safety factor. It is important to note that Eq. (85) and (86) are valid for "highly passing" particles. Only for those particles one can set $\omega_t \simeq v_{\|}/qR$ and neglect the magnetic drift frequency.

The kinetic terms involve circulating particles only. The eigenvalue equation for the stream function U is now completed, and it can be used to study kinetic effects on low-n MHD modes.

5.7 High frequency modes: the gap mode eigenvalue equation

In the high frequency limit, $\omega \sim \omega_A >> \omega_b > \omega_D$, the trapped particle resonant effects, as well as the nonresonant kinetic effects, can be neglected. The only relevant contribution comes from resonant circulating particles. For simplicity we focus on TAE modes.

Using a large aspect ratio expansion, and restricting ourselves to equilibria with circular flux surfaces, we derive the following form of the eigenvalue equation for the radial displacement: $\hat{\xi}_m \equiv U_m/r$:

$$\frac{d}{dr} r^3 \left[\sum_j \rho_j (\hat{\omega} - \omega_{*j})(\hat{\omega} - \nu_{mj}^{C}) - F^2 \right] \frac{d\hat{\xi}_m}{dr} - (m^2 - 1) r \left[\sum_j \rho_j (\hat{\omega} - \omega_{*j})(\omega - \nu_{mj}^{C}) - F^2 \right] \hat{\xi}_m$$

$$-\sum_j \rho_j \hat{\omega}(\hat{\omega}-\omega_{*j})\epsilon_0 r_0^2 \frac{d^2}{dr^2}(\xi_{m+1}+\xi_{m-1}) - \sum_j (\hat{\omega}-\omega_{*j})\left[r^2\frac{d}{dr}\hat{a}_m^C\right]\hat{\xi}_m = 0 \quad (87)$$

where $F = \mathbf{k}\cdot\mathbf{B}$ is the well-known field line bending term, $\epsilon_0 = r_0/R$ where r_0 is the gap location and

$$\nu_m^C \equiv \frac{1}{\rho_j}\left(-\Gamma_{m+1}^C - \Gamma_{m-1}^C\right) \quad (88)$$

$$\hat{a}_m^C \equiv (m-1)\Gamma_{m+1}^C - (m+1)\Gamma_{m-1}^C \quad (89)$$

In deriving Eq. (87) we have neglected any additional kinetic coupling. It is rather clear that each coupling with different harmonics introduces higher order terms unless the coupled mode has the same singular surface of the mode under consideration. According to standard MHD analysis, each mode is either singular at a rational surface (Kink modes, ballooning modes, etc) or singular at an Alfvén frequency gap location (TAE, EAE, NAE). For gap modes, the kinetic coupling must be retained only in the case it coincides with the geometrical coupling of the mode (toroidal, elliptical, triangular). The coupling, introduced by the circulating particle pressure, is mainly $k, k+2$; and therefore, it must retained only for the EAE. Similar considerations are valid for kink modes. Since two modes with the same toroidal wavenumber cannot have the same rational surface, it follows that at a given rational surface only one mode can be singular, and the coupling with other harmonics can be neglected.

After performing the integrations in the Γ^C's, one can easily show that

$$\nu_m^C(r_0) = \nu_{m+1}^C(r_0) = i\gamma_{TAE}$$

where γ_{TAE} is the growth rate of the TAE, as derived in Chapter 4. Eq. (87) can be easily solved by assuming $(\nu^C/\omega_r) << \epsilon$, $\omega_r >> \omega_{*i}$ and $\rho_h << \rho_i$. It is easily seen that to lowest order Eq. (87) is identical to Eq. (85) which yields the lowest order eigenfunction. In order to derive ω_i one can construct a quadratic form from Eq. (87). Assuming $\epsilon << 1$ it is straightforward to derive that $\omega_i = \gamma_{TAE}$.

5.8 Low frequency modes

We now consider modes with frequency $\omega \sim \omega_{*i}$. In this regime all the resonant and nonresonant kinetic effects have to be retained, and the analysis becomes very complicated. However, the geometrical coupling is usually negligible and the straight tokamak approximation will be used. The final form of the momentum conservation equation reads (for the m-th harmonic):

$$\frac{d}{dr}r^3\Big[\sum_j \rho_j(\hat{\omega}-\omega_{*j})(\hat{\omega}-\nu_m)-F^2\Big]\frac{d\hat{\xi}_m}{dr}-(m^2-1)r\left[\sum_j \rho_j\hat{\omega}(\hat{\omega}-\omega_{*j})-F^2\right]\hat{\xi}_m$$
$$-\hat{g}\hat{\xi}_m-\sum_j(\hat{\omega}-\omega_{*j})\left[\frac{d}{dr}(r^2\hat{a}_m)+r\hat{b}_m\right]\hat{\xi}_m=0 \qquad (90)$$

where

$$\hat{g}=\frac{1}{4\pi}\rho_i k_\parallel^2 B_\theta^2\Big[\frac{8\pi r p'}{B_\theta^2}+(3q+1)(q-1)\Big] \qquad (91)$$

$$\nu_m \equiv \frac{1}{\rho_j}\left(2\Gamma_{m+1,m-1}-\Gamma_{m+1,m+1}-\Gamma_{m-1,m-1}\right) \qquad (92)$$

$$\hat{a}_m \equiv 2\Gamma_{m+1,m-1}+(m-1)\Gamma_{m+1,m+1}-(m+1)\Gamma_{m-1,m-1} \qquad (93)$$

$$\hat{b}_m \equiv 2(m^2-1)\Gamma_{m-1,m+1}+(m-1)^2\Gamma_{m+1,m+1}+(m+1)^2\Gamma_{m-1,m-1} \qquad (94)$$

and

$$\Gamma_{k,l}=\Gamma_{k,l}^T+\Gamma_k^C\delta_{k,l} \qquad (95)$$

with $\delta_{k,l}$ the Kronecker symbol ($\delta_{k,l}=0$ for $k\neq l$ and $\delta_{k,l}=0$ for $k=l$).

With $\hat{g}$, we denote terms of order ϵ^4 which were not included in the starting equation [Eq. (62)]; and it becomes important only for $m=1$ that causes the well-known m^2-1 cancellation in Eq. (90). We assume that $\hat{g}$ is mainly fluid-like, and it is given by standard MHD theory. In Eq. (91) we give the expression for $\hat{g}$ valid for a straight tokamak ordering. An expression for $\hat{g}$ valid in toroidal geometry can be obtained from Ref.[14]. The reason we need to introduce the ϵ^4 terms is because (as is shown later) the order of magnitude of the nonresonant terms depends on the

mode frequency. For $\hat{\omega} < \omega_D^{(0)}$, it is readily seen that $\hat{b} \sim \epsilon^{3/2}$, with respect to the line bending term (F^2) and the kinetic effects, dominate. For $\hat{\omega} >> \omega_D^{(0)}$, it follows that $\hat{b} \sim \epsilon^{5/2}$ and the fluid response (the term $\hat{g}$) is dominant.

5.9 Applications to the $m = 1$ internal kink

We now apply the results derived in Sec. 5.7 to study the kinetic effects on the $m = 1$. Referring to the linear theory of the $m = 1$ modes as discussed in Refs. [12]-[14], we decompose the plasma domain into a narrow region around the rational $q = 1$ surface and an outer region away from it. In the second, the effects of plasma resistivity and parallel electric field can be neglected. This implies that no dissipation processes take place in the outer region. In the inner region the parallel current is generally very high and it leads to large dissipation, even in the limit of small resistivity. In the course of this chapter, we use two different models for the outer and the inner region in order to retain the essential physics.

A The outer region

Since the reconnection processes take place only in a thin layer around the rational surface, we can choose the gauge condition $A_{||} = 0$, where $A_{||}$ is the parallel component of the magnetic vector potential in the region away from the $q = 1$ surface (the outer region). The model developed in the previous section is therefore suitable to describe the plasma behavior in the outer region.

We start our analysis solving Eq. (90) using the standard tecnique given in Ref. [12]-[13] : to lowest order, the displacement has a step-function structure, $\hat{\xi}_m(r) = \xi_\infty H(r_s - r)$, while to order $\epsilon^{3/2}$, one has:

$$\frac{d\hat{\xi}_m}{dr} = -\frac{4\pi\xi_\infty}{r^3 F^2}\int_0^r dr' \left[\hat{g}(r') + \sum_j (\hat{\omega} - \omega_{*j})\left(\frac{d}{dr'}(r^2 \hat{a}_(r')) + r'\hat{b}(r')\right)\right] \qquad (96)$$

where the function $\hat{g}(r)$ and the two functions $\hat{b}(r)$ and $\hat{a}$ represent the fluid and the kinetic contribution respectively. It is important to remember that $\hat{b}$ and $\hat{a}$ are of order $\epsilon^{3/2}$ only for $\omega < \omega_D^{(0)}$.

We follow the notation introduced in Refs. [12]-[13] and define

$$\lambda_H = -\frac{4\pi^2}{s(r_s)(B_\theta)^2_{r_s}} \int_0^{r_s} \hat{g}(r')dr' \tag{97}$$

$$\lambda_K = -\frac{4\pi^2}{s(r_s)(B_\theta)^2_{r_s}} \sum_j (\omega - \Omega_j) \int_0^{r_s} dr\ r\hat{b}_j \tag{98}$$

where $s = rd\ln q/dr$. It important to note that in deriving λ_K the contribution coming from $\hat{a}$ vanishes due to the fact that $\hat{a}(r_s) = 0$. The fluid contribution λ_H can be calculated using the function $\hat{g}$ given in Eq. (91) which is valid for a straight tokamak. In toroidal geometry a more appropriate expression for λ_H would be the one derived by Bussac and co-workers which yields

$$\lambda_H = -\frac{3\pi}{2}\left(\frac{r_s}{R}\right)^2 \left[\frac{13}{144} - \hat{\beta}_p^2\right] \tag{99}$$

with $q_0 = q(r = 0)$ and

$$\hat{\beta}_p = \frac{-8\pi}{B_\theta^2(r_s)} \int_0^{r_s} dr \left(\frac{r}{r_s}\right)^2 \frac{dp}{dr} \tag{100}$$

The contribution from trapped particles can be evaluated rather easily for the case of Maxwellian distribution functions. After some straightforward manipulation, λ_K can be written in the following form

$$\lambda_K = \frac{4\sqrt{2}\pi}{s(r_s)(B_\theta)^2_{r_s}} \left(\frac{r_s}{R}\right)^{5/2} \sum_j \left(\frac{\omega}{\bar{\omega}_{Dj}} - \frac{\Omega_j}{\bar{\omega}_{Dj}}\right) \int_0^1 dx\ x^{5/2} p_j(x)$$
$$\int_0^1 d\kappa^2 \frac{K(\kappa^2)}{H(\kappa^2)} \left[\frac{3}{4} + \frac{1}{2}\mathcal{E}_r + \mathcal{E}_r^2 + \mathcal{E}_r^{5/2} Z(\sqrt{\mathcal{E}_r})\right] \left[(\cos q\theta)^{(0)}\right]^2 \tag{101}$$

where

$$\bar{\omega}_{Dj} \equiv \frac{T_j}{Z_j e B r_s R} \tag{102}$$

$$\mathcal{E}_r(r, \kappa^2) \equiv \frac{\omega}{\bar{\omega}_{Dj}} \frac{r}{r_s H(\kappa^2)} \tag{103}$$

$$H(r,\kappa^2) \approx 2(1+2s)\frac{E(\kappa^2)}{K(\kappa^2)} - 1 + 4s(\kappa^2 - 1) \tag{104}$$

$$(\cos q\theta)^{(0)}(r,\kappa^2) \approx [2 + 4(1-q)]\frac{E(\kappa^2)}{K(\kappa^2)} - 4(1-q)(1-\kappa^2) \tag{105}$$

The variable $\kappa^2 = (1/2)[1 + (R/r)(1-\Lambda)]$ was introduced in Ref. [16], the functions K and E are complete elliptical integrals, while Z is the well-known plasma dispersion function [21], modified in such a way as to only carry a resonant contribution when the mode phase velocity is in the same direction as the precession of the particle ($Re(\omega)/\omega_D > 0$). Note that we order $(r_s/R)(\Omega/\bar{\omega}_{Dj}) \sim 1$. Thus, the trapped particle contribution, λ_K, can be negative and of order $(r_s/R)^{3/2}\beta_p$ - for instance, in the limit of vanishing mode frequency. In all that follows, we shall refer to the beta-poloidal of the plasma, $\beta_p = \sum_j \beta_{pj} = (1 + T_i/T_e)\beta_{pe}$, as the quantity of relevance.

From Eqs. (96)-(98) we can finally write the boundary condition for the eigenfunction in the neighborhood of the singular layer:

$$\frac{1}{\xi_\infty}\frac{d\hat{\xi}_m}{dx}\bigg|_{x\to 0_-} = -\frac{1}{\pi}\frac{\lambda_H + \lambda_K}{s(r_s)x^2} \tag{106}$$

where $x \equiv (r - r_s)/r_s$. The factor of x^{-2} comes from $F = B_\zeta/R - B_\theta/r \approx (B_\theta/r_s)s(r_s)x$ in the neighborhood of the $q(r) = 1$ surface. This condition will be used to match the solution found here with that found within the singular layer (see the next section) and will yield the dispersion equation.

B Theory within the singular layer

The "singular" layer is the thin region, centered about $r = r_s$, where the eigenfunction has its greatest variation and where non-ideal MHD effects such as inertia, electrical resistivity, diamagnetic effects, and parallel electric field are important. In order to keep these effects we rederive Eq. (20) starting from Eq. (19) including the perturbed parallel electric field due to parallel component of the vector potential

in both the Farady's law and the perturbed distribution function that we used to calculate the pressure. For an isotropic distribution function $\tilde{f}$ can be written in the following form:

$$\tilde{f} = -\xi_\perp \cdot \nabla F + im_j(\omega - n\Omega)\frac{\partial F}{\partial \mathcal{E}}[\xi_\perp \cdot \mathbf{v} - \int_{-\infty}^{t}[\frac{\tilde{E}_\parallel v_\parallel}{i\omega} + \mathbf{v} \cdot \frac{d\xi_\perp}{dt'}]dt'. \qquad (106)$$

Note that when we calculate the perturbed pressure, the largest contribution from the $\tilde{E}_\parallel$ comes the passing particle orbit integral ($v_\parallel^{Trap} < v_\parallel^{Circ}$), and therefore, leaves $\tilde{E}_\parallel$ and $\tilde{f}$ in phase. When we apply the operator $\mathbf{e}_\parallel \cdot \nabla\times$ to the perturbed $J \times B$ equation as in Sec. 5, the perturbed pressure enters the equation through the term $\mathbf{e}_\parallel \times \kappa \cdot \nabla\tilde{p}$. Since the curvature κ is θ dependent, it follows that the parallel electric field term in the pressure gives a contribution only to the poloidal sideband $(m-1, m+1)$. We conclude that $\tilde{E}_\parallel$ enters the final layer equation only through the Faraday's law that reads

$$\tilde{B} = \nabla \times [i\frac{\tilde{E}_\parallel}{\omega}\mathbf{e}_\parallel + (\xi_\perp \times \mathbf{B})]. \qquad (107)$$

Assuming a very small layer width after some algebra, we obtain the following equation:

$$\sum_j \frac{(\hat{\omega} - \nu_1^C)(\hat{\omega} - \omega_{*j})}{\omega_A^2}\frac{d^2\bar{\xi}}{dx^2} = -x\frac{d^2\Psi}{dx^2} \qquad (108)$$

where $\bar{\xi} \equiv \xi_r/\xi_\infty$ and $\Psi \equiv -i\tilde{B}_r/s(r_s)B_\theta(r_s)$ is the perturbed poloidal magnetic flux. The parallel electric field is related to Ψ through Faraday's law $\tilde{E}_\parallel = r\omega s B_\theta \Psi$. The equation for $\tilde{E}_\parallel$ (or for Ψ) can be deduced from the parallel component of generalized Ohm's law which is given by the parallel electron momentum equation. In regimes where the resistivity plays a more important role than the electron inertia the parallel, Ohm's law can be written as

$$\mathbf{b} \cdot [\eta_\parallel \mathbf{J}_\parallel = \mathbf{E} + \frac{1}{en}\nabla p_{e\parallel}] \qquad (109)$$

where we neglect the thermo-electric force, and $\mathbf{b} = \mathbf{B}/B$. After linearizing Eq. (109) and using the equilibrium relation for the electrons and Faradays law one obtains

$$\Psi + x\bar{\xi} = i\epsilon_\eta \frac{\omega_A}{\hat{\omega} - \omega_{*e}}\frac{d^2\Psi}{dx^2} \qquad (110)$$

where $\eta_{||} = 2\pi\nu_{ei}/\omega_{pe}^2$.

Notice that in both equations [Eq. (108) and Eq. (110)] and in the resonant term ν_1, the frequency ω enter through the parameter $\hat{\omega} = \omega + n\omega_E$. We conclude that the presence of an equilibrium electric field has only the effect of providing a real frequency to the mode.

In deriving the above equation we have neglected the parallel electron Landau damping in the perturbed parallel pressure. In the regime where the electron collision frequency is large enough, ($\nu_e > \omega_i$) this is certainly a reasonable assumption. In high temperature plasmas the parallel electron Landau damping should be included. This leads to an additional term in Eq. (110). In particular, the denominator on the RHS should be replaced by $(\hat{\omega} - \omega_{*e} - \nu_{||})$ with $\nu_{||}$ proportional to the standard Z function. Since $k_{||}$ vanishes at the $q = 1$ surface, a resonant layer has to be considered, and the Z function turns out to be dependent on x and a numerical solution of the equation becomes necessary. This effect has been studied by other authors, and it has been concluded that the parallel electron Landau damping does not appreciably affect the stability of the resistive kink. A detailed treatment on the effects of the electron Landau damping on the $m = 1$ mode can be found in Ref.[27].

C The circulating particle resonant term

The transit resonance enters the dispersion relation through the term

$$\rho_j(\omega - \omega_*)\nu^C. \tag{110}$$

In order to calculate ν^C for $m = 1$, we use Eq. (88) and Eq. (86) in the limit of $\omega_r << \omega_t$ and $\omega_i \to 0$. With ω_t we denote the transit frequency $\omega_t \equiv v_{th}/R$. Since the condition for a particle to be circulating is roughly $v_{||} > \sqrt{2\epsilon}v_\perp$, we expect to find two different results according to the value of $\epsilon = r_s/R$.

In the small ϵ limit, with $\omega_t > \omega_r > \sqrt{2\epsilon}\omega_t$, almost all of the resonant particles are circulating and a straightforward calculation yields

$$\nu^C(\epsilon \to 0) = -\frac{\pi^{1/2}}{2}\omega_t \tag{111}$$

which is a very large value when compared to the real frequency of a kink mode ($\omega_r \sim \omega_{*i}$). This result was previously found in Ref. [26]. For finite ϵ the result can be very different. Eq. (86), which is valid for "highly passing" particles, could not in principle be used for low frequency modes, because the passing particle portion of the velocity space can be very small. However a simple estimate can still be done. Since the resonant velocity is the wave phase velocity, it follows that Γ_m^C can be written in the following form:

$$\Gamma_m^C \simeq -\frac{i\pi^2 m^2}{2|k_{\|m}|R^2}\int_0^u \left(\frac{v_\perp^2}{2} + v_\|^2\right)^2 \frac{\partial F}{\partial \mathcal{E}} v_\perp dv_\perp \tag{113}$$

where

$$u \simeq \frac{\omega_r}{|k_{\|m}|\sqrt{2\epsilon}} \tag{114}$$

In the limit $\omega_r < \sqrt{2\epsilon}\omega_t$, the integration over the circulating particle domain in velocity space yields

$$\nu^C \simeq -\frac{\pi^{1/2}}{2}\omega_t \left(\frac{\omega_r}{\omega_t}\right)^6 f(\epsilon) \tag{115}$$

where

$$f(\epsilon) = \left[\frac{1}{48\epsilon^3} + \frac{1}{4\epsilon^2} + \frac{1}{\epsilon}\right]. \tag{116}$$

Note that for realistic value of ϵ and frequencies of the order of the ion diamagnetic frequency, ν turns out to be much smaller than its value in the cylindrical limit. However a better estimate should be done including the θ modulation of ϵ and performing a change of variables in μ, ϵ and Λ.

Since the simple estimate given in Eq. (115) leads to vanishingly small values of ν^C, we will neglect the effects of the transit resonance in the course of this Chapter.

For realistic values of the aspect ratio ($\epsilon \simeq 1/3$) and for realistic β's, ν^C turns out to be vanishingly small for low frequency modes ($\omega \sim \omega_{*i}$) and therefore it will be neglected in the course of this Chapter.

D The dispersion relation

Equations (108)-(110) are most easily solved in conjugate (k-) space through the introduction of generalized Fourier transforms (cf. [24]). A single, second order differential equation involving the transform of the parallel perturbed current is obtained:

$$\sigma\frac{d^2J}{d\sigma^2} - \frac{1}{2}\frac{dJ}{d\sigma} - \frac{1}{4}Q^2(1+\sigma)J(\sigma) = 0 \tag{117}$$

where $\sigma \equiv \delta^2 k^2$,

$$\delta \equiv \left[-i\epsilon_\eta \frac{\hat{\omega}(\hat{\omega}-\omega_{*i})}{\omega_A(\omega-\omega_{*e})}\right]^{1/4} \tag{118}$$

represents the characteristic width of the singular layer, and

$$Q \equiv -i\delta^2 \frac{\hat{\omega}-\omega_{*e}}{\epsilon_\eta \omega_A} \tag{119}$$

The solution of Eq. (117), which decays at infinity, is

$$J(\sigma) = J_0 \exp(-\sigma/2)\ U[\frac{Q-1}{4}, -\frac{1}{2}, \sigma] \tag{120}$$

where U is a confluent hypergeometric function (Kummer's function). This solution must have $Re(\delta) > 0$ in order to converge at infinity and must obey the global boundary condition:

$$J(\sigma < 1) \propto 1 - \frac{1}{2}(\delta_{in}k^2) + \delta_{in}^2|k|^3(\lambda_H + \lambda_K) \tag{121}$$

where $\delta_{in} \equiv -\hat{\omega}(\hat{\omega}-\omega_{*i})/\omega_A^2$ is the width of the inertial layer. This global condition is the generalized Fourier transformation of the condition (on the current) that corresponds to the boundary condition (106) on the displacement (cf. [24]). Using the asymptotic form for Kummer's function, and matching it to the form given by Eq. (102), the dispersion relation is obtained:

$$\left[-\frac{\hat{\omega}(\hat{\omega}-\omega_{*i})}{\omega_A^2}\right]^{1/2} = \frac{1}{8}\left[\lambda_H + \lambda_K(\omega)\right]\ \frac{\Gamma[(Q-1)/4]}{\Gamma[(Q+5)/4]}Q^{3/2} \tag{122}$$

Eq. (122) is the desired form of the dispersion relation for resistive internal kink modes. Because of the complicated functional dependence of Λ_K on the mode

frequency, a numerical solution is necessary. We have solved Eq. (122) in the ideal regimes ($\eta \to 0$) and the results are reported below.

E Discussion

Although Eq. (122) is valid in both resistive and ideal regimes, we analyze in detail only the ideal case ($\eta \to 0$) and we give only qualitative indication of the kinetic effects on resistive modes. We also consider only kinetic bulk ions and we will discuss the case of kinetic electrons at the end of this section.

For $\epsilon_\eta \to 0$, Eq. (122) can be easily solved yielding the following dispersion relation

$$\sqrt{\hat{\omega}(\hat{\omega} - \hat{\omega}_{*i})} = i\omega_A(\lambda_H + \lambda_K(\hat{\omega})). \tag{123}$$

Since we expect the growth rate to be small compared to ω_A and the real frequency of the mode to be of the order of ω_{*i}, we define a reference frequency $\omega_A\delta$ with $\delta = 5 \cdot 10^{-3}$ and rewrite the Eq. (123) in a dimensionless form

$$\sqrt{\bar{\omega}(\bar{\omega} - \bar{\omega}_{*i})} = i(\bar{\lambda}_H + \bar{\lambda}_K) \tag{124}$$

where $\bar{\omega} = \omega/\delta\omega_A$, $\bar{\omega}_{*i} = \omega_{*i}/\delta\omega_A$, $\bar{\lambda}_H = \lambda_H/\delta$ and $\bar{\lambda}_K = \lambda_K/\delta$.

For a rigid rotor distribution function $\bar{\lambda}_K$ can be written in the following form

$$\bar{\lambda}_K = (\bar{\omega} - \bar{\omega}_{*i})\hat{\lambda}_K(\bar{\omega}) \tag{125}$$

where $\hat{\lambda}_K$ is a complex number having the real part representing the nonresonant particle contribution and the immaginary part related to the trapped particle resonance with the precession drift ω_{Dh}. In order to derive some qualitative results we neglect the resonant particle contribution (the numerical solution will include the resonant effects). With $\hat{\lambda}_K$ real, we can exactly solve the dispersion relation [Eq. (124)] and find for the following expression for the growth rate

$$\bar{\omega}_i^2 = \frac{1}{1+\hat{\lambda}_K^2}\left[\bar{\lambda}_H^2 - \frac{(\bar{\omega}_{*i} + 2\bar{\lambda}_H\hat{\lambda}_K)^2}{4(1+\hat{\lambda}_K^2)}\right] \tag{126}$$

Note that for $\hat{\lambda}_K = 0$ the standard FLR-MHD dispersion relation is recovered. It is also important to remember that $\bar{\lambda}_H + Real[\bar{\lambda}_K]$ has to be positive for the eigenfunction to exist. Eq. (126) can be solved for $\bar{\lambda}_H$ at marginal stability, giving the following results

$$\bar{\lambda}_H = \frac{1}{2} \frac{\bar{\omega}_{*i}}{\sqrt{1 + \hat{\lambda}_K^2} - \hat{\lambda}_K} \tag{127}.$$

The following conclusions can be extracted from Eq. (127).

Positive $\hat{\lambda}_K$ enhances the FLR stabilization term. On the contrary negative values of $\hat{\lambda}_K$ lower the instability threshold. In Fig. 9 a plot of $\hat{\lambda}_K$ versus $\omega_r/\bar{\omega}_{Dh}$ for $\omega_i = 0$ shows that if $\omega_r >> \omega_{Dh}$ then $\hat{\lambda}_K < 0$ and the stability threshold is lowered and if $\omega_r << \omega_{Dh}$ then $\hat{\lambda}_K > 0$ and the stability threshold is higher. Since two branches of the internal kink mode exist (the high frequency branch at $\omega_r \simeq \omega_{*i}$, and the low frequency branch at $\omega_r \simeq 0$), we expect a reduction of the FLR stabilization mechanism on the high frequency branch and an enhancement on the low frequency branch.

More interesting is the case when the equilibrium distribution function is not of the "rigid-rotor" form. Combining the procedure used in Chapter 4 where an arbitrary dependence on ϵ and P_ϕ has been retained for the equilibrium distribution function, it is easy to show that the correct result can be obtained by simply replacing

$$\Omega \frac{\partial F}{\partial \mathcal{E}} \rightarrow \frac{1}{Ze} \frac{\partial F}{\partial P_\phi} \tag{128}$$

in the expression for λ_K given in Eq. (101). For simplicity we neglect the equilibrium electric field and consider the ion species confined by the Lorentz force only. After a straightforward calculation, assuming flat density profiles and a maxwellian distribution function

$$F = n_0 \left(\frac{m}{2\pi T(\Psi)}\right)^{3/2} exp[-\frac{\mathcal{E}}{T(\Psi)}] \tag{129}$$

one finds the following expression for λ_K

$$\lambda_K = \frac{4\pi^2}{s(r_s) B_\theta^2(r_s)} \int_0^{r_s} (\omega - \alpha\omega_{*i}) r \hat{b}(r) \tag{130}$$

and where $\hat{b}$ is given in Eq. (94) and

$$\alpha = \frac{\int_0^\infty \frac{x^{5/2}e^{-x}}{x-\mathcal{E}_r}(x-\frac{3}{2})dx}{\int_0^\infty \frac{x^{5/2}e^{-x}}{x-\mathcal{E}_r}dx} \tag{131}$$

where the term ϵ_r is a function of the mode frequency and it can be written in the following form

$$\mathcal{E}_r = \frac{\omega}{\bar{\omega}_{Dh}} \frac{r}{r_s H(\kappa^2)} \tag{132}$$

with $\bar{\omega}_{Dh}$ and $H(\kappa^2)$ given in Eq. (102) and (104) respectively. The term λ_K in Eq.(130) can be rewritten as the sum of the λ_K that we had obtained with a rigid-rotor distribution function and a new term which depends on the choice of the distribution function,

$$\lambda_K = (\omega - \omega_{*i})\hat{\lambda}_K + (1-\alpha)\omega_{*i}\hat{\lambda}_K \tag{133}$$

Fig. 10a shows the dependence of $Real[\hat{\Lambda}_K] = (1-\alpha)\hat{\lambda}_K(s_0\sqrt{2}/\beta_p)$ on the the real mode frequency. Notice that for $\bar{\omega} > 1.17$, $Real[\hat{\Lambda}_K]$ is positive. Fig. 10b shows a plot of $Real[\hat{\Lambda}_K]$ versus $\bar{\gamma} \equiv \bar{\omega}_i$ for $Real[\bar{\omega}] \rightarrow 1.17$. Note the strong dependence of $Real[\hat{\Lambda}_K]$ on the growth rate. Those results are important for the analysis that follows.

For mode frequencies $\omega >> \bar{\omega}_{Dh}$, Eq.(131) yields $\alpha = 2$ and for $\omega << \bar{\omega}_{Dh}$ gives $\alpha = 1$. Assuming a constant ω_{*i}, the $\omega << \bar{\omega}_{Dh}$ case leads to the previous results obtained with a "rigid-rotor" distribution function. The case $\omega >> \bar{\omega}_{Dh}$ leads to a very interesting conclusion. In the limit $\omega_{*i} >> \omega_{Dh}$ the stability treatment of the high frequency branch of the internal kink requires $\alpha \simeq 2$. Eq. (104) can therefore be replaced with

$$\bar{\lambda}_K = (\bar{\omega} - 2\bar{\omega}_{*i})\hat{\lambda}_K \tag{134}$$

with $\hat{\lambda}_K$ computed with a maxwellian distribution function.

The new marginal stability condition can now be written in the following form

$$\bar{\lambda}_H = \bar{\omega}_{*i}\left[\hat{\lambda}_K + \frac{1}{2}\frac{1}{\sqrt{1+\hat{\lambda}_K^2} - \hat{\lambda}_K}\right]. \tag{135}$$

Since for $\bar{\omega} >> \bar{\omega}_{Dh}$, $\hat{\lambda}_K$ is negative we conclude that for sufficiently large $|\hat{\lambda}_K|$ the stability threshold can be reached at negative values of $\bar{\lambda}_H$. This kinitically induced instability will be denoted as Kinetic Kink Mode (KKM).

Fig. 11 shows the growth rate of the (KKM) as a function of $\beta_p \equiv 2\mu_0 p(0)/B_\theta^2(r_s)$, for $\omega_{*i}/\bar{\omega}_{Dh} = 5$, $(r_s/a) = 1/3$ and $q_0 = 0.9$. The growth rate is normalized to $5 \cdot 10^{-3}\omega_A$. Note that the mode is unstable also for small values of β_p. At large values of β_p the instability is mainly driven by the nonresonant contribution (as described above), but for small values of β_p the resonant particle contribution become large because the real frequency decreases and approaches $\bar{\omega}_{Dh}$. The numerical solution in Fig. 11 shows a sharp threshold in β_p.

From the numerical solution of the dispersion relation it turns out that a somewhat stringent condition for instability is $\omega_{*i}/\bar{\omega}_{Dh} \geq 4$. In the cylindrical limit it is readily found that

$$\frac{\omega_{*i}}{\bar{\omega}_{Dh}} = -\left(\frac{r}{T}\frac{dT}{dr}\right)_{r_s}\frac{R}{r_s} \tag{134}$$

For typical tokamak profiles with $T = T_0(1 - r^2/a^2)^2$, one finds

$$\frac{\omega_{*i}}{\bar{\omega}_{Dh}} \simeq 4\left(\frac{r_s}{a}\frac{R}{r_s}\right) \tag{134}$$

Since $R/a = 3$ in many tokamak the instability condition requires $r_s > a/3$.

However it must be considered that the instability threshold is a strong function of $\omega_{Dh}(\mathcal{E}, \Lambda)$ (not to be confused with $\bar{\omega}_{Dh}$). As pointed out by C.Z. Cheng[28] the inclusion of finite β and finite ellipticity effects can strongly affect the magnitude and the sign of ω_{Dh} and therefore deeply change the stability threshold for the KKM.

Since $\omega_{*e} \simeq -\omega_{*i}$ the trapped electrons give a stabilizing contribution. However , the magnetic drift frequency of trapped elctrons and the real frequency of the mode have equal sign and therefore the denominator of the trapped electron term is expected to be larger than the one of the trapped ion term. We conclude that the electron stabilizing effect is smaller than the ion destabilizng driver.

For the low frequency branch $\bar{\omega} < \bar{\omega}_{Dh}$, the sign of $\hat{\lambda}_K$ is positive and therefore is stabilized by the trapped ions. Hence we expect the resistive kink to be more stable than what predicted by the fluid theory.

5.10 Conclusions

In this Chapter we have derived a general eigenvalue equation for low-n kinetically modified MHD modes. The kinetic effects of trapped and circulating particles have been retained. In particular we have found that trapped bulk ions can destabilize the high frequency branch of the internal kink. The instability is driven by the nonresonant trapped ions and requires a somewhat large value of ω_{*i}/ω_{Dh}. The numerical solution of the dispersion relation indicates that a sharp threshold in β_p exists for the instability to grow and that stabilizing effects come from the trapped electron response. Although a more detailed analysis is needed, these preliminary studies indicates that the trapped electrons are not able to bring the mode to a complete stabilization.

CHAPTER 6.

Experimental data on gap modes: Comparison with theory

6.1 Introduction

In TFTR and DIII-D , experiments have been carried out that employ neutral beam injection to create an energetic ion population that simulates alpha particles. The main difference between an alpha and a beam induced hot ion species is in the distribution function which is isotropic for the alphas and highly anisotropic for injectd beams. Since the gap modes are driven unstable by resonant interaction with circulating particles, we expect tangential beams to properly simulate passing particles and the anisotropy of the beam to play only a minor role on the evolution of the instability. In addition, the present design of the International Thermonuclear Reactor (ITER) relies on 1.3Mev neutral beams to drive the tokamak current. Therefore, neutral beam experiments are also important to investigate the physics of future steady state tokamaks.

For the Ellipticity Induced Alfvén Eigenmode (EAE) and the Toroidicity Induced Alfvén Eigenmode (TAE), a necessary condition for instability is $v_b > v_A/3$ and $v_b > v_A/2$ respectively, where v_b is the beam velocity and v_A is the Alfvén velocity. From the expression of the TAE growth rate given in Sec. 4.5, we notice that the resonance at $v_{||} = v_A/3$ is weaker than the resonance at $v_{||} = v_A$, therefore,

a better threshold for the TAE would be $v_b > v_A$. In order to satisfy these conditions, a tokamak operation at high density, low magnetic field, and high energy beam is required.

6.2 The TFTR experiment

In TFTR, up to 14 MW of nearly balanced deuterium neutral beams with 110-kev maximum energy were tangentially injected into a deuterium plasma with the following parameters: $B > 1T$, $q(a) > 2.8$, $R_0 = 240cm$, $a = 75cm$, $n_e \simeq 3 \times 10^{13} cm^{-3}$, $T_e(0) \sim 2Kev$. For sufficiently high plasma density (i.e. low Alfvén velocity and high beam velocity) ($v_b > .7v_A$), bursts of magnetic fluctuations at a frequency of about 82 kHz were detected on the Mirnov coils signals. The mode was identified as having toroidal mode number $n = 2$ and poloidal mode number $m = 6$ and $m = 8$. The latter was measured at two different locations ($m = 6$ at $R_0 = 291$ cm and $m = 8$ at $R_0 = 310$ cm) close to the the plasma edge. A TAE with $n = 2$, $m = 6 - 7$ would resonant at the $q = 13/4$ surface that is located in proximity of the plasma boundary. As suggested by the Princeton group, the resonant surface could be in the interior of the plasma despite the detected high m number that resonates at the outer region of plasma column. A tentative explanation would be the following: the TAE with $n = 2$ has a stronger poloidal coupling if the frequency gap is wide enough to generate an open "channel" passing through the Alfvén continuum as shown in fig. 10. In such a configuration, all gap modes with different poloidal harmonics ($m = 2 - 3, m = 3 - 4, m = 4 - 5, \ldots$) are strongly coupled. It follows that the eigenfunction of the TAE with a fixed n number results from a combination of many gap modes , where we define gap modes as the modes originating from the coupling of only two poloidal harmonic. If the resonant surface is well inside the plasma column and a low-m gap mode is destabilized, measurements of poloidal harmonics at the plasma edge would always observe high-m numbers.

Drops in neutron emission rates have been detected and correlated to hot ions loss and magnetic fluctuations amplitudes. A substantial beam particle loss up to

7% has been observed during the high frequency bursts. The TFTR experiment is certainly the first experimental evidence of the existence of Toroidicity Induced Alfvén Eigenmodes destabilized by energetic particles.

6.3 The DIII-D experiment

Of greater interest for the theoretical predictions developed in the course of this thesis are the experiments conducted on elliptical plasmas as in DIII-D. In this section we will search experimental evidence of the existence of the Ellipticity Induced Alfvén Eigenmode in the DIII-D data. For this purpose we will thoroughly analyze the results presented in Ref.[2].

DIII-D is well suited for Alfvén gap mode studies. Its low aspect ratio ($a = 65cm$, major radius $R_0 = 167cm$ and elongation ($\kappa \simeq 2$) permit low toroidal field ($< 1T$), moderate density ($< n_e > \simeq 5 \times 10^{13} cm^{-3}$), moderate current ($\sim 1MA$) operation without encountering density or q limits. Its neutral beams are intense ($< 20MW$), energetic ($< 80kev$), and fairly tangential (Fig.12). In the discharge we are going to describe $13.1Mw$ of deuterium beam was injected in a deuterium plasma in the direction of the plasma current. The plasma parameters at $1745ms$ from the beginning of the discharge were: $B_\phi = .8T$, $I_p \simeq .7MA$ and $< n_e >= 3.8 \times 10^{13} cm^{-3}$. As shown in Fig. 13, high frequency bursts of magnetic fluctuation were observed on the signal of the Mirnov coils located near the outer midplane. In Fig. 14, the cross power (a) and coherence (b) spectra of two B_θ signals between 1745.4 and $1747.4ms$ are shown. The peaks are labeled with their toroidal mode number. The high frequency mode analysis is shown in Table 2, where the frequency, the toroidal, and the poloidal mode numbers of the mode are reported. Drops in the neutron emission rate are correlated with the high frequency bursts implying that energetic beam particles are lost due to MHD activity.

A The mode frequency

Table 2 shows that a mode with frequency $64kHz$ and toroidal mode number $n = 3$ is excited. Notice that the poloidal mode number is mainly $m = 4 - 6$. An EAE with $m = 4 - 6$ could be a good candidate for the burst at $64kHz$. Using Eq. (81) in Sec.2.6 where the EAE frequency is derived in the limit of small ellipticity, one finds $f_{EAE} \simeq 74kHz$. ThE frequency of an $n = 3$, $m = 4 - 5$ TAE would also be close to the measured value ($f_{TAE} \simeq 54$kHz). The predicted frequency seems to be close to the measured one. Unfortunately in a rotating and high-β plasma like the one in DIII-D, the theoretical prediction of the mode frequency must account for the effects of the plasma rotation and the bulk ion finite larmor radius effects. The measured plasma rotational frequency is $f_R \sim (10-17)kHz$ and the bulk ion diamagnetic drift frequency for $n = 1$ is $f_{*i} = \omega_{*i}/2\pi n \simeq 6kHz$. The next step is to compute the frequency of an Alfvén wave in the laboratory frame, including the finite diamagnetic frequency and the plasma rotation effects.

We consider a plasma consisting of bulk ions (i), bulk electron and and energetic ion species. Each species is rotating rigidly with flow velocity $\mathbf{U_j} = -R\Omega_j \mathbf{e}_\phi$. The dispersion relation for shear Alfvén waves in such a plasma can be deduced from Sec. 7 in Chapter 5.

Defining ρ_j as the density of the species j, the dispersion relation reads

$$\sum_j \rho_j(\hat{\omega} - \omega_{*j})\hat{\omega} = k_{||}^2 B^2 \tag{1}$$

where $\hat{\omega} = \omega + n\omega_E$ and $\omega_E = d\Phi/d\Psi$ (Φ is the electrostatic potential). The rotational frequency is related to ω_E and ω_* through the equilibrium relation

$$n\Omega_j = -n\omega_E + \omega_{*j} \tag{2}$$

Substituting Eq. (2) into Eq. (1) and solving for ω in the limit $\omega_A >> \omega_{*_i}$ and $n_b\omega_{*b} \sim n_i\omega_{*i}$, yields

$$\omega = n\Omega_i + \frac{1}{2}\left(\frac{n_b}{n_i}\omega_{*b} - \omega_{*i}\right) + \omega_A. \tag{3}$$

If we assume that the equilibrium electric field is large enough to balance the Lorentz force and the pressure gradient of the bulk ions then $n\Omega_i$ and ω_{*i} have opposite signs.

The next step is to calculate the beam contribution to the mode frequency. For an estimate of the ratio n_b/n_i, we use the fact that the average beam beta is about equal to the average bulk ion beta ($< \beta_b > \simeq < \beta_i > \sim 3\%$). Evaluating the hot ion temperature with a slowing down distribution function leads to a constant value

$$T_b \simeq \frac{1}{6} E_b \tag{4}$$

where E_b is the beam energy. It then follows that

$$\frac{n_b}{n_i} \simeq \frac{6T_i}{E_b}. \tag{5}$$

For $T_i \simeq 3Kev$ and $E_b \simeq 70Kev$ one finds

$$\frac{n_b}{n_i} \simeq \frac{1}{4}. \tag{6}$$

A simple estimate for ω_{*b} can be easily found by relating ω_{*b} to ω_{*i} as follows

$$\omega_{*b} = \frac{d\ln n_b}{d\ln T_i} \frac{T_b}{T_i} \omega_{*i}. \tag{7}$$

For peaked hot ion species, density profiles with $d\ln n_b/d\ln T_i \sim 3$ and $T_b/T_i \sim 4$, Eq. (7) yields

$$\omega_{*b} \sim 12\omega_{*i}. \tag{8}$$

Substituting into Eq.(3) yields the following relation for the mode frequency in the laboratory frame

$$f = f_A \pm n[|f_R| - |f_{*i}|] \tag{9}$$

where $f_{*i} \equiv \omega_{*i}/2\pi|n|$, $f_R = \Omega/2\pi$ and $f_A = \omega_A/2\pi$. Using the estimated value of $f_{*i} = 6kHz$ and $f_R = 12kHz$ one finds the following frequencies for the first three modes in Table 2 if they really were EAE ($n = 3$) and TAEs ($n = 4$ and $n = 5$):

Table 3

EAE	**n=3**	**m=4-6**	**f=59-95 kHz**
TAE	**n=4**	**m=5-6**	**f=34-82kHz**
TAE	**n=5**	**m=6-7**	**f=31-91kHz.**

The dispesion relation for shear Alfvén waves in a rotating plasma gives two values of the frequency in the laboratory frame (for each n number). In Fig. 14 we can notice the presence of double peaks corresponding to the same n number. With some degree of approximation we can relate the two frequencies of each mode in table 3 to a couple of peaks in Fig.14 except for the $n = 5$. Because of the high number of modes that have been excited, it is however very difficult to find both peaks of the doppler shifted frequencies.

6.4 Stability of gap modes in DIII-D

In the DIII-D experiment, the cross power of the B_θ oscillation has been measured through a poloidal array of Mirnov coils. The power content of each poloidal harmonic indicates the poloidal structure of the mode. Table 2 shows the toroidal and the main poloidal mode numbers corresponding to the high frequency bursts shown in Fig.14. In order to make a reasonable comparison with our low-n gap mode theory, we focus on the first three modes of table 2 with $n < 5$.

First we notice that the lower poloidal mode number is $n + 1$. From the expressions of the growth rate given in Chapter 4 , we notice that the alpha particle instability driver is proportional to $nq_{gap} \propto m$. On the other hand, when m is much larger than n, the resonant surface $q = q_{gap}$ is very close to the plasma boundary where few energetic particles are present. Therefore, the theory predicts an optimum m number for instability that is slightly larger than n and is in general agreement with the experiment. The next step is to consider the $(n = 3, m = 4-6)$ mode in Table 2 as an EAE and the $(n = 4, m = 5-6)$, $(n = 5, m = 6, 7)$ as TAEs. The stability analysis for the EAEs and TAEs is carried out using an expression

for the growth rate slightly different from the one derived in Sec. 5.5 where the α particle density profile was consistently derived. In the NBI experiment, the beam deposition profile is very uncertain. Therefore, we let the hot particle density gradient scale length be a free parameter. We consider a gaussian hot ion species density profile given by

$$n_b = n_{b0} e^{-\frac{r^2}{L_b^2}}$$

where L_b can vary in the range $0 < L_b < a$. A reasonable value of L_b would be $.3 - .5a$. In fig. 16 (a,b,c), the marginal stability boundaries for the gap modes in Table 2 are plotted in a $< \beta_b >$, L_b/a plane. The value $< \beta_b >= 3\%$, represented by the horizontal line, indicates a reasonable approximation of the beam beta calculated with beam deposition codes. Fig. 16a shows that the EAE $n = 3$, $m = 4 - 6$ has a lower marginal stability threshold than the TAE $n = 3$, $m = 4 - 5$. Fig. 16b and 16c show that TAEs $n = 4$, $m = 5 - 6$ and $n = 5$, $m = 6 - 7$ are more unstable than the correspondent EAEs with the same toroidal and the same first poloidal wave number in exact agreement with the experiment. Furthermore, the $n = 5$ is predicted to be the most unstable mode. This is also in agreement with the experimental results presented in Fig.14 where the cross power is maximum for $n = 5$. Ref. [2] mentions the disagreement between the stability threshold calculated with the original formula of Fu and Van Dam for TAEs, the actual beam power necessary to excite these modes has turned out to be an order of magnitude larger than predicted. Our estimate of the growth rate which includes the ion Landau damping gives a threshold for instability higher than the Fu and Van Dam prediction and considers the electron Landau damping as the only stabilizing effect. For typical DIII-D parameters the ion Landau damping is about five times larger than the electron Landau damping. Thus our prediction can be considered to be in general agreement with the experiments. The theoretical analysis of the $n = 6$ and $n = 7$ modes detected in the experiment and reported in Table 2, requires the development of an high-n gap mode theory which is urgently needed. According to the computer simulations reported in Ref.[3], the high-n modes can induce a larger hot particle losses than low-n. However very high n have been found to be stable

when the finite radial excursion of the α particles orbits is taken into account. We conclude that an optimum n number exists which is an intermidiate value, for which the growth rate is maximum (as also observed in the experiments).

6.5 Conclusions

In this chapter we have reviewed the experimental evidence of Alfvén gap modes and we have attempted an analysis of the experimental data. Both the measured and predicted frequencies match with a good degree of accuracy. The stability analysis show that the EAEs and TAEs are unstable in DIII-D. The theory also predicts a beam power larger than the one orginally considered to excite these modes. Although this evidence are not conclusive to proof the existence of Alfvén gap modes, it is certainly indicative of the resonance particle destabilization of electromagnetic waves in high temperature plasmas.

CHAPTER 7.

Concluding Remarks.

Through the various chapters of this thesis we have attempted to investigate how kinetic effects can affect the stability of MHD modes. We have considered toroidal high temperature plasmas in regimes of interests to thermonuclear fusion research. The most promising device for plasma confinement are toroidal machines with a strong magnetic field. The success of the magnetic fusion program relies on the prospect that plasma heating provided by the charged fusion reaction products can compensate for all forms of energy loss. Recent experimets have shown that the confinement of energetic particles is strongly dependent on the presence of macroscopic magnetic fluctuations. During minority ions heating in JET[1], it has been observed that plasma relaxation oscillations of the central part of the plasma column with structure dominated by the $m = 1$ and $n = 1$ poloidal and toroidal components (namely the sawtooth oscillations) causes a large loss of energetic particles. In TFTR and DIII-D recent experiments of tangential neutral beam injection have shown that high frequency MHD activity induces considerable losses of the beam particles. These high frequency magnetic perturbations are believed to be originated by the resonant interaction of Alfvén waves with circulating energetic particles.

The MHD stability of the plasma core is therefore crucial to guarantee alpha particle confinement in ignited tokamaks. In this thesis we have studied the effects of energetic particles on global Alfvén waves such as "gap modes" and the stability of the $m = 1$,$n = 1$ internal kink when kinetic effects are included.

The Alfvén Gap Modes

It has been recently shown that in toroidal plasma the poloidal coupling induced by toroidicity induces gaps in the Alfvén continuum and that within these gap, discrete modes (TAE) exist with poloidal structure dominated by two neighboorhing poloidal component. In Chapter 2 we have shown that the ellipticity of the plasma cross section has a similar effect. In particular, since many tokamaks have finite ellipticity ($\kappa - 1 \sim \epsilon$) as compared to a small toroidicity ($\epsilon << 1$), the ellipticity induced Alfvén eigenmode (EAE) may have a more global structure than the TAE. The poloidal structure of the EAE is mainly $m, m+2$ and its frequency is higher than the correspondent TAE's.

In the presence of an energetic particle population such as alpha particles, the gap modes can be destabilized by resonant interaction with circulating particles. In Chapter 3 we have derived an exact sufficient condition for stability against any high frequency perturbation. The criterion is valid for arbitrary apect ratio, arbitrary β, noncircular, axisymmetric tori. Its fluid-like nature, makes possible accurate evaluation in realistic geometries with only minor modifications to any one of the existing ideal MHD stability codes.

The growth of the gap modes is derived in Chapter 3 where a drift kinetic description of each particle species has been employed. It is found that the growth or damping of these modes depends upon a competition between the alpha particle driver, electron and ion Landau damping. The electron Landau damping turns out to be particular important for the $m = 1, n = 1$ EAE in highly elongated plasmas ($\kappa \sim 2$). We have also shown that the ion Landau damping can stabilize the TAE at high density regimes. For sufficiently high densities and toroidal mode number $n > 1$ the EAE can have a stability threshold lower than that of the corresponding TAE. Both the EAE and the TAE need further investigation to determine how detrimental their effects can be on alpha particle comfinement in ignited tokamak.

Experimental data on high frequency magnetic fluctuations induced by ener-

getic particle tangentially injected in tokamaks (TFTR and DIII-D) are anlyzed in Chapter 6. We conclude that there can be some possibility that ellipticity induced Alfvén eigenmodes have been detected in DIII-D.

The $m = 1$ internal kink mode

It has been recently shown[2,3] that kinetic effects are of great importance for the stability of the $m = 1$ internal kink. Previous theoretical investigations have been mostly concerned with the effect of trapped hot ions. It was concluded that a small population of trapped energetic particles can stabilize the ideal and resistive kink. Recent experements in JET have also confirm the theory. During ICRH heating in JET[4], the internal relaxation oscillations of the electron temperature have been suppressed for a period up to 3.2 sec. These sawtooth-free discharges are charachterized by the presence of anisotropic (mostly trapped) high energy ions, accelerated by radio frequency fields at the ion-cyclotron resonance.

In Chapter 5 we studied the effects of bulk trapped ions and electron on the stability of the internal kink mode. We have concluded that trapped ions can destabilize the high frequency branch ($\omega \sim \omega_{*i}$) of the $m = 1$ mode. The instability is driven by the nonresonant trapped particle population precessing toroidally at the magnetic drift frequency. The first analysis of this mode seems to show the presence of a threshold in β_p which in principle can be a very low value. The resonant interaction of the mode with the precessing ions gives an additional destabilizing contribution. The trapped electrons are usually stabilizing but since they mostly precess in the same direction of the rotational frequency of the mode, their effect is not sufficient to reach complete stabilization. Although these first results shows the existence of this new instability, a more detailed investigation is certainly needed.

References of Chapter 1

[1]Ya.I. Kolesniscenko, Nucl. Fusion **20**,727 (1980).

[2]R.B. White, M.S. Chance, J.L. Johonson, H.E. Mynick, F.W. Perkins and A.H. Reiman in Plasma Physics and Controlled Nuclear Fusion Research , **2**, 111, 1988

[3]J.D. Strachan, B.Grek, W. Heidbrink, D. Johonson, S.M. Kaye, H.W. Kugel, B. leBlanc and K. McGuire, Nuclear Fusion **25**, 863 (1985)

[4]L. Chen, R. B. White and M. N. Rosenbluth, Phys. Rev. Lett. **52**, 1122 (1984).

[5]B. Coppi and F. Porcelli, Phys. Rev. Lett. **57**, 2272 (1986).

[6]B. Coppi. S. Migliuolo and F. Porcelli, Phys. Fluids **31**, 1630 (1988).

[7]K. McGuire et al.,Phys. Rev. Lett. **50**, 891 (1983)

[8]K.L. Wong et al.,Phys. Rev. Lett. **66**, (1991).

[9]W.W. Heidbrink, E.J. Strait, E. Doyle, G.Sager and R. Snider, General Atomics, Report GA-A20254.

[10]D.J. Sigmar, C.T. Hsu, R. White and C.Z. Cheng , MIT-PFC, Report PFC/ja-89-59.

[11]D. Campbell et al., Phys. Rev. Lett. **60**, 2148 (1988).

[12] F. Porcelli, Bulletin of the European Physical Society , Berlin, 1991

[13] B. Coppi, R. J. Hastie, S. Migliuolo, F. Pegoraro, and F. Porcelli, *Phys. Lett.* **A132**, 267 (1988).

[14] M. N. Rosenbluth, S. T. Tsai, J. W. VanDam, and M. G. Engquist, Phys. Rev. Lett. **51**, 1967 (1983).

[15]D.A. Spong, D.J. Sigmar, K.T. Tsang, J.J. Ramos, D.E. Hastings and W.A. Cooper, Physica Scripta **T16** , 18 (1987).

References of Chapter 2

[1]S. Riyopoulos, S. Mahajan, Phys. Fluids **29**, 731 (1986)

[2]C. Z. Cheng, M. S. Chance, Phys. Fluids **29**, 3659 (1986).

[3]R. Betti, J. P. Freidberg, Phys. Fluids **B3**, 538 (1991).

[4]J.P. Freidberg, Ideal Magnetohydrynamics, Pergamon Press

[5]G. Bertin, A. Einaudi in Comments on Plasma Physics

[6]K. Appert,R. Gruber,F.Troyon and J. Vaclavik, Plasma Phys. **24**, 1147 (1982)

[7]D. Edery, G. Laval, R. Pellat, J. L. Soulé, Phys. Fluids **19**, 260 (1976).

[8]S. P. Hakkarainen, R. Betti, J. P. Freidberg, R. Gormley, Phys. Fluids **B2**, 1565 (1990).

[9]R. Betti, J. P. Freidberg, Phys. Fluids **B3**, 1865 (1991).

[10]G. Y. Fu, J. W. Van Dam, Phys. Fluids B1, 2404 (1989).

[11]G. Y. Fu, J. W. Van Dam, Phys. Fluids B1, 1949 (1989).

[5]J. W. Van Dam, G. Y. Fu, C. Z. Cheng, Fus. Tech. **18**, 461 (1990).

[12]R. Betti, J. P. Freidberg, submitted to Phys. Fluids

[13]F. Zonca, L. Chen, Bull. Am. Phys. Soc. **35**, 2069 (1990).

[14]Z. Guo, H. L. Berk, J. W. Van Dam, D. E. Baldwin, C. Z. Cheng, Bull. Am. Phys. Soc. **35**, 1923 (1990).

[15]G. Bertin and B. Coppi, Astrophysical Journal, **298**, 387 (1985)

References of Chapter 3

[1]R. A. Dandl, H. O. Eason, G. E. Guest, C. L. Hedrick, H. Ikegami and D. B. Nelson in *Plasma Physics and Controlled Nuclear Fusion Research 1974*, Proceedings of the 5th International Conference, Tokyo (IAEA, Vienna, 1975) Vol. 2, p. 141.

[2]G. B. Guest, C. L. Hedrick and D. B. Nelson, Phys. Fluids **18**, 871 (1975).

[3]L. Chen, R. B. White and M. N. Rosenbluth, Phys. Rev. Lett. **52**, 1122 (1984).

[4]B. Coppi and F. Porcelli, Phys. Rev. Lett. **57**, 2272 (1986).

[5]B. Coppi. S. Migliuolo and F. Porcelli, Phys. Fluids **31**, 1630 (1988).

[6]R. B. White, F. Romanelli and M. N. Bussac, Phys. Fluids **B2**, 745 (1990).

[7]K. Appert, R. Gruber, F. Troyon and J. Vaclavik, Plasma Phys. **24**, 1147 (1982).

[8]D. W. Ross, G. L. Chen and S. M. Mahajan, Phys. Fluids **25**, 652 (1982).

[9]S. M. Mahajan, D. W. Ross and G. L. Chen, Phys. Fluids **26**, 2195 (1983).

[10]S. M. Mahajan, Phys. Fluids **27**, 2238 (1984).

[11]B. Hoffman, Ch. Hollenstein, B. Joye, R. Keller, A. Lietti, J. B. Lister, J.-M. Moret, S. Nowak, J. O'Rourke, A. Pochelon and W. Simm, Plasma Phys. Controlled Fusion **26**, 173 (1984).

[12]Y. M. Li, S. M. Mahajan and D. W. Ross, Phys. Fluids **30**, 1466 (1987).

[13]G. Y. Fu and J. W. Van Dam, Phys. Fluids **B1**, 2404 (1989).

[14]M. N. Rosenbluth and P. H. Rutherford, Phys. Rev. Lett. **34**, 1428 (1975).

[15]K. T. Tsang, D. J. Sigmar and J. C. Whitson, Phys. Fluids **24**, 1508 (1981).

[16]C. Z. Cheng and M. S. Chance, Phys. Fluids **29**, 3659 (1986).

[17]G. Y. Fu and J. W. Van Dam, Phys. Fluids **B1**, 1949 (1989).

[18]S. I. Braginskii in *Reviews of Plasma Physics*, edited by M. A. Leontovich, (Consultants Bureau, New York, 1965) Vol. 1.

[19]S. P. Hirshman and D. J. Sigmar, Nucl. Fusion **21**, 1079 (1981).

[20]C. E. Seyler and J. P. Freidberg, Phys. Fluids **23**, 331 (1980).

[21]Y. Z. Zhang, H. L. Berk and S. M. Mahajan, Nucl. Fusion **29**, 848 (1989).

[22]B. Coppi, P. Detragiache, S. Migliuolo, F. Pegoraro and F. Porcelli, Phys. Rev. Lett. **63**, 2733 (1989).

[23]J. F. Krall, PhD Thesis, Cornell University, "Stability of an Axisymmetric Mirror with an Energetic Ion Component," 1987.

References of Chapter 4

[1] R. Betti and J. P. Freidberg, Phys. Fluids **B3**, 538 (1991).

[2] K. L. Wong, R. J. Fonck, S. F. Paul, D. R. Roberts, E. D. Fredrickson, R. Nazikian, H. K. Park, M. Bell, N. L. Bretz, R. Budny, S. Cohen, G. W. Hammett, F. C. Jobes, D. M. Meade, S. S. Medley, D. Mueller, Y. Nagayama, D. K. Owens and E. J. Synakowski, Phys. Rev. Lett. **66**, (1991).

[3] C. Z. Cheng and M. S. Chance, Phys. Fluids **29**, 3659 (1986).

[4] G. Y. Fu and J. W. Van Dam, Phys. Fluids **B1**, 1949 (1989).

[5] C. Z. Cheng, Fus. Tech. **18**, 443 (1990).

[6] J. W. Van Dam, G. Y. Fu and C. Z. Cheng, Fus. Tech. **18**, 461 (1990).

[7] R. Betti and J. P. Freidberg, Phys. Fluids **B3**, 1865 (1991).

[8] K.T. Tsang, D.J. Sigmar and J.C. Whitson, Phys. Fluids **24**, 1508 (1981).

[9] J. Tataronis, J. Plasma Phys. **13**, 87 (1975).

[10] L. Chen and A. Hasegawa, Phys. Fluids **17**, 1399 (1974).

[11] F. Zonca and L. Chen, Bull. Am. Phys. Soc. **35**, 2069 (1990).

[12] Z. Guo, H.L. Berk, J.W. Van Dam, D.E. Baldwin and C.Z. Cheng ,Bull. Am. Phys. Soc. **35**, 1923 (1990).

References of Chapter 5

[1] S. von Goeler, W. Stodiek, and N. Sauthoff, *Phys. Rev. Lett.* **33**, 1201 (1974).

[2] B. B. Kadomtsev, *Sov. J. Plasma Phys.* **1**, 389 (1975).

[3] D. J. Campbell, D. F. H. Start, J. A. Wesson, D. V. Bartlett, V. P. Bhatnagar, M. Bures, J. G. Cordey, G. A. Cottrell, P. A. Dupperex, A. W. Edwards, C. D. Challis, C. Gormezano, C. W. Gowers, R. S. Granetz, J. H. Hamnen, T. Hellsten, J. Jacquinot, E. Lazzaro, P. J. Lomas, N. Lopes Cardozo, P. Mantica, J. A. Snipes, D. Stork, P. E. Stott, P. R. Thomas, E. Thompson, K. Thomser, and G. Tonetti, *Phys. Rev. Lett.* **60**, 2148 (1988).

[4] D. Meade and the TFTR Group, in *Plasma Physics and Controlled Nuclear Fusion Research 1990* (IAEA, Vienna, 1991).

[5] B. Coppi, R. J. Hastie, S. Migliuolo, F. Pegoraro, and F. Porcelli, *Phys. Lett.* **A132**, 267 (1988).

[6] B. Coppi, P. Detragiache, S. Migliuolo, F. Pegoraro, and F. Porcelli, *Phys. Rev. Lett.* **63**, 2733 (1989).

[7] R. B. White, P. H. Rutherford, P. Colestock, and M. N. Bussac, *Phys. Rev. Lett.* **60**, 2038 (1988).

[8] R. B. White, M. N. Bussac, and F. Romanelli, *Phys. Rev. Lett.* **62**, 539 (1989).

[9] Y. Z. Zhang, H. L. Berk, and S. M. Mahajan, *Nucl. Fusion* **29**, 848 (1989).

[10] Y. Z. Zhang and H. L. Berk, *Phys. Lett.* **A143**, 250 (1990).

[11] S. Migliuolo, F. Pegoraro, and F. Porcelli *Phys. Fluids* (in press, 1991).

[12] B. Coppi, R. Galvão, R. Pellat, M. N. Rosenbluth, and P. H. Rutherford, *Sov. J. Plasma Phys.* **2**, 533 (1976).

[13] G. Ara, B. Basu, B. Coppi, G. Laval, M. N. Rosenbluth, and B. V. Waddell, *Ann. Phys.* (NY) **112**, 443 (1978).

[14] M. N. Bussac, R. Pellat, D. Edery, and J. L. Soulé, *Phys. Rev. Lett.* **35**, 1638 (1975).

[15] R. Betti and J.P. Freidberg,*Phys. Fluids* **B3**, 538 (1991)

[16] B. Coppi and G. Rewoldt, in **Advances in Plasma Physics**, edited by A. Simon and W. B. Thompson (Interscience, NY, 1976), vol. 6, p. 421.

[17] R. Betti and J. P. Freidberg (in preparation, 1991).

[18] G. Rewoldt, W. M. Tang, and M. S. Chance, *Phys. Fluids* **25**, 480 (1982).

[19] B. Coppi, *Riv. Nuovo Cimento* **1**, 357 (1969).

[20] B. Coppi, J. Greene, and J. Johnson, *Nucl. Fusion* **6**, 101 (1966).

[21] B.D. Freid and S.E. Conte, *The Plasma Dispersion Function*, (Academic, New York, 1961)

[22] S. I. Braginskii, in **Reviews of Plasma Physics**, edited by M. A. Leontovich (Consultants Bureau, 1965), vol. 1 , p. 214.

[23] K.V. Roberts and J.B. Taylor, *Phys. Rev. Lett.* **8**, 197 (1962)

[24] F. Pegoraro and T. J. Schep, *Plasma Phys. Cont. Fusion* **28**, 647 (1986).

[25] B. Coppi, S. Migliuolo, F. Pegoraro, and F. Porcelli, *Phys. Fluids* **B2** , 927 (1990).

[26] F. Romanelli, L. Chen and R.B. White, *Nucl. Fusion*, **31** 631, (1991)

[27] B. Coppi and P. Detragiache, submitted to *Phys. Rev. Lett.*

[28] C.Z. Cheng, *PPPL-2604*, 1989

References of Chapter 6

[1]K.L. Wong et al.,Phys. Rev. Lett. **66**, (1991).

[2]W.W. Heidbrink, E.J. Strait, E. Doyle, G.Sager and R. Snider, General Atomics, Report GA-A20254.

[3]D.J. Sigmar, C.T. Hsu, R. White and C.Z. Cheng , MIT-PFC, Report PFC/ja-89-59.

References of Chapter 7

[1] G. Sadler, Contibution to the IAEA Technical Committee Meeting on α-particles in Fusion Research, Aspenas, Sweden, 1991

[2] B. Coppi, R. J. Hastie, S. Migliuolo, F. Pegoraro, and F. Porcelli, *Phys. Lett.* **A132**, 267 (1988).

[3] B. Coppi, P. Detragiache, S. Migliuolo, F. Pegoraro, and F. Porcelli, *Phys. Rev. Lett.* **63**, 2733 (1989).

[4] D. J. Campbell, D. F. H. Start, J. A. Wesson, D. V. Bartlett, V. P. Bhatnagar, M. Bures, J. G. Cordey, G. A. Cottrell, P. A. Dupperex, A. W. Edwards, C. D. Challis, C. Gormezano, C. W. Gowers, R. S. Granetz, J. H. Hamnen, T. Hellsten, J. Jacquinot, E. Lazzaro, P. J. Lomas, N. Lopes Cardozo, P. Mantica, J. A. Snipes, D. Stork, P. E. Stott, P. R. Thomas, E. Thompson, K. Thomser, and G. Tonetti, *Phys. Rev. Lett.* **60**, 2148 (1988).

Appendix A: Calculation of b^+ and b^-

The coefficient b_m can be accurately estimated by variational techniques. The appropriate Lagrangians for b_m^- and b_m^+, corresponding to Eq. (36), are given by

$$\mathcal{L}^- = \int_0^{1-\epsilon} y f_m \left[y^2 \xi_m'^2 + (m^2-1)\xi_m^2\right] dy - c^2 f_m'(1) \ln \epsilon \qquad (A1)$$

$$\mathcal{L}^+ = \int_{1+\epsilon}^{k} y f_m \left[y^2 \xi_m'^2 + (m^2-1)\xi_m^2\right] dy + c^2 f_m'(1) \ln \epsilon \qquad (A2)$$

where $y = r/r_0, k = a/r_0$ and in Eqs. (A1) and (A2), $c = 1/b_m^-$ and $c = 1/b_m^+$ respectively. This variational principle is valid only if ξ_m satisfies the following two conditions. First, near the singular layer

$$\xi_m(y) = 1 + c \ln |y-1|. \qquad (A3)$$

Second, ξ_m must be properly normalized by choosing the solutions at $r = 0$ and $r = a$ to be regular, with amplitude independent of c: that is, $\xi_m(0) \approx a_1 y^{m-1}$ and $\xi_m(k) \approx a_2(k-y)$ with a_1 and a_2 independent of c.

In the analysis c is treated as a variational parameter to be evaluated in the limit $\epsilon \to 0$. The validity of the variational principle can be easily verified by standard techniques using the relations $\delta\xi(1) = \delta c \ln \epsilon$ [from Eq. (A3)] and $\delta\xi(k) = 0$ (from the normalization). A convenient choice of trial functions is as follows

$$\xi_m^- = \xi_1(y) + c\xi_2(y)$$
$$\xi_m^+ = \xi_3(y) + c\xi_4(y) \qquad (A4)$$

where

$$\xi_1 = y^{m-1}$$
$$\xi_2 = y^{m+1} \ln\left(\frac{1-y^2}{2}\right)$$
$$\xi_3 = y^{-m-1}\left(\frac{k^{2m}-y^{2m}}{k^{2m}-1}\right) \qquad (A5)$$
$$\xi_4 = y^{-m-1}\left(\frac{k^{2m}-y^{2m}}{k^{2m}-1}\right)\left(\frac{k^2-y^2}{k^2-1}\right)\ln\left(\frac{y^2-1}{2}\right).$$

Substituting into the Lagrangian yields expressions of the form

$$\mathcal{L} = I_0 + 2cI_1 + c^2 I_2. \tag{A6}$$

Minimizing with respect to c we obtain

$$\begin{aligned} b_m^- &= -I_2^-/I_1^- \\ b_m^+ &= -I_2^+/I_1^+ \end{aligned} \tag{A7}$$

In the limit $\epsilon \to 0$, the integrals can be written as

$$\begin{aligned} I_1^- &= \int_0^1 y f_m \left[y^2 \xi_1' \xi_2' + (m^2-1)\xi_1 \xi_2\right] dy \\ I_2^- &= \int_0^1 \left\{ y f_m \left[y^2 \xi_2'^2 + (m^2-1)\xi_2^2\right] + \frac{f_m'(1)}{1-y} \right\} dy \\ I_1^+ &= \int_1^k y f_m \left[y^2 \xi_3' \xi_4' + (m^2-1)\xi_3 \xi_4\right] dy \\ I_2^+ &= \int_1^k \left\{ y f_m \left[y^2 \xi_4'^2 + (m^2-1)\xi_4^2\right] - \frac{f_m'(1)}{y-1} \right\} dy + f_m'(1)\ln(k-1). \end{aligned} \tag{A8}$$

Note that in the expression for I_2^- and I_2^+, the integrands are finite as $y \to 1$. Equations (A7) and (A8) are the desired expressions for b_m^- and b_m^+.

Appendix B. Electrostatic modification of $\tilde{f}$

In this appendix we show that the existence of an equilibrium electric field $\mathbf{E}_0 \equiv -\nabla\phi_0$ does not fundamentally alter Eq. (27) upon which our stability analysis is based. To lowest order in r_{Le}/a the electrons are isothermal and therefore neglecting the electron inertia, the parallel electron momentum equation can be written as

$$\mathbf{E}_{\|} = -\nabla_{\|}\frac{1}{e}\int\frac{dp_e}{n_e}. \tag{B1}$$

Linearizing Eq. (B1) gives the following expression of the perturbed parallel electric field

$$E_{\|1} = -\mathbf{b}\cdot\nabla(\boldsymbol{\xi}_\perp\cdot\mathbf{E}_0). \tag{B2}$$

The definition of the $\mathbf{E}\times\mathbf{B}$ displacement can be rewritten as follows:

$$\mathbf{E}_1 \equiv i\omega\boldsymbol{\xi}_\perp\times B_0 - \nabla(\boldsymbol{\xi}_\perp\cdot\mathbf{E}_0) \tag{B3}$$

an Eq. (19) becomes

$$\mathbf{E}_1\cdot\mathbf{v} = -i\omega\frac{m_j}{q_j}\left[\frac{d}{dt}(\boldsymbol{\xi}_\perp\cdot\mathbf{v}) - \mathbf{v}\cdot\frac{d\boldsymbol{\xi}_\perp}{dt}\right] - \frac{d}{dt}(\boldsymbol{\xi}_\perp\cdot\mathbf{E}_0). \tag{B4}$$

Substituting these results into Eq. (17) leads to the following form of Eq. (20)

$$f_{1j} = -q_j\left[\frac{\partial F_j}{\partial p_\phi}\boldsymbol{\xi}_\perp\cdot\nabla\psi + \frac{\partial F_j}{\partial\epsilon}\boldsymbol{\xi}_\perp\cdot\nabla\phi_0\right] + im_j\left(\omega\frac{\partial F_j}{\partial\epsilon} - n\frac{\partial F_j}{\partial p_\phi}\right)\left[(\boldsymbol{\xi}_\perp\cdot\mathbf{v}) - \int_{-\infty}^{t}\mathbf{v}\cdot\frac{d\boldsymbol{\xi}_\perp}{dt'}dt'\right]. \tag{B5}$$

Following the averaging procedure described in section IID leads to an unchanged form of Eq. (27)

$$f_{1j} \approx -\boldsymbol{\xi}_\perp\cdot\nabla F + im_j(\omega-\hat{\omega}_j^*)\frac{\partial F}{\partial\epsilon}\left[\boldsymbol{\xi}_\perp\cdot\mathbf{v} - \int_{-\infty}^{t}a_0dt'\right].$$

However, in the calculation of the divergence of the pressure tensor, the equilibrium electric field contributes through an inertial term $\simeq \sum_j \rho_j\omega\omega_E$; where ρ_j is the density of the species j, and $\omega_E \equiv k_\perp\cdot\frac{E_0\times B_0}{B_0^2}$. For Alfvén waves ($\omega\sim\omega_A$) and for small α particle population ($\rho_i \gg \rho_\alpha$), the ion inertia dominate ($\rho_i\omega^2 \gg \rho_j\omega\omega_E$) and the equilibrium electric field contribution can be neglected.

Appendix C. Calculation of B

In this Appendix we show how to compute the term B necessary to evaluate the continuum damping effect. Our formula is restricted to the case of only one "intersection" with the continuum, i.e. there is only one Alfvén wave of the continuum spectrum with the same frequency of the gap mode. However the simple theory presented here can easily be extended to the general case of multiple interaction.

For simplicity we consider TAE modes (the same procedure can be applied to EAE and NAE) and we write the eigenvalue equation in the following form

$$D\xi_m + \epsilon F \xi_p = 0 \qquad (C.1)$$

$$D\xi_p + \epsilon F \xi_m = 0 \qquad (C.2)$$

where $p = m + 1$, and

$$D = \frac{d}{dr}[r^3\rho(\omega^2 - \omega_A^2)]\frac{d}{dr} - \rho r(\omega^2 - \omega_A^2)(m^2 - 1) \qquad (C.3)$$

$$F = \rho_g r_0^3 \omega_g^2 \frac{d^2}{dr^2}. \qquad (C.4)$$

. With ω_g we denote the Alfvén frequency at the gap location, r_g. We also assume that the intersection with the continuum takes place with the spectrum of the mth harmonic. Following the standard procedure presented in Sec. 2.5 and 4.6, we write the eigenfunction as combinations of a regular (ξ_{rm}, ξ_{rp}) and a singular part (ξ_{sm}, ξ_{sp}) which presents a logarithmic behavior about the continuum resonance surface $r = r_0$. According to the previuos analysis we order

$$\xi_{sm} \sim B \sim \xi_{rm}(\frac{\hat{\gamma}}{\epsilon})^{1/2} \qquad (C.5)$$

$$\xi_{pr} \sim \xi_{mr}. \qquad (C.6)$$

Rewriting Eq. (C.1) and (C.2) in terms of these new variables and after some straightforward manipulations one finds

$$\xi_{sm} = -\frac{\int_0^r dr'\left(\xi_{rm}^*[D\xi_{rm} + \epsilon F \xi_p] + \xi_{sm} D\xi_{rm}^*\right)}{\rho r^3(\omega^2 - \omega_{Am}^2)\xi_r^*} + constant \qquad (C.7)$$

where $\xi_p = \xi_{rp} + \xi_{sp}$, ξ^* is the complex conjugate of ξ , $\omega_{Am} = (n - m/q)v_A/R$ and $r < r_0$. In the neighborhood of r_0 we expect ξ_s to be of the form

$$\xi_{sm}(r \simeq r_0) = B \ln(i\hat{x} + \hat{\gamma}) \tag{C.8}$$

where $\hat{x}$ and $\hat{\gamma}$ have been defined in Eq. (89) and (102). In the limit of $r \to r_0$, from Eq. (C.8) it follows

$$L(r \to r_0)\frac{d\xi_s}{dr} = \frac{B}{\hat{x} - i\hat{\gamma}} sgn\left(\omega_r \frac{d \ln \omega_A^2}{dt}\right)\frac{d \ln \omega_a^2}{dr}) \tag{C.9a}$$

In order to find B we use a standard matching procedure. We consider the limit for $r \to r_0$ of Eq. (C.7). After some straightforward manipulations one finds

$$L(r \to r_0)\left[\frac{d\xi_{sm}}{dr} + \epsilon \frac{\rho_0 r_0^3 \omega^2}{\rho r^3(\omega^2 - \omega_{Am}^2)} \frac{d^2\xi_{sm}}{dr^2}\right] =$$

$$L(r \to r_0)\left[\frac{\xi_{sm}\xi'_{rm}}{\xi^{*2}_{rm}} - \frac{\int_0^r \left(\xi^*_{rm}[D\xi_{rm} + \epsilon F \xi_{pr}] + \xi_{sm} D\xi^*_{rm}\right)dr}{\rho r^3(\omega^2 - \omega_{Am}^2)\xi^*_{rm}}\right] \tag{C.9b}$$

We now evaluate ξ_{sp} by solving Eq. (C.1) and (C.2) in the neighborhood of the continuum resonance surface.

Following the adopted ordering one finds that for $r \simeq r_0$ Eq. (C.1) and (C.2) yield

$$\frac{d^2\xi_{sp}}{dr^2} = -\epsilon \frac{\omega^2}{\omega^2 - \omega_{Ap}^2(r_0)} \frac{d^2\xi_{sm}}{dr^2}. \tag{C.10}$$

Substituting into Eq. (C.9b) and keeping only the lowest order terms gives

$$L(r \to r_0)\frac{d\xi_{sm}}{dr} = -\frac{\int_0^{r_0} \xi^*_{rm}[D\xi_{rm} + \epsilon F \xi_{pr}]dr'}{\rho_0 r_0^2(\omega^2 - \omega_A^2(r_0) - \epsilon^2\Omega^2)\xi^*_{rm}} \tag{C.11}$$

where

$$\Omega^2 \equiv \frac{\omega^4}{\omega^2 - \omega_{Ap}^2(r_0)} \tag{C.12}$$

Note that the toroidal coupling induces a small ($\sim \epsilon^2$) shift of the continuum resonance surface with respect to the cylindrical case. Comparing Eq. (C.11) with Eq. (C.9a) and after integarting by parts, one finds the following expression for B

$$B = -\frac{\int_0^{r_0} \left(\rho r(\omega^2 - \omega_A^2)[r^2|\xi'_{rm}|^2 + (m^2 - 1)|\xi_{rm}|^2] - \epsilon \xi^*_{rm} F \xi_{rp}]\right)dr'}{\rho_0 r_0^2 \omega^2 |\frac{d \ln \omega_A^2}{dr}|\xi^*_r(r_0)} \tag{C.13}$$

Eq. (C.13) is the desired form for B which turns out to depend on the regular part of the eigenfunction only. This result can be also applied to the cylindrical case ($\epsilon = 0$) to compute the damping of a continuum Alfvén wave.

To lowest order in ϵ the largest contribution of ξ_{rp} in the numerator of Eq. (C.13) comes from the layer around the gap location ($r = r_g$). In the neighborhood of r_g Eq. (C.1) can be written in the following form

$$\frac{d}{dr}(\omega^2 - \omega_{Am}^2)\frac{d\xi_m}{dr} = -\epsilon\omega^2\frac{d^2\xi_p}{dr^2} \qquad (C.14)$$

Substituting into Eq. (C.12) and integrating by parts yields

$$B = -\frac{P\int_0^{r_0}\left(\rho r(\omega^2 - \omega_A^2)|r^2|\xi'_{rm}|^2 + (m^2-1)|\xi_{rm}|^2|\right)dr'}{\rho_0 r_0^2\omega^2|\frac{d\ln\omega_A^2}{dr}|\xi_r^*(r_0)} \qquad (C.15)$$

where $P\int_0^{r_0} = \int_0^{r_g^-} + \int_{r_g^+}^{r_0}$ denotes an integration out of the gap region. From Eq. (C.15) we deduce that the calculation of B requires the knowledge of the regular part of the eigenfunction outside the gap region. An easy tecnique to calculate ξ_r can be found in Appendix A.

From Eq. (C.15) we expect B to be indeed small. First we notice that if $r_0 < r_g$, the continuum resonance takes place close to the magnetic axis and the integration domain in the numerator of (C.15) is small. If instead $r_0 > r_g$, the term $(\omega^2 - \omega_A^2)$ in the integral in the numerator of (C.15) changes sign, causing the numerator to be small. Furthermore if the continuum resonance surface is close to the plasma edge, then the term $(\partial \ln\omega_A^2/\partial r_0)$ is large causing B to be small. Although we have not reached an exact quantitative estimate of B, (that can be obtained only after obtaining ξ_r from Appendix A) we have shown that B is small and we think that an appropriate ordering is $B \sim \epsilon$. Substituing into Eq. (106) this give a continuum damping of order $\Gamma \sim \epsilon^3$.

Figure Captions

Fig. 1 Plot of $\omega(r)R_0/v_a \equiv k_p R_0$ vs $q(r)$ for the $n = 1$, $m = 1, 2, 3$ cylindrical eigenmodes.

Fig. 2 Plot of $\omega_A^2(r)R_0^2/v_a^2$ vs r/a for an inverted shear configuration. Note the minimum in ω_a^2

Fig. 3 Plot of $\omega(r)R_0/v_a \equiv k_p R_0$ vs $q(r)$ for the following elliptical spectra (a) $m = 1$, $n = 1$ and $m = 3$, $n = 1$; (b) $m = 2$, $n = 2$ and $m = 4$, $n = 2$; (c) $m = 3$, $n = 3$ and $m = 5$, $n = 3$; (d) $m = 4$, $n = 4$ and $m = 6$, $n = 4$.

Fig. 4 Plot of $\omega(r)R_0/v_a \equiv k_p R_0$ vs $q(r)$ for the following toroidal spectra (a) $m = 1$, $n = 1$ and $m = 2$, $n = 1$; (b) $m = 2$, $n = 2$ and $m = 3$, $n = 2$; (c) $m = 3$, $n = 3$ and $m = 4$, $n = 3$; (d) $m = 4$, $n = 4$ and $m = 5$, $n = 4$.

Fig. 5 Plot of $\omega(r)R_0/v_a$ vs $q(r)$ for the continuum ($n = 2, m = 2 - 4$) in an elliptical plasma with equilibrium density profile $n = n_0\sqrt{1 - r^2/a^2}$. The dashed line represents the frequency of an EAE $n = 2, m = 2 - 4$. Note the intersection with the continuum.

Fig. 6 Plot of the stability domain in the (n_e, T) for BPX-like parameters ($B_0 = 8.1$ T, $a = .79$ m, $R_0 = 2.59$ m, $q(0) = 1$, $q(a) = 3.5$): (a) $m = 1, n = 1$; (b) $m = 3, n = 3$; (c) $m = 5, n = 4$.

Fig. 7 Plot of the stability domain in the (n_e, T) space of the TAE $m = 1, n = 1$ for BPX, including ion Landau damping (solid line) and neglecting it (dashed line).

Fig. 8 Plot of the stability domain in the (n_e, T) space of the EAE $m = 1, n = 1$ for BPX, for different values of the plasma elongation and with $q(a) = 4$.

Fig. 9 Plot of the real part of $\hat{\lambda}_K\sqrt{2}s_0/\beta_p$ versus the real part of the eigenfrequency $\bar{\omega}_r$. Note that for $\bar{\omega} > 1.17$ the sign of $\bar{\Lambda}_K$ is negative and therefore destabilizing.

Fig. 10a Plot of the real part of $\hat{\Lambda}_k \equiv (1-\alpha)\hat{\lambda}_K\sqrt{2}s_0/\beta_p$ versus the real part of the eigenfrequency $\bar{\omega}_r$. Note that for $\bar{\omega} > 1.17$ the sign of $\hat{\Lambda}_K$ is positive and therefore destabilizing.

Fig. 10b Plot of the real part of $\hat{\Lambda}_K \equiv (1-\alpha)\hat{\lambda}_K\sqrt{2}s_0/\beta_p$ versus the immaginary part of the eigenfrequency $\hat{\gamma} \equiv \bar{\omega}_i$. Note that $\hat{\Lambda}_K$ is positive and and has a maximum at $\hat{\gamma} \simeq 1$.

Fig. 11 Plot of the real and immaginary part of the eigenfrequency $(\bar{\omega}, \bar{\gamma})$ versus the poloidal β $(\hat{\beta}_p = 2\mu_0 p(0)/B_\theta^2(r_s))$. Note the threshold in β_p.

Fig. 12 Plan view of the DIII-D tokamak.

Fig. 13 Signals from a Mirnov coil.

Fig. 14 Cross-power (a) and coherence (b) spectra of two B_θ signals.

Fig. 15 High frequency mode analysis (Table 2)

Fig. 16 Marginal stability boundaries in a $< \beta_{beam} >, L_b/a$ diagram for the discharge of Fig. 14, for the following modes: (a) EAE $n = 3, m = 3-5$ and TAE $n = 3, m = 3-4$, (b) EAE $n = 4, m = 5-7$ and TAE $n = 4, m = 5, 6$, (c) EAE $n = 5, m = 6-8$ and TAE $n = 5, m = 6, 7$. The parameter $< \beta_b >$ represents the average β of the beam, and L_b the hot beam particle density gradient scale length. The horizontal solid line indicates the estimated $< \beta_b >$ of 3 percent.

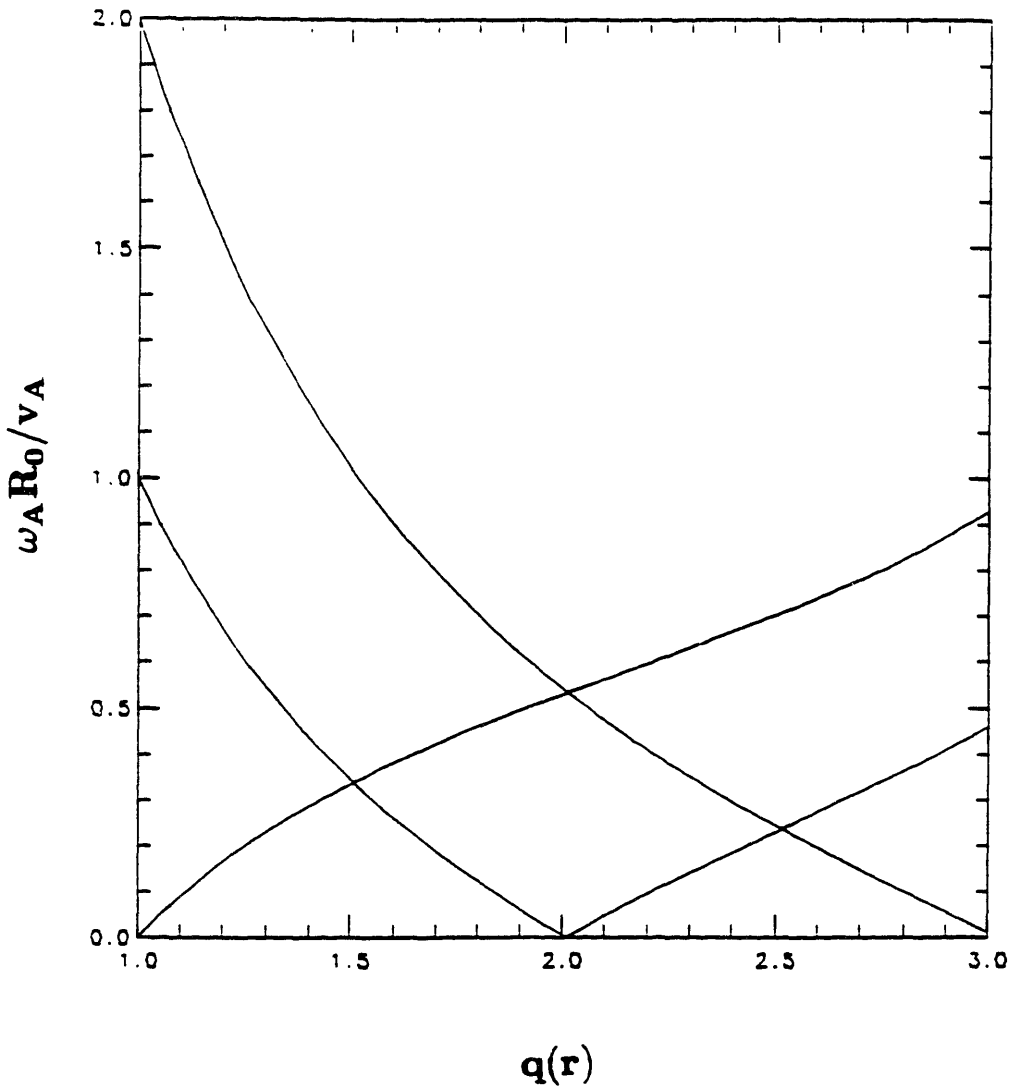

Figure 1

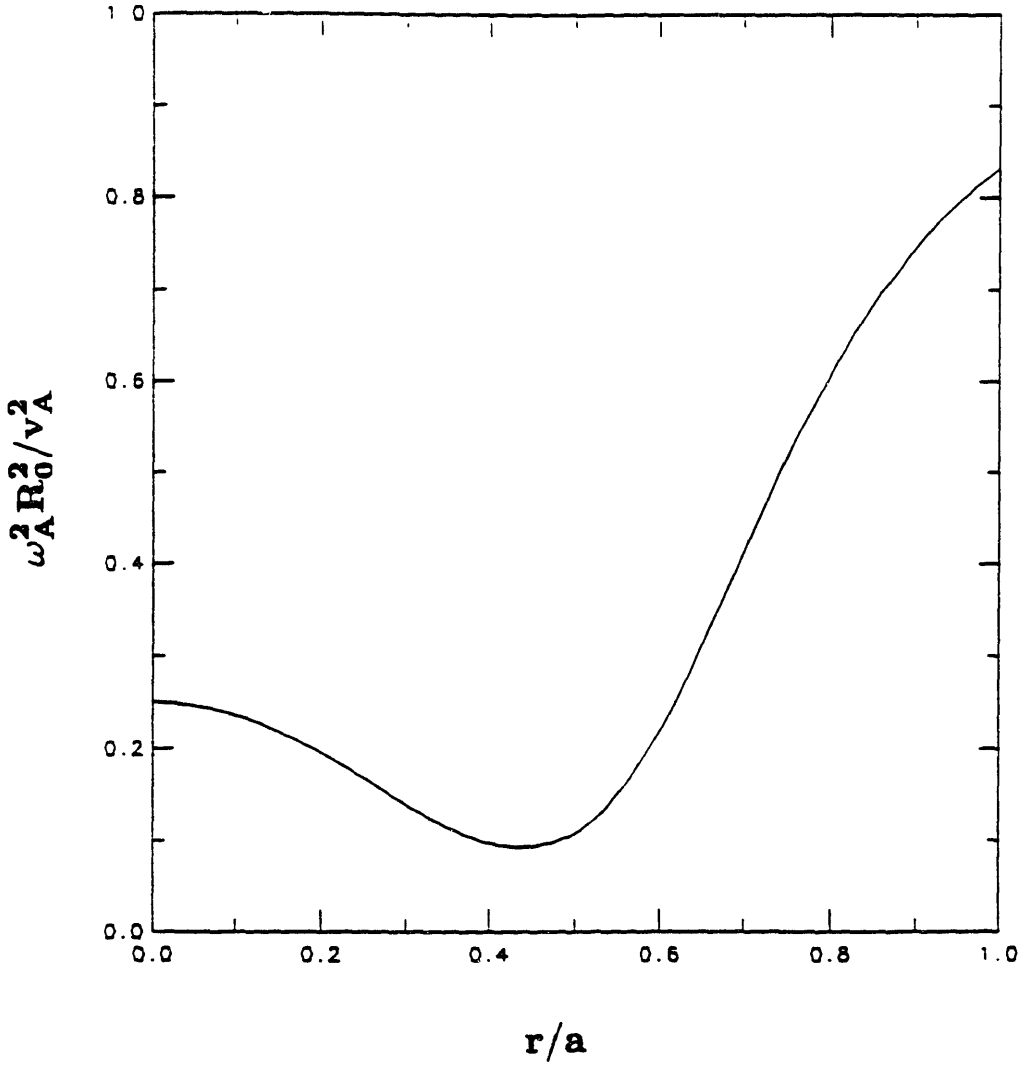

Figure 2

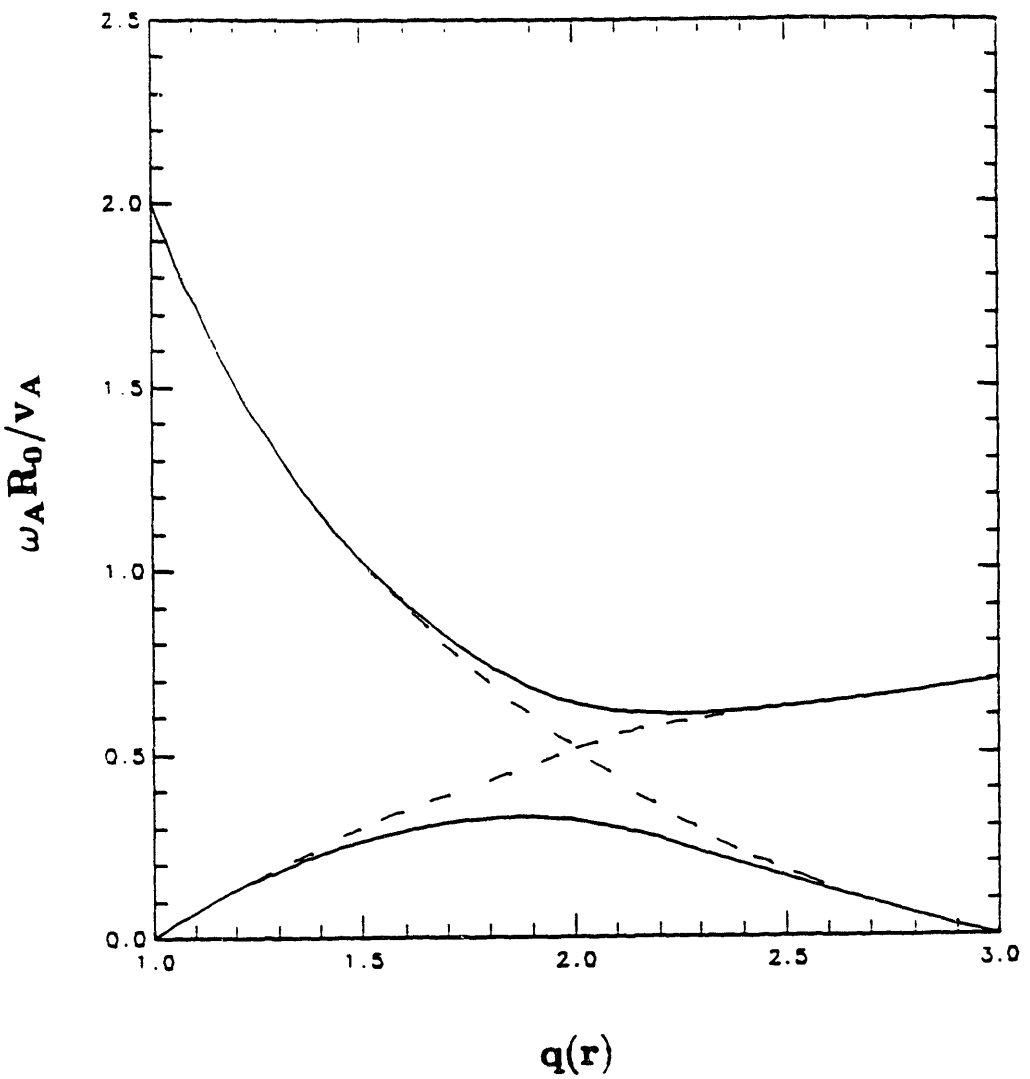

Figure 3a

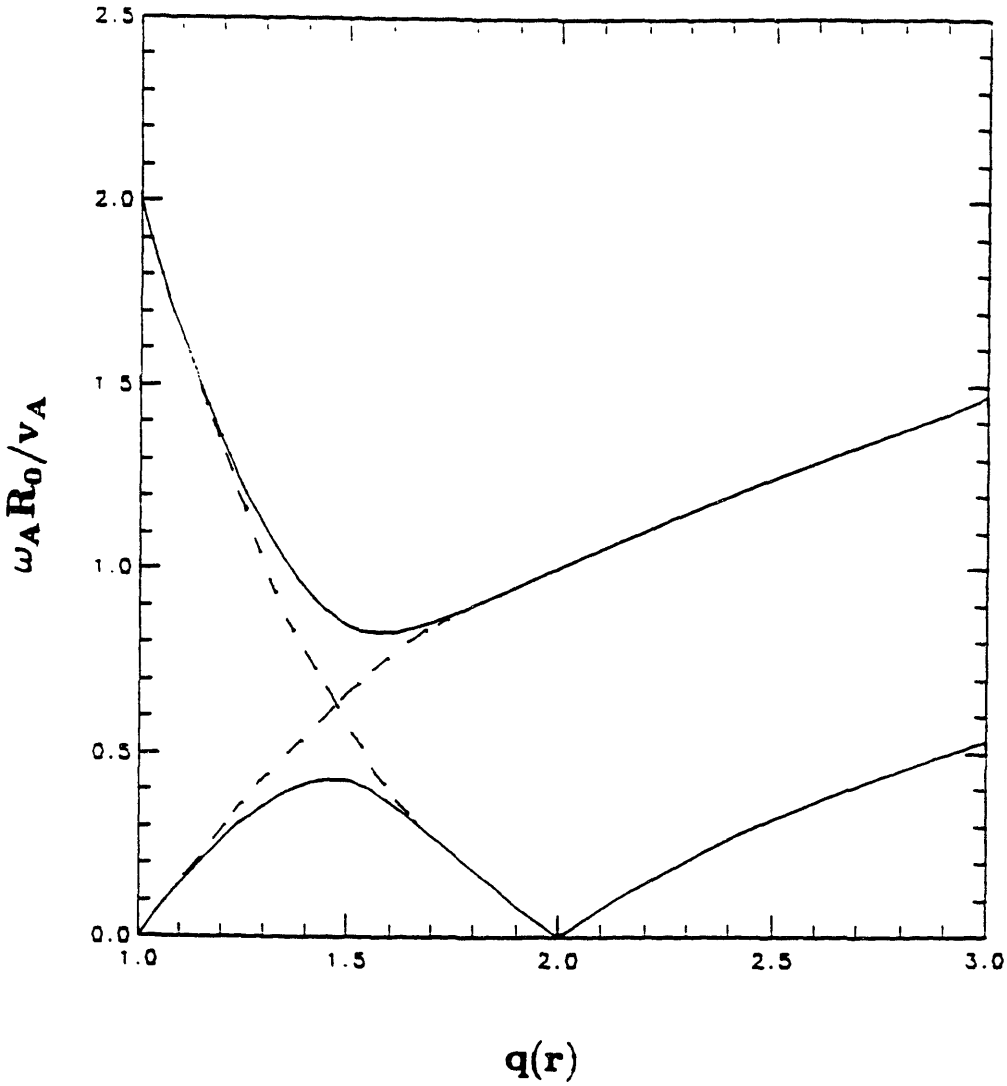

Figure 3b

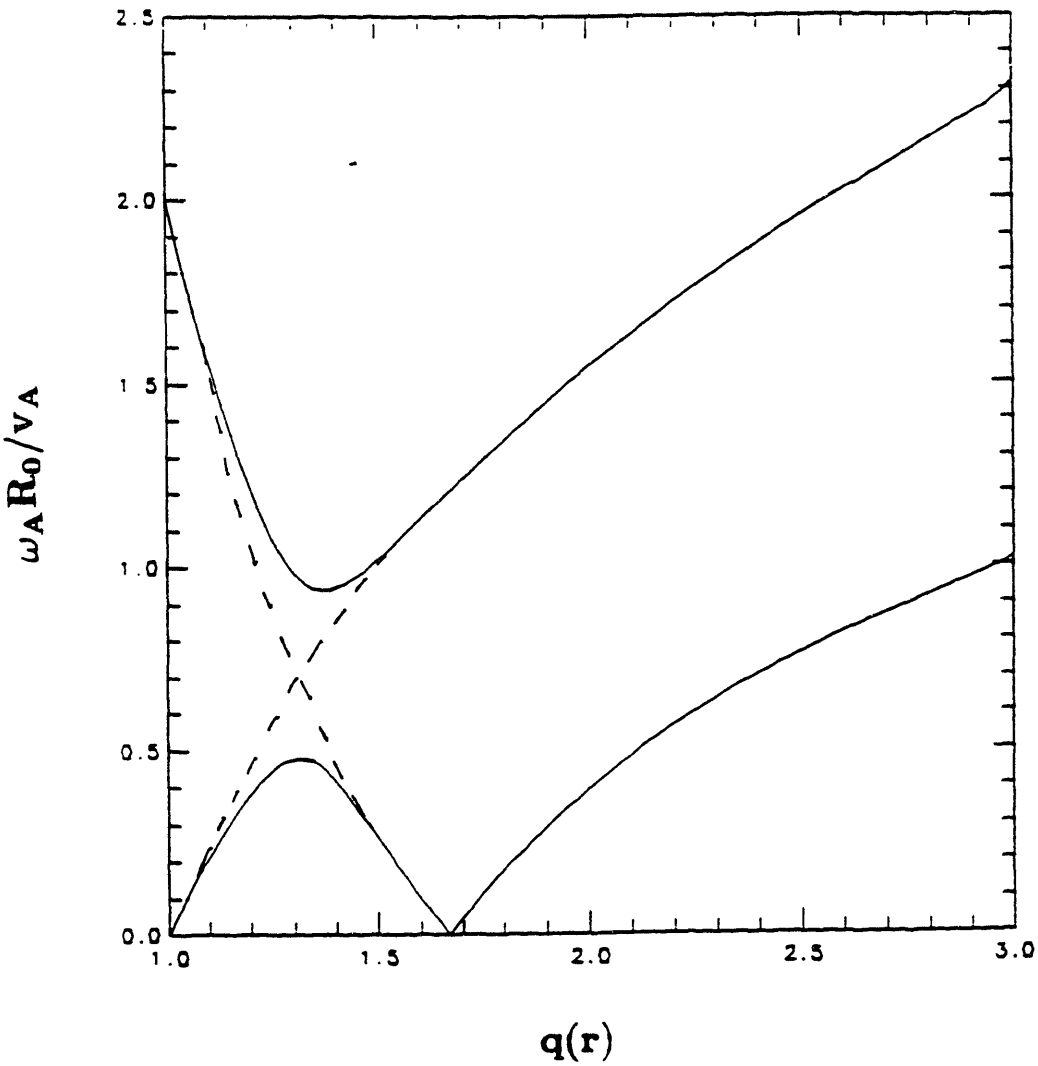

Figure 3c

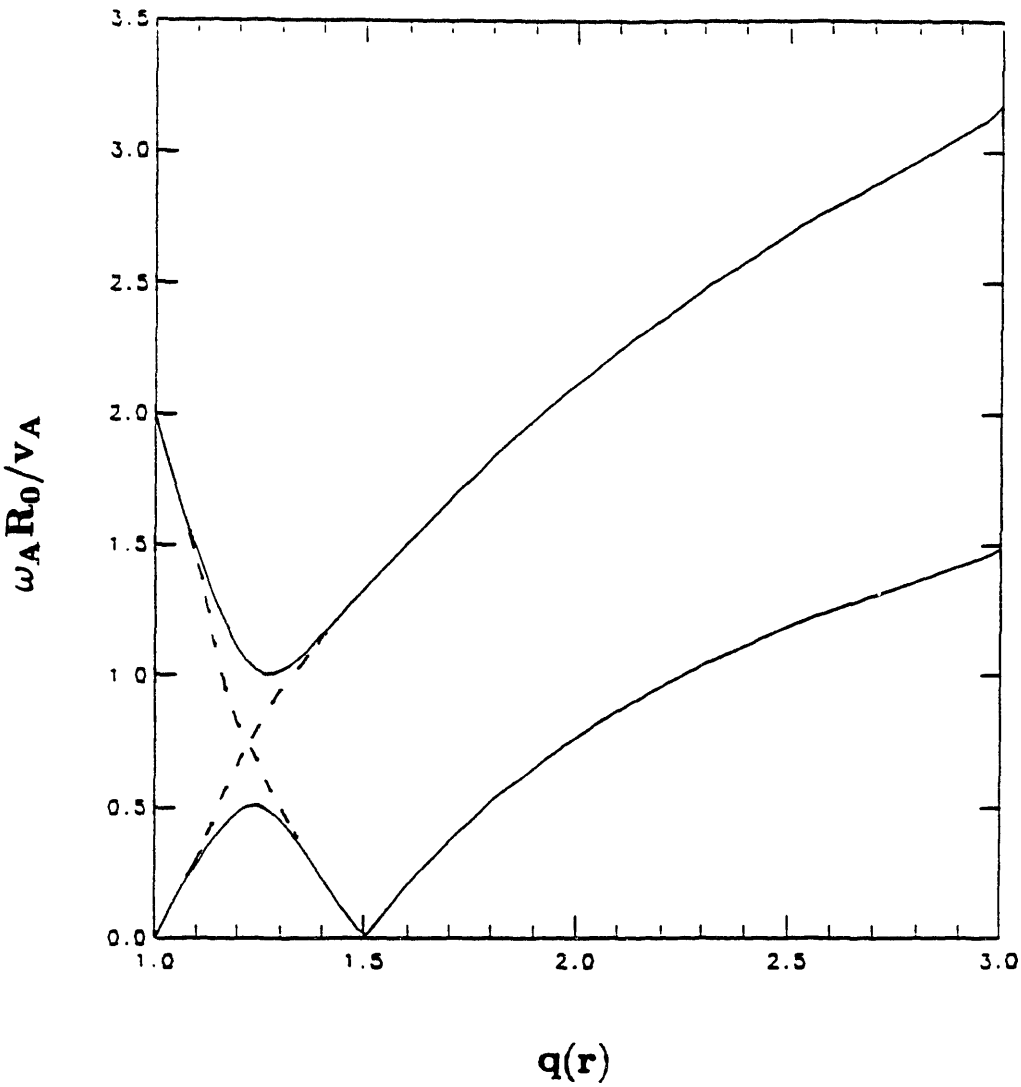

Figure 3d

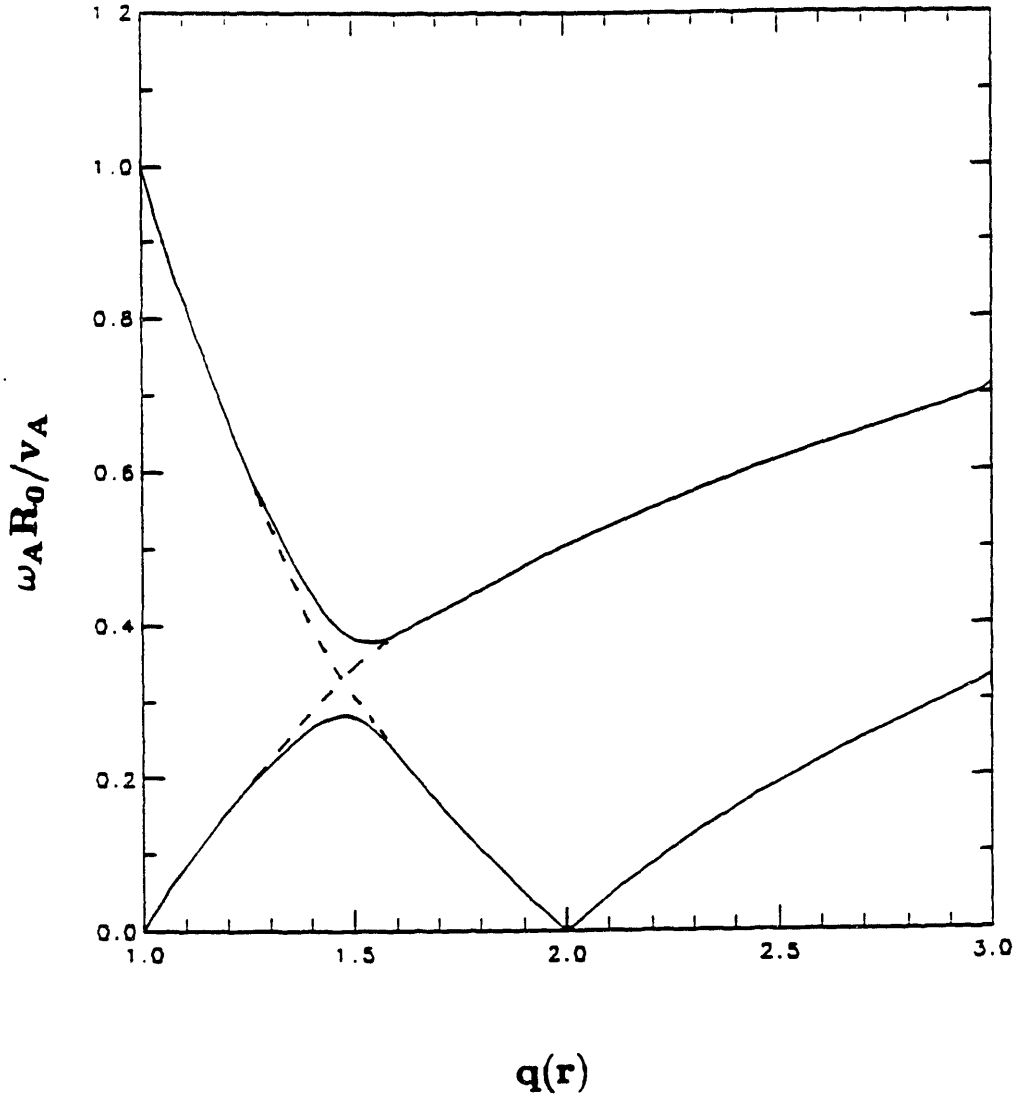

Figure 4a

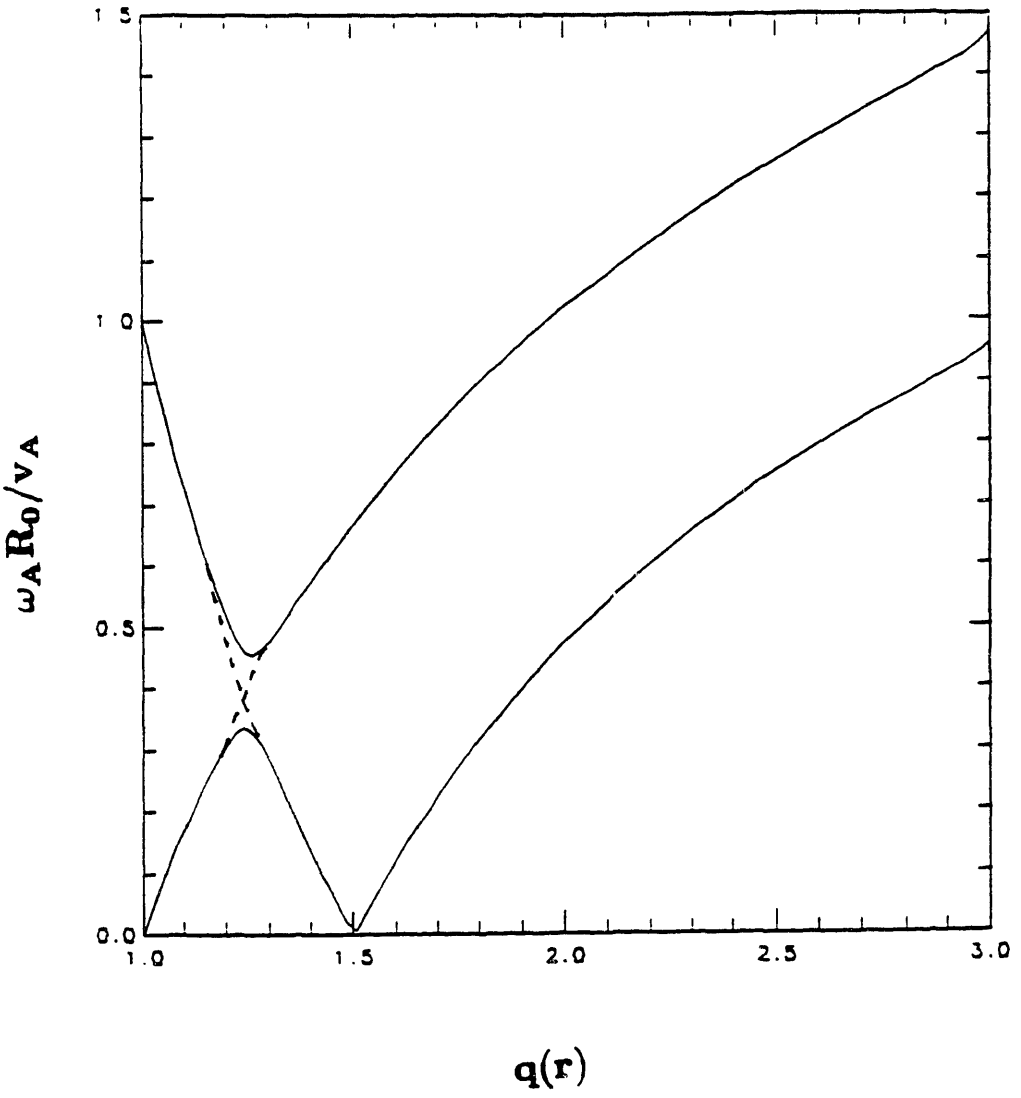

Figure 4b

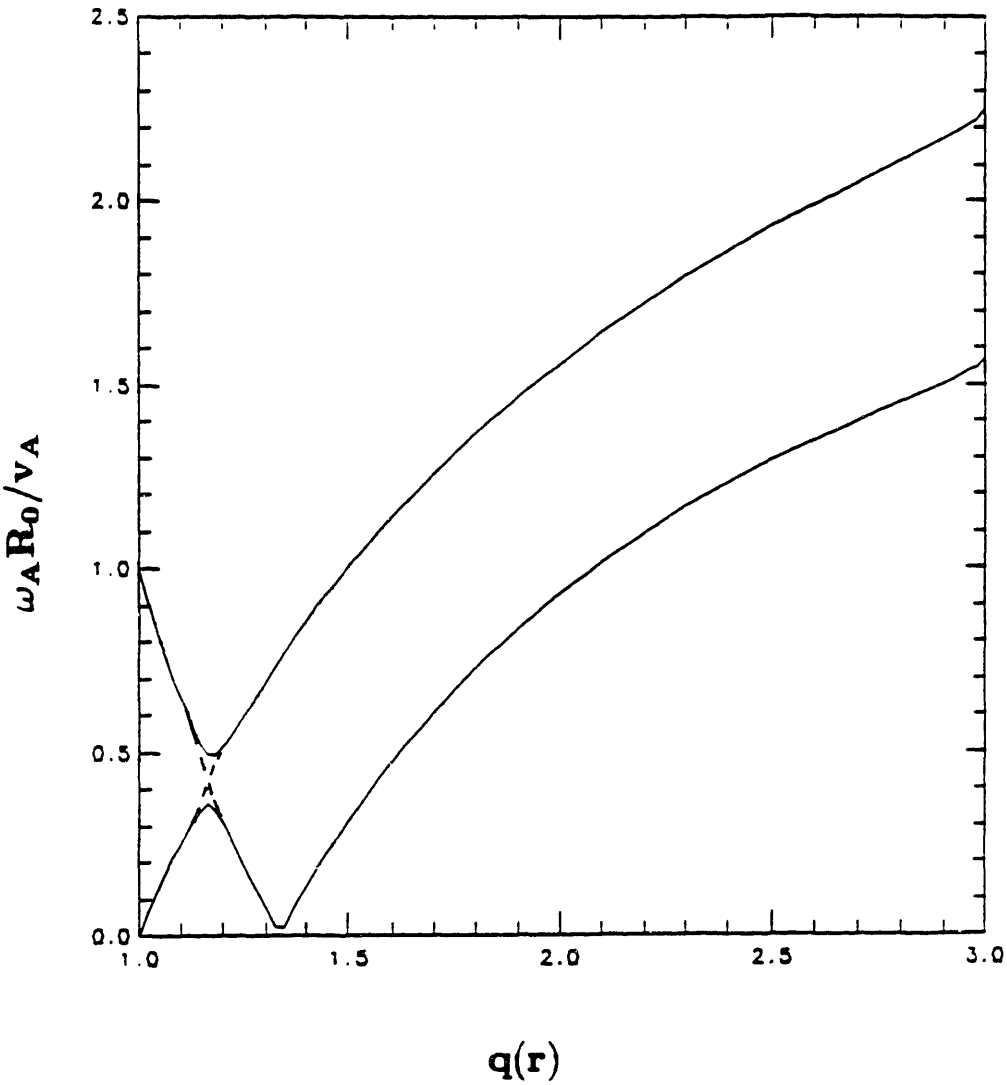

Figure 4c

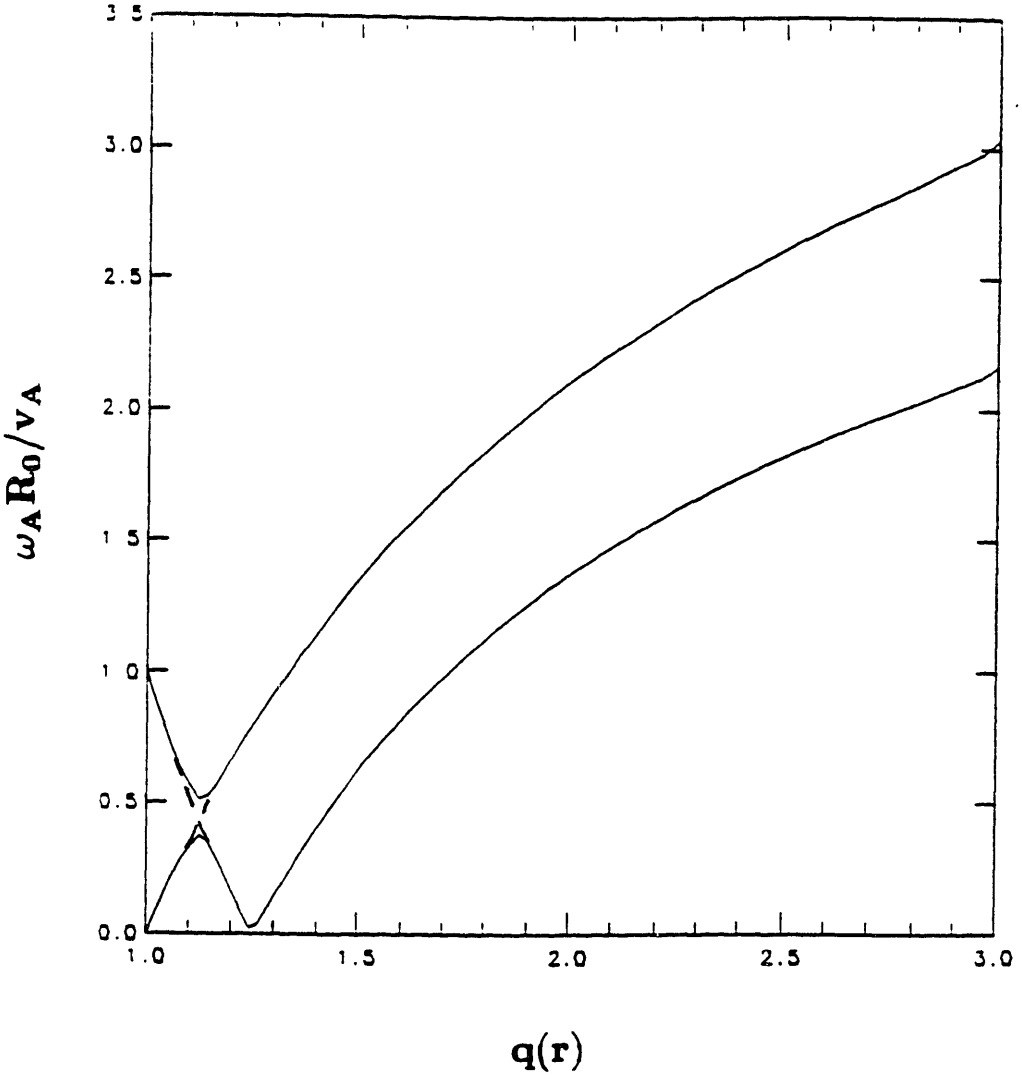

Figure 4d

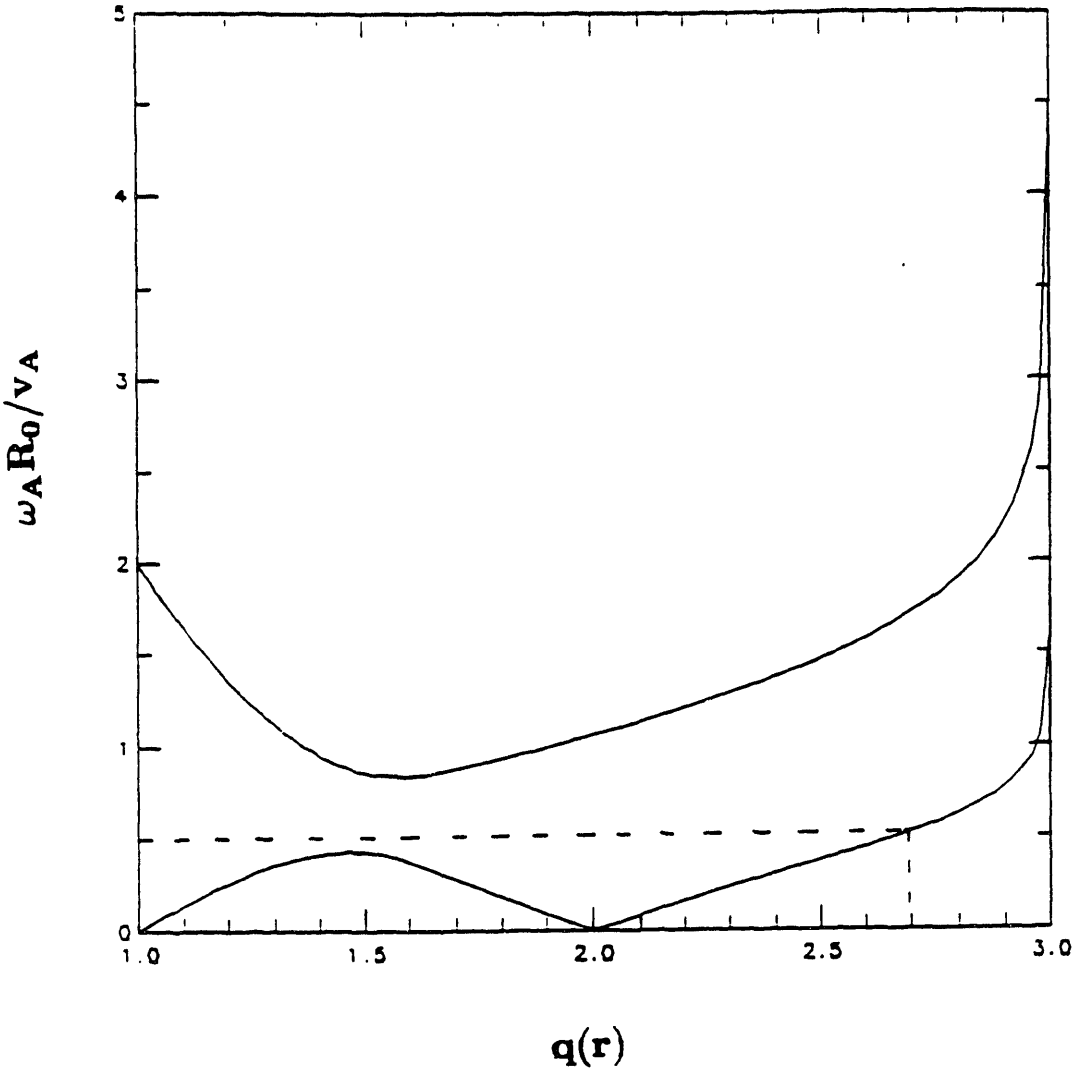

Figure 5

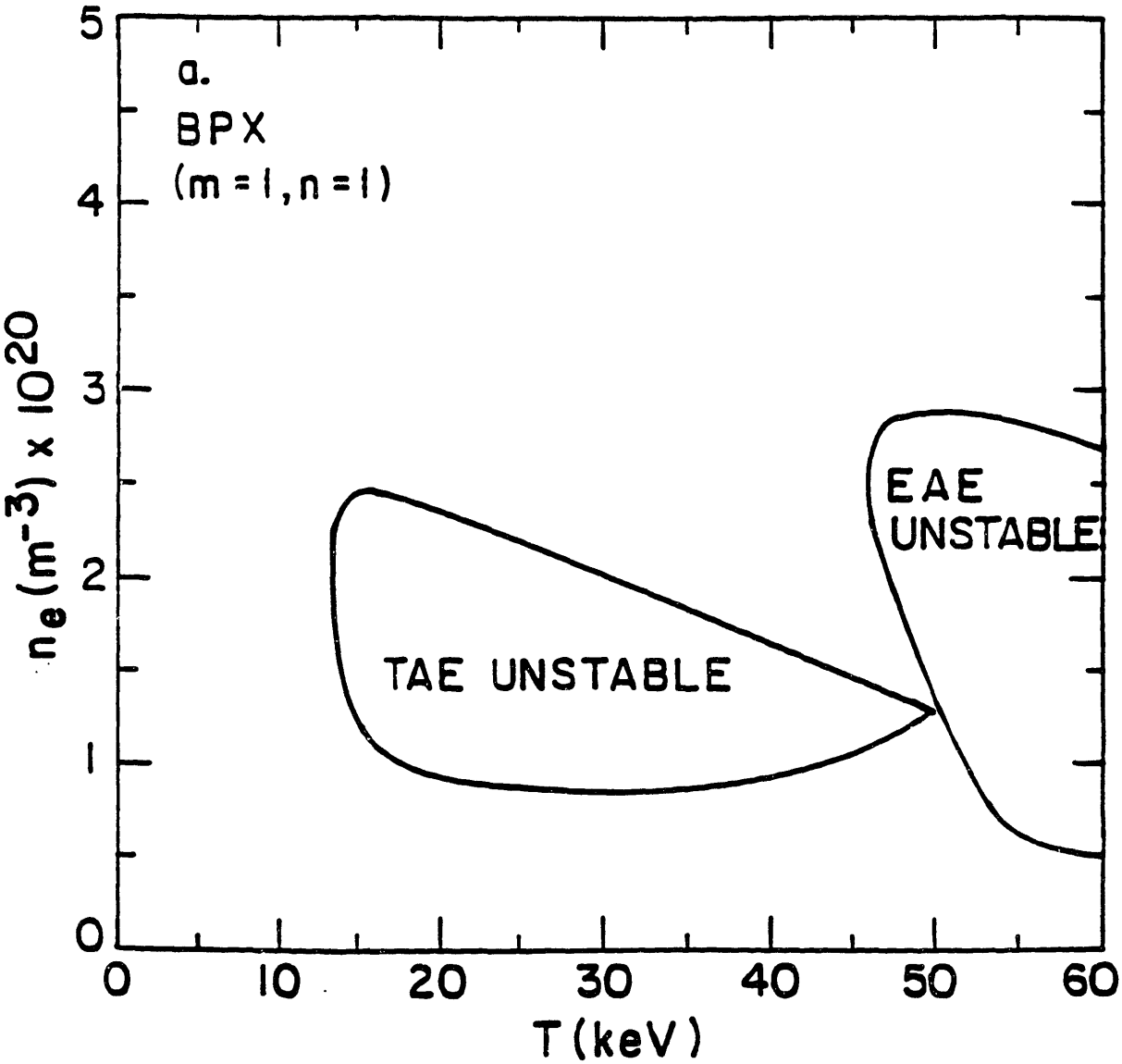
a.
BPX
(m = 1, n = 1)
TAE UNSTABLE
EAE
UNSTABLE
$n_e (m^{-3}) \times 10^{20}$
T (keV)
0
1
2
3
4
5
0
10
20
30
40
50
60

Figure 6a

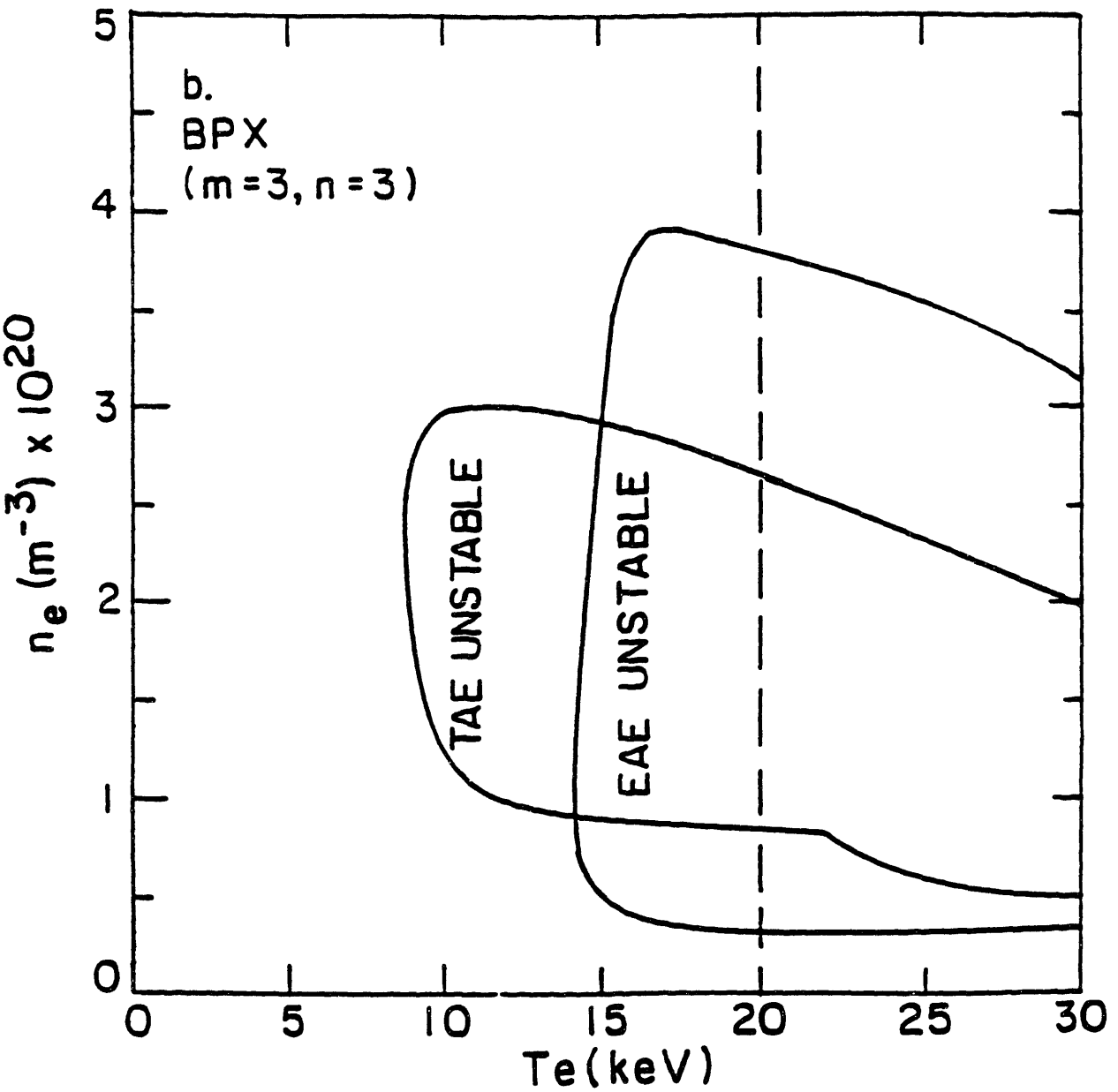
b.
BPX
(m=3, n=3)
TAE UNSTABLE
EAE UNSTABLE
$n_e\,(m^{-3}) \times 10^{20}$
Te(keV)
0
1
2
3
4
5
0
5
10
15
20
25
30

Figure 6b

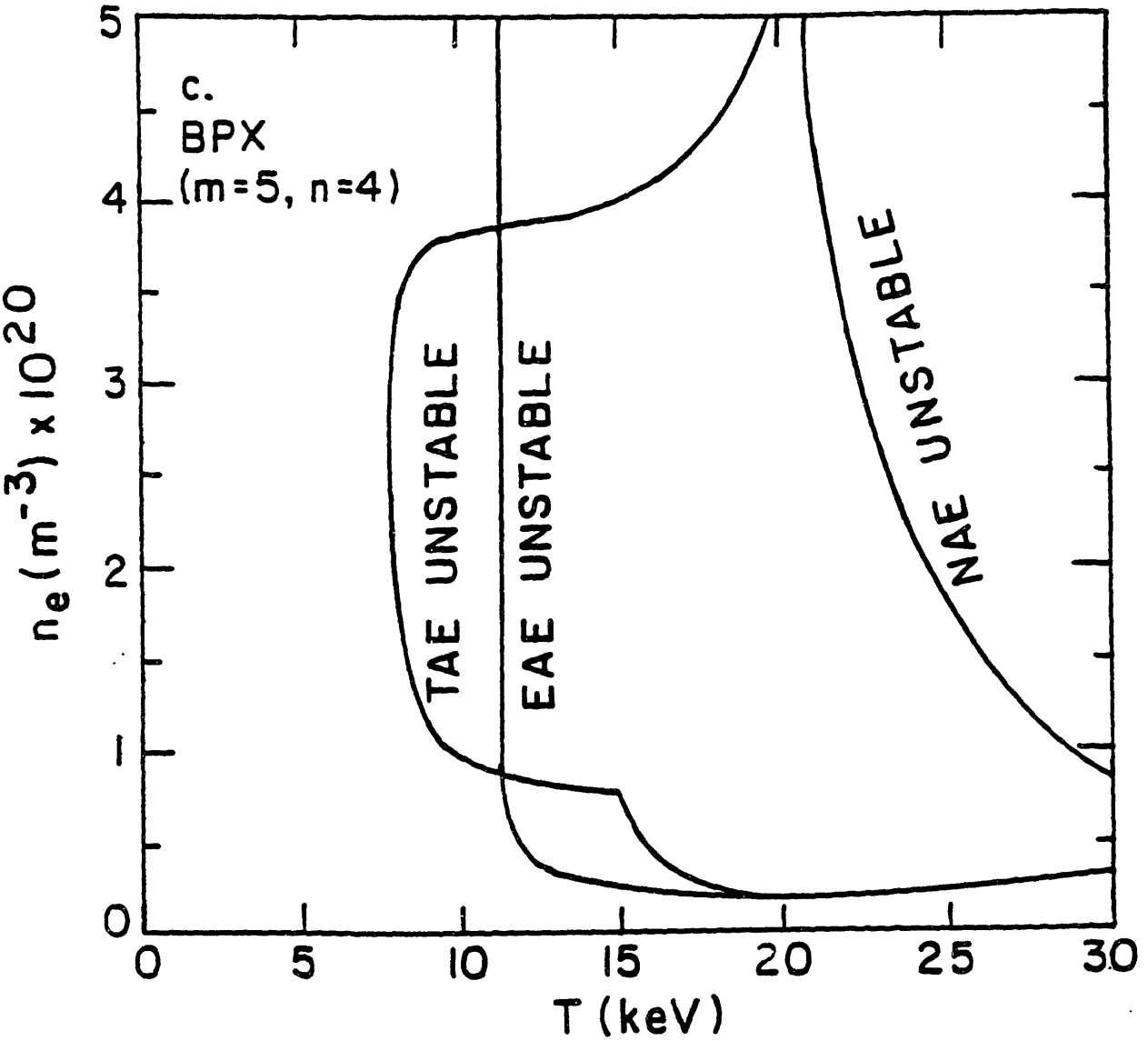
c.
BPX
(m=5, n=4)
TAE UNSTABLE
EAE UNSTABLE
NAE UNSTABLE
$n_e(m^{-3}) \times 10^{20}$
T (keV)
0
1
2
3
4
5
0
5
10
15
20
25
30

Figure 6c

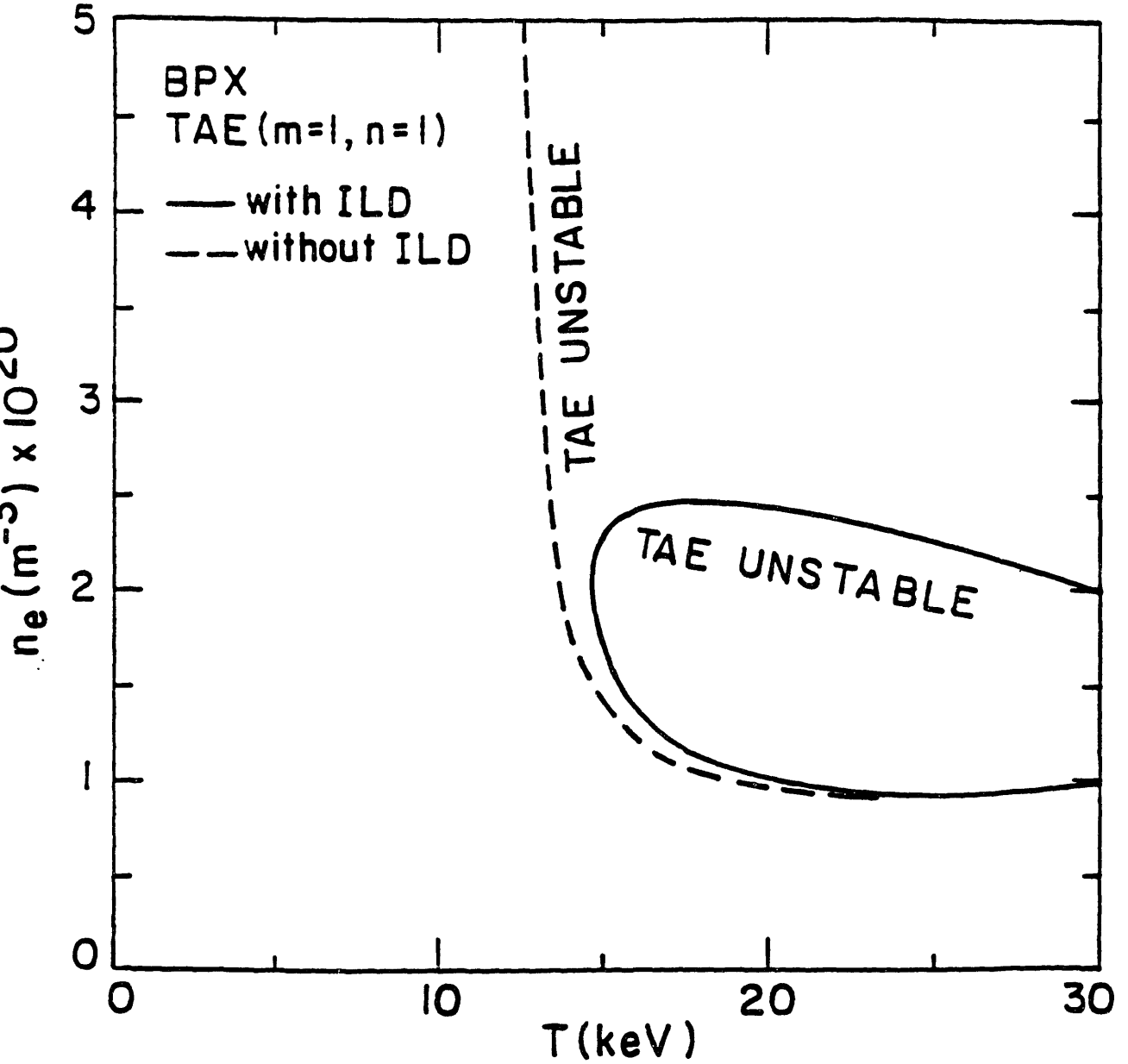
BPX
TAE (m=1, n=1)
—— with ILD
– – without ILD
TAE UNSTABLE
TAE UNSTABLE
$n_e (m^{-3}) \times 10^{20}$
T (keV)
0
1
2
3
4
5
0
10
20
30

Figure 7

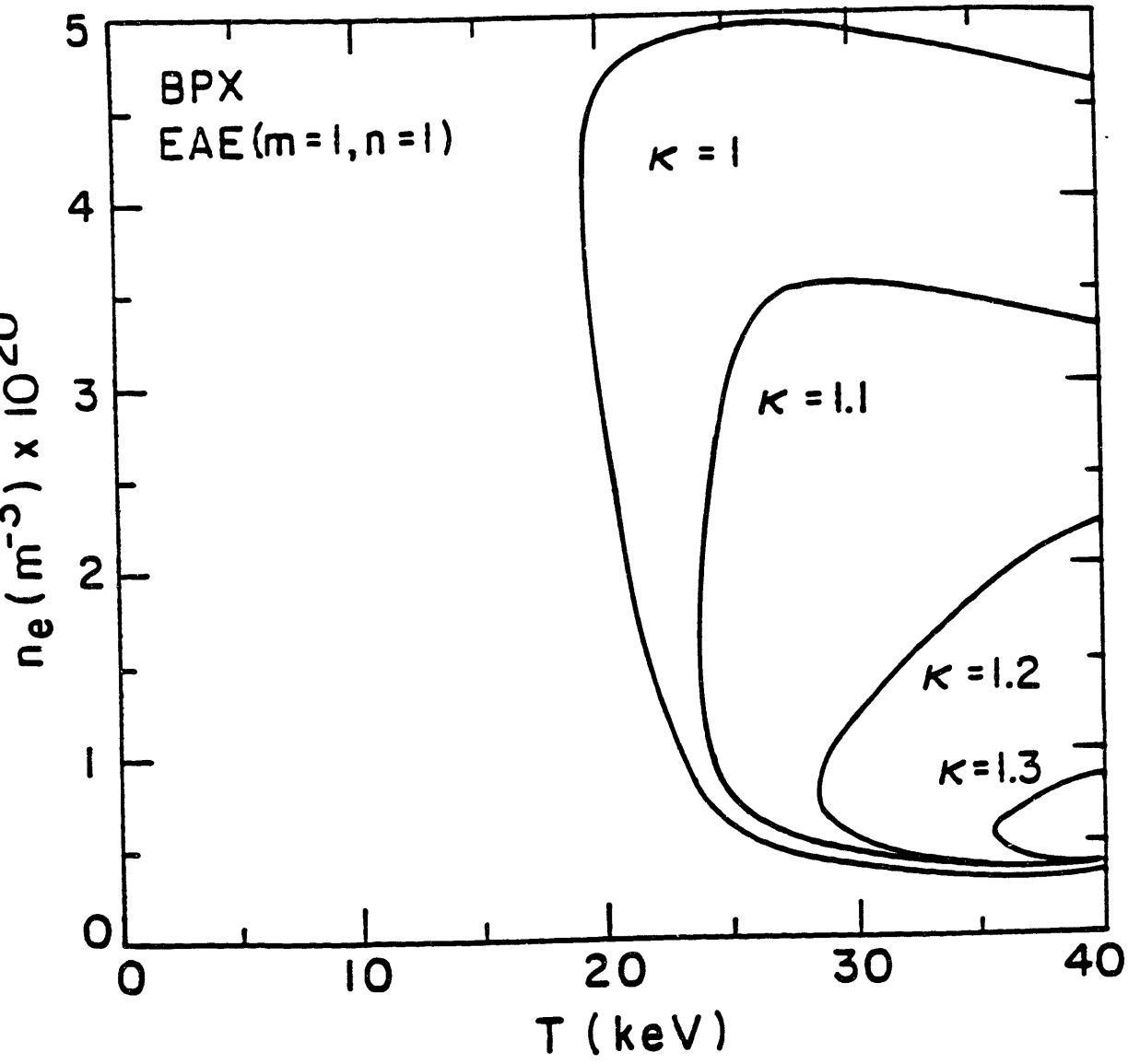
BPX
EAE(m=1, n=1)
κ = 1
κ = 1.1
κ = 1.2
κ = 1.3
$n_e(m^{-3}) \times 10^{20}$
T (keV)
0
1
2
3
4
5
0
10
20
30
40

Figure 8

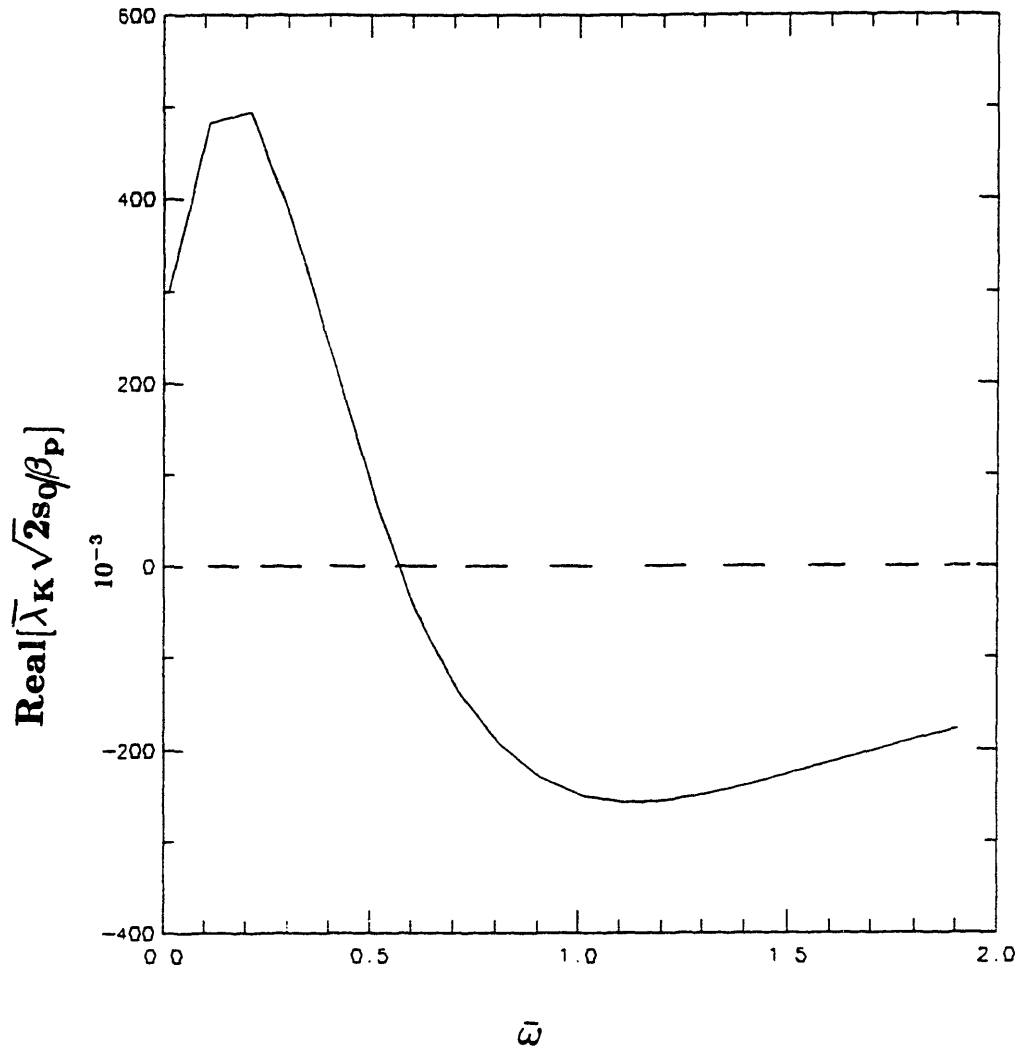
600
400
200
0
-200
-400
0 0
0.5
1.0
1 5
2.0
$\mathbf{Real}[\bar{\lambda}_K \sqrt{2} s_q / \beta_p]$
10^{-3}
$\bar{\omega}$

Figure 9

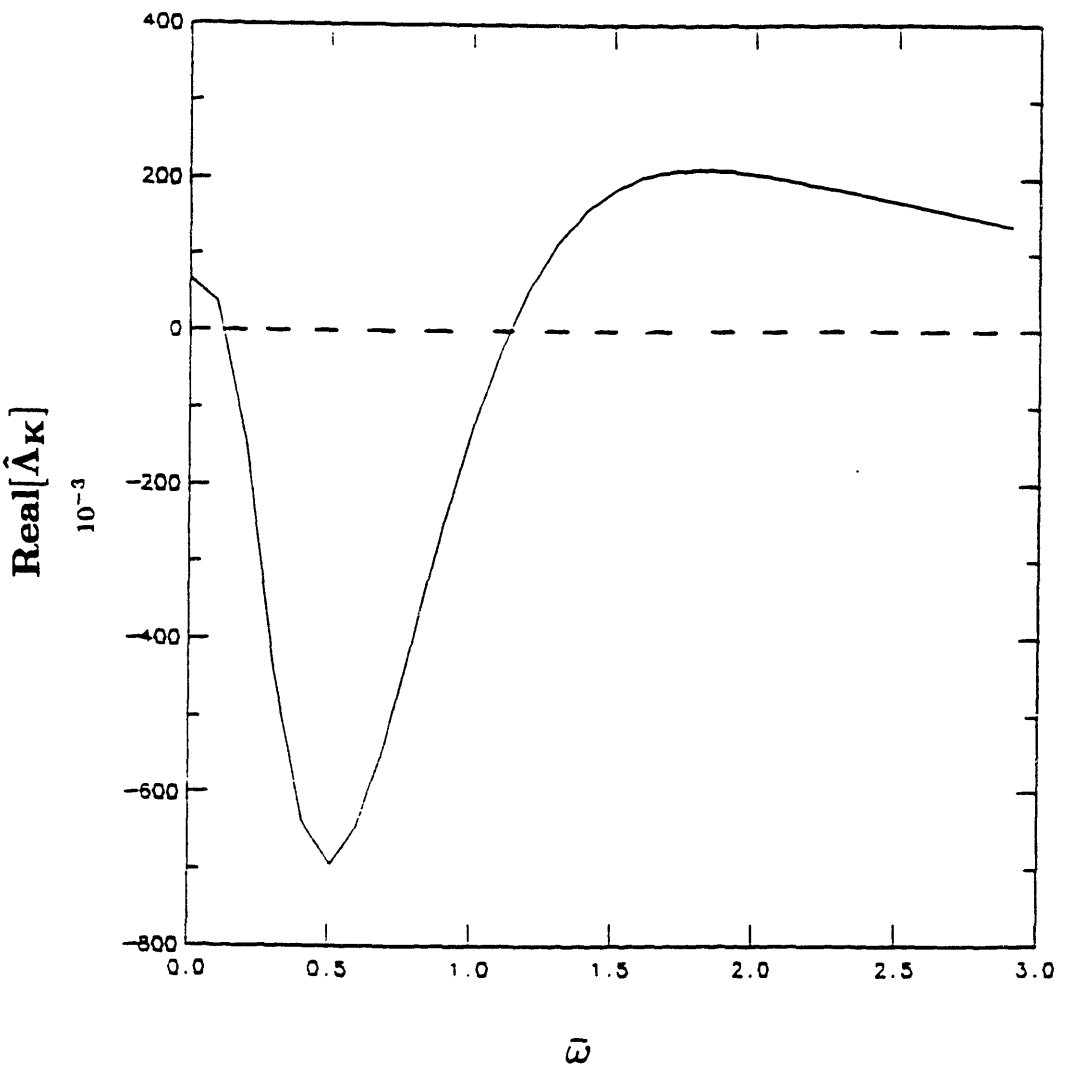
400
200
0
-200
-400
-600
-800
0.0
0.5
1.0
1.5
2.0
2.5
3.0
Real[$\hat{\Lambda}_K$]
10^{-3}
$\bar{\omega}$

Figure 10a

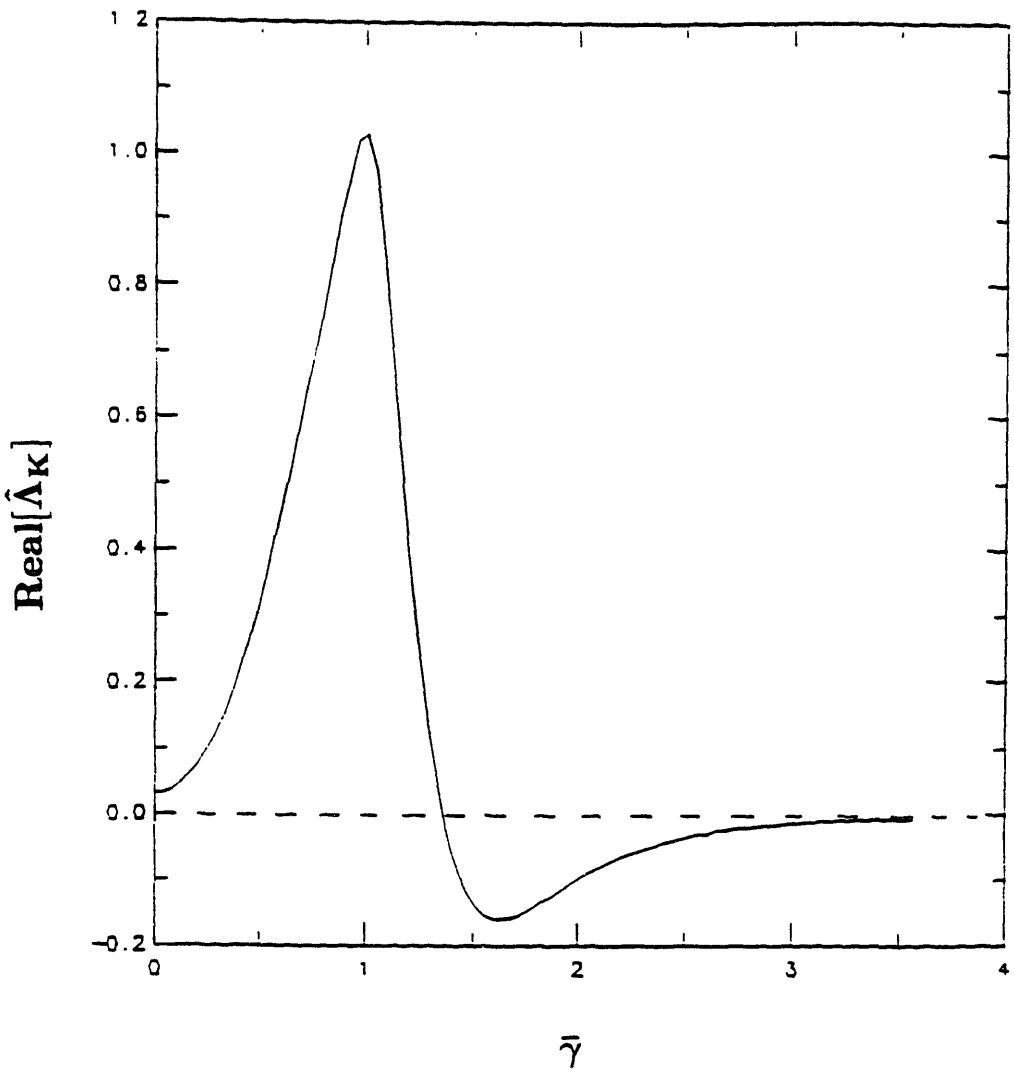

Figure 10b

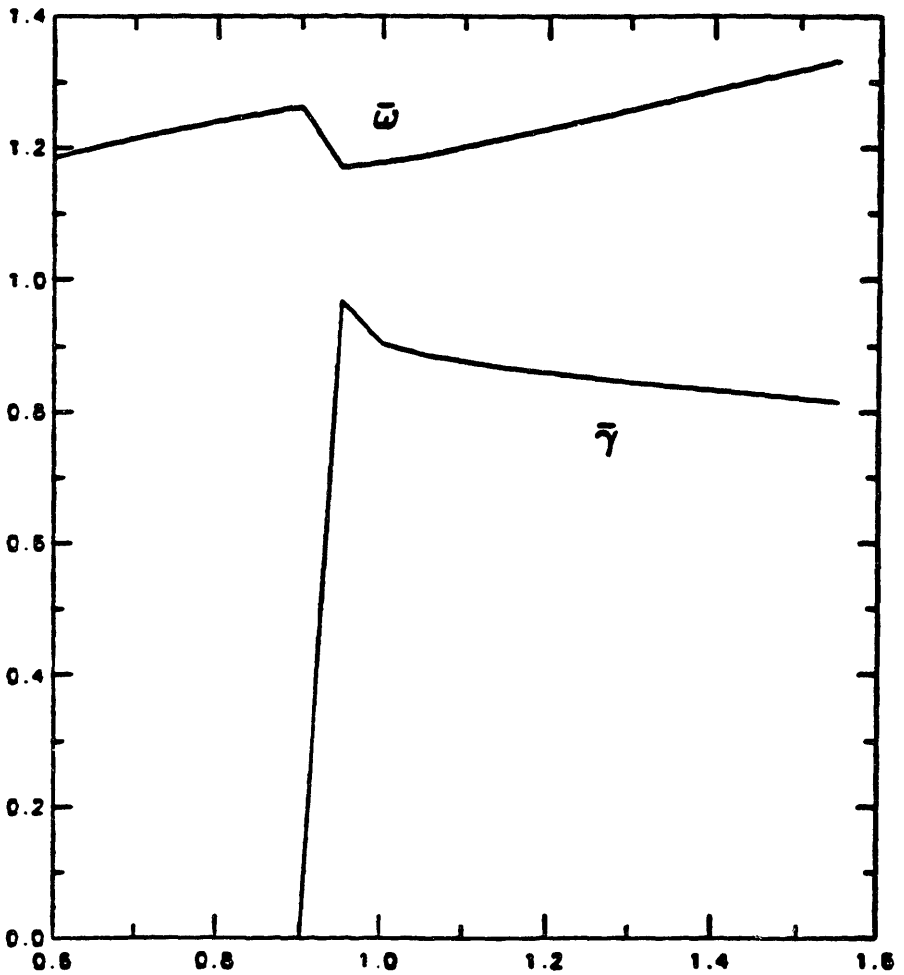

$$\hat{\beta}_p \equiv 2\mu_0 p(0)/B_\theta^2(r_s)$$

Figure 11

From W.W. HEIDBRINK, E.J. STRAIT, E.DOYLE, G.SAGER, and R. SNIDER, General Atomics, Report GA-A20254

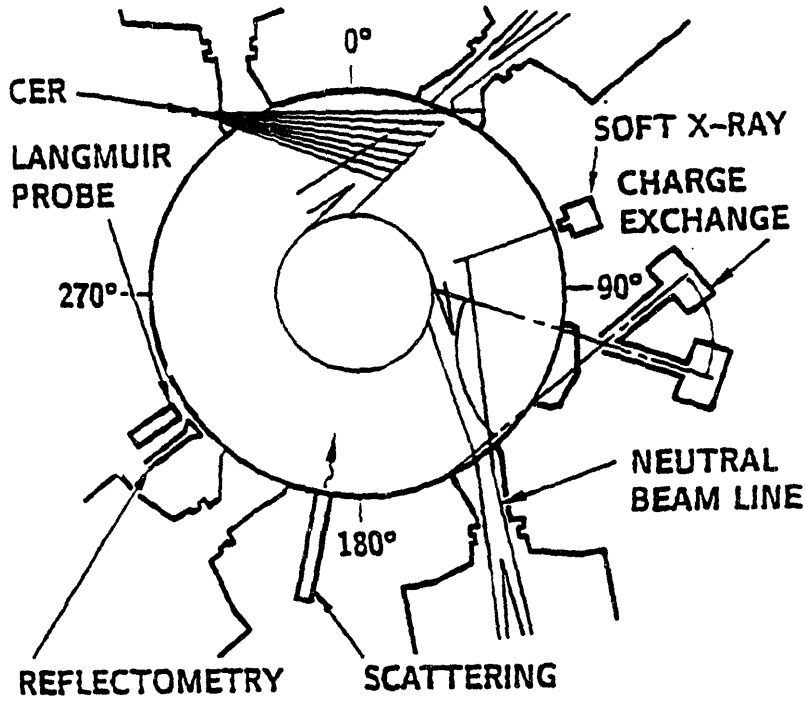

Plan view of the DIII–D tokamak. Eight neutral beam sources housed in four beam boxes inject neutrals in the direction of the plasma current. Active charge-exchange measurements are obtained by modulating one of the heating beams at 150°. The neutral deposition is measured by the CER diagnostic that views the nominally identical beam at 30°. Fluctuation diagnostics include soft x-ray cameras, a laser scattering diagnostic, microwave reflectometry, a midplane Langmuir probe, and numerous Mirnov coils (not shown).

Figure 12

From W.W. HEIDBRINK, E.J. STRAIT, E.DOYLE, G.SAGER, and R. SNIDER, General Atomics, Report GA-A20254

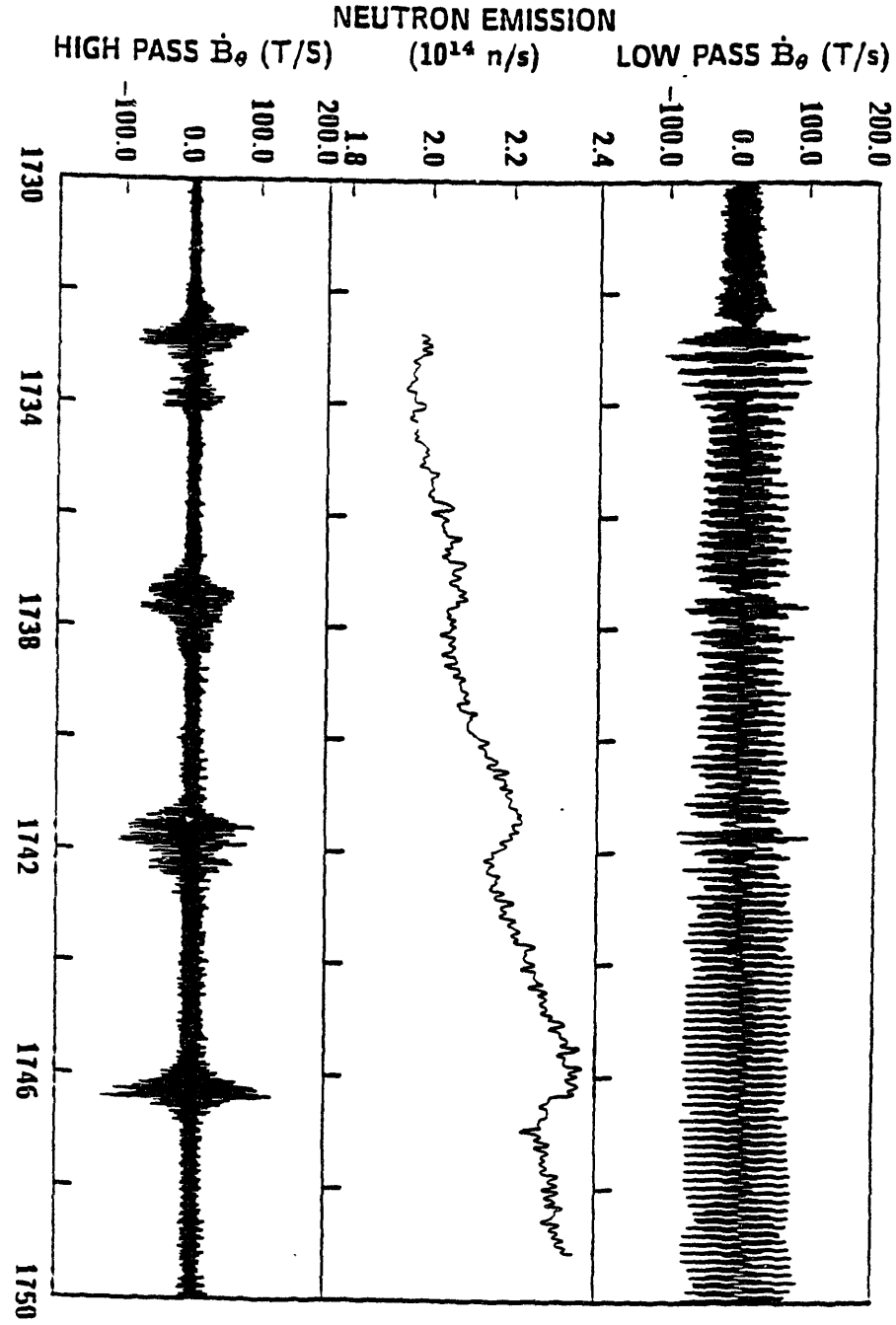

Signal from a Mirnov coil located near the outer midplane after digital filtering to remove frequencies above 50 kHz (a) and below 100 kHz (c), together with the signal from a plastic scintillator (b). *Reductions in neutron emission correlate with high*

Figure 13

From W.W. HEIDBRINK. E.J. STRAIT. E.DOYLE, G.SAGER, and R. SNIDER. General Atomics. Report GA-A20254

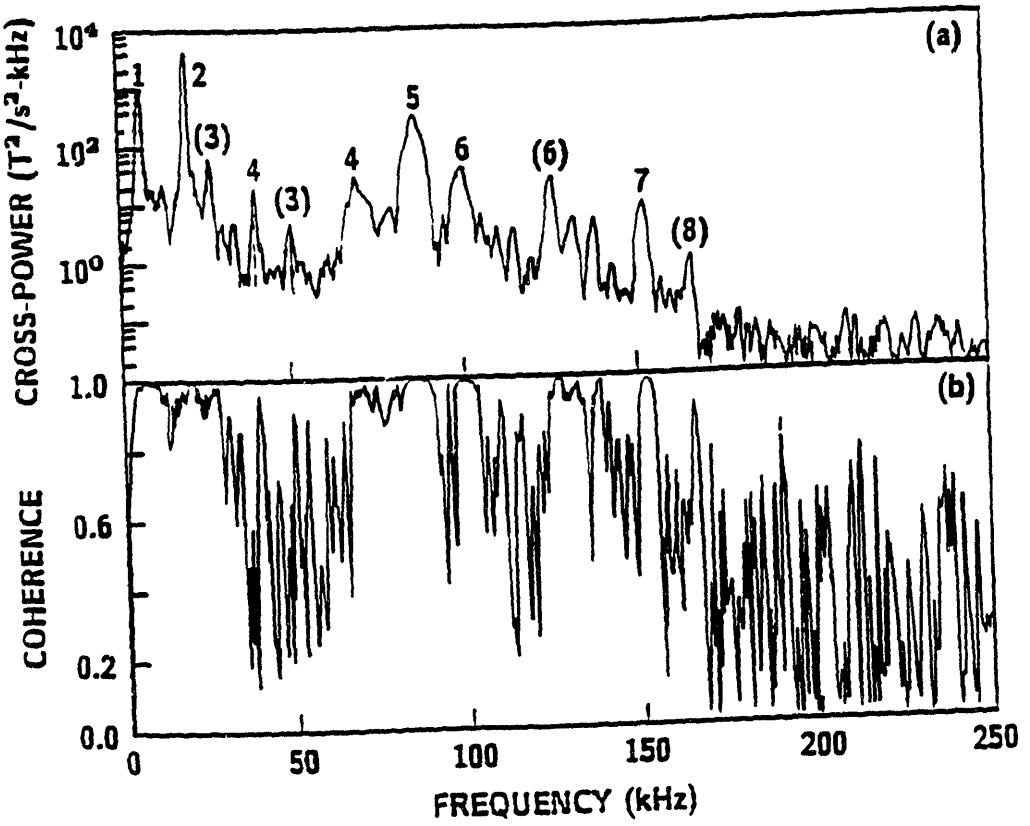

Cross-power (a) and coherence (b) spectra of two $\dot{B}_\theta$ signals between 1745.4–1747.4 ms in the discharge shown in Fig. 2. The coils are at the same poloidal location on the outer wall displaced 45° from one another. The peaks are labeled with their toroidal mode number; a parenthesis indicates that the identification is somewhat uncertain.

Figure 14

From W.W. HEIDBRINK. E.J. STRAIT. E.DOYLE. G.SAGER, and R. SNIDER. General Atomics. Report GA-A20254

TABLE 2
High Frequency Mode Analysis

f (kHz)	n	m
64	3	4–6
78	4	5–6
92	5	6–7
104	6	6–8
121	7	7–9

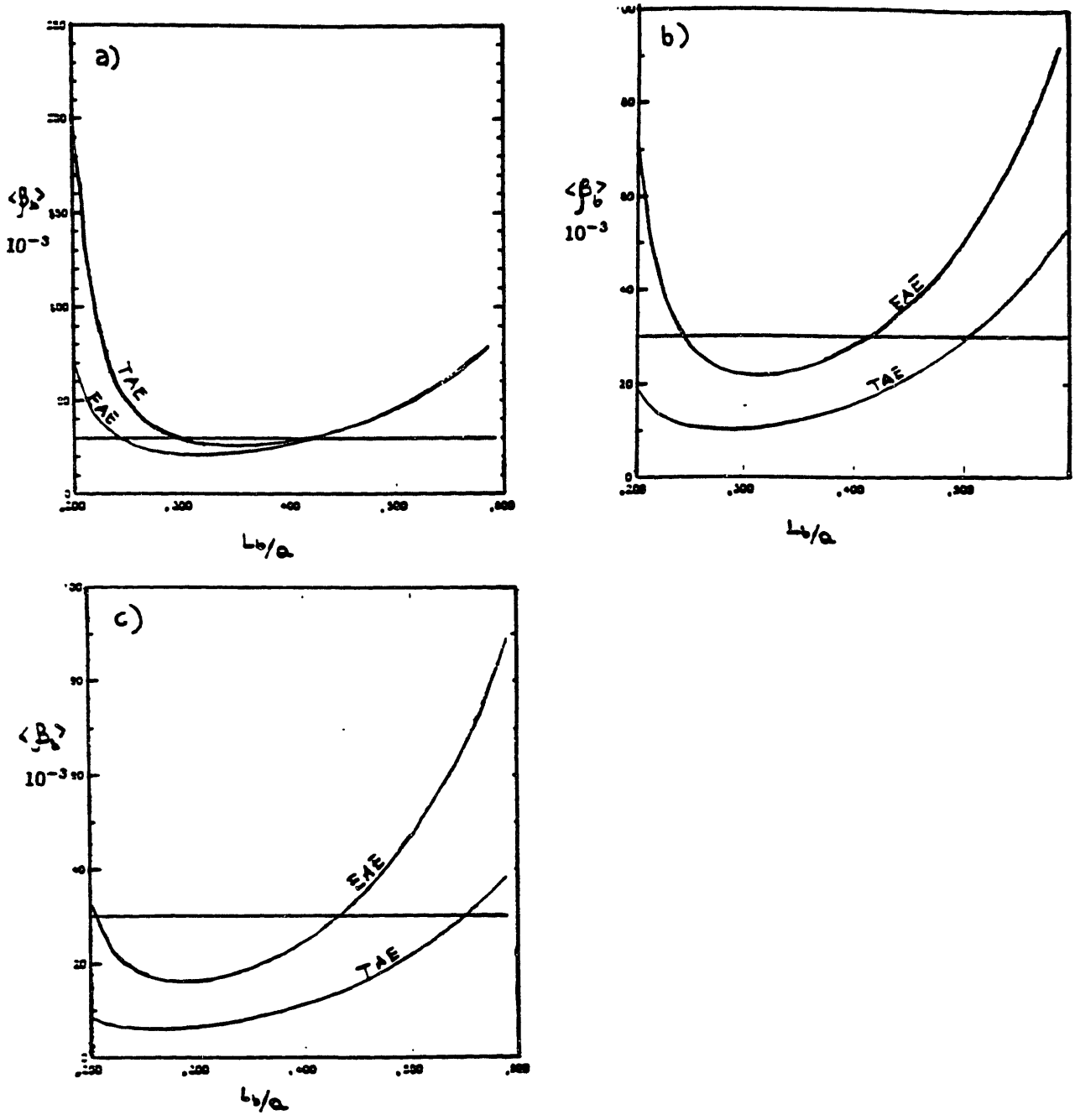

Figure 16